THE DEVELOPMENT OF A MEMBRANE REACTOR FOR THE DEHYDROGENATION OF ISOPROPANOL.

by

DUANE WILMOT MOUTON

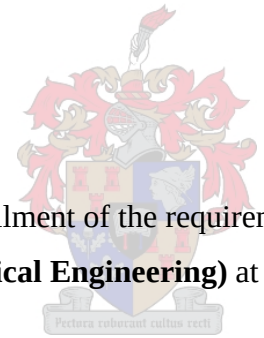

Thesis submitted in partial fulfillment of the requirements for the degree of Master of Science in Engineering **(Chemical Engineering)** at the **University of Stellenbosch.**

Supervisors: Prof.L.Lorenzen
Dr. J.N. Keuler

April 2003

DECLARATION

I, the undersigned hereby declare that the work contained in this thesis is my own original work, except where it was stated otherwise, and has not previously in its entirety or in part been submitted at any university for a degree.

……. ……..

Signature Date

SYNOPSIS

Both porous and dense hydrogen selective membranes have recently been an active area of research. The combination of a reactor and a separator in the form of a membrane reactor is seen as a feasible application in which to perform dehydrogenation reactions. These reactions are equilibrium limited so that the removal of the product H_2 by a selective membrane can improve the process effectiveness. Early Pd-based membranes were made of thin-walled tubes. In an attempt to increase permeation rates, thin supported Pd membranes have been developed.

This study investigated the development and performance of a catalytic membrane reactor. The membrane reactor consists of a tubular alumina membrane support coated on the inside with a film of palladium or a palladium-copper alloy. This reactor was used for the dehydrogenation of isopropanol. The thin film was coated on the alumina support using an electroless plating process. This process occurs in a liquid medium where palladium and copper are deposited by electrolysis or electroless means. With these methods alloys can also be deposited on the support. By plating a thin film of palladium on the alumina membranes, will attract hydrogen molecules from the reaction product, which will increase the reaction rate. The electroless plating process consists of four major components:

(i) reducing agent (0.04 M hydrazine),
(ii) temperature bath,
(iii) stabilised source of metal ions, and
(iv) support membrane (α-alumina).

Heat treatment was carried out on the coated membranes for 5 hours in a hydrogen atmosphere at 450°C. The plated membranes supplied by Atech were characterised using X-ray diffraction (XRD), scanning electron microscopy (SEM) and particle induced X-ray emission (PIXE) before and after heat treatment. SEM photographs showed that the pore size of the membranes was doubtful and due to that the films were not of a dense

nature. XRD results revealed that heat treatment led to the formation of smaller Pd and Cu crystallites. The concentration profiles constructed from the PIXE results indicated that Cu and Pd penetrated deep into the pores of the membrane during film preparation.

Different catalysts (Al_2O_3, MgO and SiO_2) were tested and the best one was chosen as catalyst in the membrane reactor. These catalytic runs were done in a plug flow (fixed-bed) reactor. Different particle sizes of catalysts were also tested. A 9.2 Cu wt % on silica achieved the highest acetone yields for the temperatures tested. Two different types of alumina membrane reactors were used. These were supplied from SCT. One membrane only coated with palladium and the other coated with palladium and copper. Selectivity and permeability tests were also carried out on these membranes. Selectivities of up to 90.6 could be reached with the palladium coated membrane. The palladium-copper plated membrane only achieved selectivities of up to 13. With heat treatment this value decreased even more. The palladium coated membrane also achieved much better conversion to acetone in the dehydrogenation of 2-propanol. The reason for that is its better selectivity. The palladium-copper membrane reactor did not show much better results than the fixed-bed reactor.

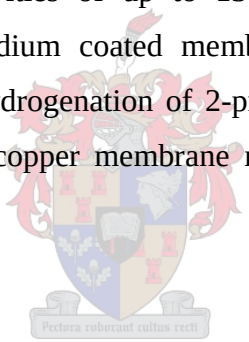

OPSOMMING

Hierdie studie ondersoek die ontwikkeling en werk verrigting van ‘n katalitiese membraan reaktor. Die membraan reaktor bestaan uit ‘n dun film palladium of palladium-koper allooi wat aan die binnekant van ‘n silindriese alumina membraan geplateer word. Die alumina dien as membraanbasis. Hierdie reaktor sal gebruik word vir die dehidrogenering van isopropanol.

Die dun films van metaal word neergeslaan op die alumina basis deur ‘n elektrodelose platerings proses. Hierdie proses vind plaas in ‘n vloeistof medium waar palladium en koper neerslag plaasvind op ‘n elektrodelose wyse. Met hierdie metode kan metaal allooie geplateer word op basis membrane. Deur ‘n dun palladium lagie aan die binnekant van die alumina membrane te plateer sal veroorsaak dat waterstof molekules uit die reaksie volume sal weg beweeg. Dit sal ‘n verhoging in reaksie tempo meebring. Die platerings proses bestaan uit vier komponente:

(i) reduseermiddel (0.04M Hidrasien),
(ii) temperatuur water bad,
(iii) stabiliseerde bron van metaal ione (Pd/Cu kompleks oplossing), en
(iv) basis membraan (α-alumina).

Hittebehandeling vir 5 uur is uitgevoer op hierdie geplateerde membrane by 450°C in ‘n waterstofatmosfeer. Die geplateerde membrane is daarna gekarakteriseer- voor en na hittebehandeling. Dit is gekarakteriseer deur X-straal diffraksie (XRD), skanderings elektron mikroskopie (SEM) en partikel geïnduseerde X-straal emissie (PIXE). XRD eksperimente het gewys dat die koper en die palladium ‘n allooi gevorm het. Veranderinge in kristaltekstuur het voorgekom na hittebehandeling. Tydens hittebehandeling was kleiner palladium en koper kristalle gevorm. SEM resultate het getoon dat die film nie baie dig was nie en die porie grootte van die membrane was ook nie korrek nie. PIXE resultate het die konsentrasieprofiele van beide koper en palladium

oor die dikte van die membraan bepaal. Dit het gewys dat die Cu en Pd diep binne die membraan penetreer het tydens voorbereiding van die membraan.

Verskillende soorte kataliste (Al_2O_3, MgO and SiO_2) is ondersoek vir die dehidrogenering van isopropanol. Hierdie katalitiese ondersoek is gedoen in ‘n propvloei reaktor. Die beste katalis is gekies om in die membraan reaktor te gebruik. Verskillende partikel groottes is ook ondersoek. ‘n 9.2 Cu massa % koper op silika katalis het die beste omsetting na asetoon verkry vir die temperature waarvoor toetse gedoen is. Twee tipes membraan reaktors is gebruik. Een met net ‘n palladium film, terwyl ‘n palladium-koper allooi op die ander membraan reaktor gedeponeer was. Selektiwiteits- en deurlaatbaarheids toetse is op altwee membrane gedoen. Selektiwiteite van 90.6% kon verkry word met die palladium membraan. Die palladium-koper membraan kon slegs ‘n selektiwiteit van 13% bereik. Met hittebehandeling daarvan het die selektiwiteit selfs meer afgeneem. Die palladium membraan het ook hoër omsettings na asetoon getoon. Die rede hiervoor is die membraan se hoë selektiwiteit. Die palladium-koper membraan het nie veel beter resultate as die propvloei reaktor gelewer nie.

TABLE OF CONTENTS

LIST OF FIGURES

Chapter 4

Chapter 5

Chapter 6

Chapter 7

LIST OF TABLES

Chapter 4

Chapter 5

Chapter 6

ACKNOWLEDGEMENTS

Gratitude and pleasure has given me the opportunity to thank the following people/institutions:

I would like to thank **my parents** for motivation and encouragement.

Prof. L Lorenzen and **Dr. JN Keuler** for guidance, leadership and technical support during the project.

Me. H Botha and the rest of the personnel at the Department of Chemical Engineering who assisted me with analysis.

The **Microscope Unit** at the University of Cape Town for assisting with SEM work.

Mr. HS Pienaar (US Geology Department) for helping with X-ray diffraction experiments.

Dr. V Prozesky (previously National Acceleration Center, now Itemba Labs) who assisted with PIXE experiments.

SASOL for sponsoring the project.

The **NRF** for financial contribution towards the project.

List of symbols

A	= frequency factor	[-]
A_r	= cross section area of reaction side of reactor	[m^2]
a_i	= adjustment factor	[-]
a	= Knudsen parameter	[$mol.K^{0.5}/m.s.kPa$]
b	= viscous parameter	[mol.K/m.kPa]
C_i	= concentration of *i*-th component	[mol/dm^3]
D_i	= diffusivity of *i*-th component	[$m^2.s^{-1}$]
d	= diameter	[m]
Da	= Damkohler number	[-]
$D_{F,i}$	= surface diffusivity parameter in Equation (2.48)	[mol/m.s.kPa]
$D_{s,i}$	= surface diffusivity of *i*-th component	[m^2/s]
$D_{s,i}^{o}$	= diffusivity constant	[m^2/s]
E	= parameter in a Langmuir isotherm	[kPa^{-1}]
E'	= parameters in a Langmuir isotherm	[mol/kg.kPa]
E_a	= activation energy	[kJ/mol]
$E_{s,i}$	= activation energy of surface diffusion of *i*-th component	[kJ/mol]
F_i	= flow rate of *i*-th component	[$mol.m^2.s^{-1}$]
$\hat{f}_i$	= fugasity of *i*-th omponent	[-]
h_i	= henry's-law constant for *i*-th component	[-]
J_i	= permeation flux of *i*-th component	[$mol.m^{-2}.s^{-1}$]
K_i	= Chemical-equilibrium constant of *i*-th component	[-]
k_i	= specific reaction rate constant	[$mol/m^3.Pa^{-1}$]
k_S	= permeability constant defined by Sieverts law	[$mol.m^{-1}.Pa^{-0.5}$]
k_{Ki}	= permeability constant defined by Knudsen diffusion	[$mol.m^{-1}.Pa^{-0.5}$]
L_i	= length	[m]
LHSV	= liquid hourly space velocity	[h^{-1}]
l	= membrane thickness	[microns]
M_i	= molecular weight of *i*-th component	[$g.mol^{-1}$]
m	= constant	[-]
n	= number of surface active sites	[-]

P_i	= partial pressure of *i*-th component	[kPa]
q_i	= the amount of species *i* adsorbed	[mol/kg]
R	= universal gas constant	[8.314 $J.mol^{-1}.K^{-1}$]
r_i	= reaction rate of *i*-th component	[$mol.m^{-3}.s^{-1}$]
S_i	= selectivity towards *i*-th component	[%]
Sol	= solubility of hydrogen in palladium	[$mol.m^{-3}.Pa^{-0.5}$]
S_t	= membrane specific surface area	[m^2/kg]
T	= Temperature	[K]
V_t	= specific volume of the adsorbed phase	[m^3/mol]
v	= average pore size of the composite membrane	[nm]
W	= catalyst mass	[mg]
X	= conversion	[%]
x_i	= molar fraction of species *i* on feed side	[-]
y_i	= molar fraction of species *i* on permeate side	[-]
Z	= constant of adsorption	[-]

Greek symbols:

α_{av}	= measure of permeance through a composite membrane	[$mol/m^2.s.Pa$]
β_{av}	= measure of the viscous flow through a composite membrane	[$mol/m^2.s.Pa^2$]
ε	= void fraction of porous membrane	[-]
λ	= parameter in Equation (2.42)	
ρ_{app}	=apparent density of the membrane	[kg/m^3]
θ	= radius of porous membrane	[m]
τ	= tortuosity factor	[-]
μ	= viscosity of the gas	[$N.s/m^2$]
ΔH	= heat of reaction	[kJ/mol]
ω	=parameter in Equation (2.41)	

Subscripts:

B = benzene

C = cyclohexane

H = hydrogen

R = reaction side

A = acetone

P = isopropanol

PR = propene

g = gas flow

s = surface flow

1 = feed side

2 = permeate side

alc = alcohol

u = upstream

d = downstream

av = average

RI = reactor from inlet

eq = equilibrium

M = membrane

o = pore

1. Introduction

In recent years, a lot of effort has gone into the development of membrane reactors. The advantages of membrane reactors can be exploited by the following type of generic reversible reaction:

$$A + B \leftrightarrow C + D \qquad (1.1)$$

The reaction (**equation 1.1**) has a limited conversion, which is a function of the temperature. The conversion can be increased by shifting the reaction equilibrium towards the product side. This can be done by selectively removing either or both the products through the membrane.

Palladium based membranes have been studied extensively due to their extremely high hydrogen permselectivity and well-known catalytic activity for many reactions. Even at elevated temperatures, palladium will maintain its thermal and corrosive resistance. Palladium alloys are favoured over pure palladium for hydrogen separation, because of several considerations. These include resistance to embrittlement at temperatures below 298 °C in a hydrogen atmosphere; the fact that with alloys such as niobium and tantalum the hydrogen flux is higher by an order of magnitude, and the price per meter for alloys is lower (Buxbaum, 1993).

The improvements in the preparation techniques of membranes with very thin palladium or palladium alloy films, should make such processes more economically attractive in the future. Thin films are advantageous since the hydrogen permeation flux is inversely proportional to the film thickness for thicker films. For thinner films (< 2.0 μm), the flux will become independent of thickness (Keuler, 2000), because of a change in the H_2 transport mechanism from the diffusion limited to adsorption limited through the film. Membranes can be made mechanically stronger and cheaper by depositing a thin layer of palladium on a thicker porous inorganic support such as alumina. These membranes are often used for reactions like dehydrogenation, because of their H_2 separation

characteristic. Palladium and palladium alloy composite membranes also catalyse dehydrogenation reactions.

In this investigation, α-alumina membranes were used as supports. These membranes were coated with palladium by an electroless plating method. This is probably the best technique to prepare a thin defect free film on the inside of a tubular membrane. Between 20 and 40 wt % copper were added to the palladium films. These metal films were heat treated in a hydrogen atmosphere for 5 hours. This was done to form a homogeneous alloy between the copper and the palladium. The plated membranes were characterised using SEM (topography of surface), XRD (crystal structure) and PIXE (concentration of elements across the membrane). These processes were performed before and after the heat treatment of the membranes. Copper serves as a catalyst for the dehydrogenation of alcohols and it will reduce production costs of defect free films, by reducing the Pd content of the alloy films.

The gas phase dehydrogenation of isopropanol was investigated in a fixed-bed reactor and in a membrane reactor. The dehydrogenation of isopropanol to acetone was chosen as a test reaction due to its high selectivity and catalytic activity. SiO_2, Al_2O_3 and MgO supports were tested for this reaction. Between 5 and 33 wt % Cu was impregnated into these supports to provide active catalytic centers. Eight different Cu catalysts were investigated. The purpose of this study was to compare the performance of both the fixed-bed reactor and the membrane reactor by doing the same reaction in both reactors.

2. Literature study

2.1 Membrane processes

A membrane can be classified as a semipermeable active barrier, which permits preferential passage of one or more selected species of a gaseous or liquid mixture. This will occur under a driving force such as pressure, concentration or a voltage difference across the membrane. The species that passes through the pores of the membranes are called the permeate and the species that are rejected by the membrane is called the retentate. **Table 2.1** shows different membrane processes.

Table 2.1 Membrane separation processes

Process	Driving force	Typical permeate	Typical retentate
Microfiltration	Pressure difference	Water and dissolved species	Suspended materials
Ultrafiltration	Pressure difference	Water and salts	Biologicals and colloids
Reverse osmosis	Pressure difference	Water	Suspended and dissolved materials
Electrodialysis	Voltage	Ions	All non-ionic and macromolecular species
Gas separation	Pressure difference	Gases and vapours	Membrane impermeable gases
Dialysis	Concentration difference	Ions and low molecular-weight organics	Dissolved and suspended materials with molecular weight > 1.00

Adapted from Lonsdale (1982)

The separation performance of a membrane can be explained by two important factors. These two factors are permeability and permselectivity. Permeability describes the ability

of the membrane to process the permeate. Thus a high permeability means a high throughput. Permselectivity is the ability of the membrane to separate the permeate from the retentate.

Organic membranes were the main focus of membrane science and technology during the early stages of membrane development. In the early to middle twentieth century, membrane science began to evolve from a fairly narrow scientific discipline with limited practical applications to a broader field with diverging applications that support a unique industry which started in the late 1960s and early 1970s. Membrane processes became more economical than conventional separation processes, such as distillation, due to lower energy costs for membrane processes. A summary of the current status of membrane technology is found in **Table 2.2**. Membrane technology is a very good separation method for small volumetric flow rate applications when the purity level required is in the 95 to 99% range.

Table 2.2 Current status of membrane technology

	Problems		
Process	**Major**	**Minor**	**Mostly solved**
Microfiltration	Reliability	Cost	Selectivity
Ultrafiltration	Reliability	Cost	Selectivity
Reverse osmosis	Reliability	Selectivity	Cost
Electrodialysis	Fouling Temperature stability	Cost	Selectivity Reliability
Gas separation	Selectivity Flux	Cost	Reliability
Pervaporation	Selectivity Reliability	Cost	
Coupled and facilitated transport	Reliability (membrane stability)		

Adapted from Baker et al. (1991)

The use of a membrane in a process to transform chemical substances is among the frontier developments in the field of inorganic membranes. This means that the membrane will not only be used as a separator, but also as part of a reactor. Inorganic membranes are potential candidates for these processes because of their better thermal stability.

In this literature study, the following definitions will be used:

(i)	Permeability	[mol.m/m^2.Pa.s]
(ii)	Permeance	[mol/m^2.Pa.s]
(iii)	Permeation or permeation flux	[mol/m^2.s]
(iv)	Permselectivity (ratio of permeance)	[no unit]

2.2 Types of inorganic membranes

Structurally, inorganic membranes can be divided into two categories: dense and porous membranes. The structure influences the performance of the membranes. Dense membranes are free of any pores. The effectiveness of dense membranes depends on the material its made of, the species to be separated and their reactions with the membrane. Electron microscopy can be used to investigate the pore structure of the membrane and to distinguish different types of membranes.

When the separation layer and the support layer are indistinguishable, i.e. they show a homogeneous structure and composition in the direction of the membrane thickness, it is called a symmetric or isotropic membrane. Since the flow rate through a diffusion limited membrane is inversely proportional to the membrane thickness, it is very desirable to make the homogeneous membrane layer as thin as possible. The mechanical structure, however, of thin membranes is not very strong and is not able to withstand high pressure gradients found in many applications. A solution to this dilemma is to make composite membranes, where the support and the separation layer are different. The support should be a mechanically strong and porous material and it should not significantly contribute towards the flow resistance of the membrane.

2.3 Catalytic membrane reactors

Membrane separation has been practised for a few decades, but new applications are still being actively explored. One such frontier technology area is the membrane reactor (or sometimes referred to as membrane catalyst system). It represents a variety of reactor configurations, which include a membrane as part of the system for separation or purification. The technology combines the permselectivity of a membrane with a reaction, particularly a heterogeneous catalytic reaction. Two types of reactions can take place in a membrane reactor, namely biological and catalytic reactions. Biological reactions are not considered in this study.

A major part of catalytic membrane reactor applications involves reversible reactions, which reach a thermodynamically limited conversion level in a conventional reactor. One or more products can continuously permeate through the membrane when the reactions are performed in a membrane reactor. The conversion which is then obtained, is much larger than in a conventional reactor. The membrane materials are usually either porous ceramic materials with Å-size pores or thin palladium films. Porous ceramic materials with Å-size pores usually pass small or linear molecules, while palladium films pass only hydrogen.

2.4 Catalytic palladium-based membrane reactors

Palladium-based membranes are well known for their high hydrogen permselectivity. Gryaznov and his Russian co-workers explored the dehydrogenation of hydrocarbons by the use of palladium membrane reactors since the early 1960s (Gryaznov, 1977). The use of pure palladium membranes for hydrogen separation is restricted, since H_2 embrittlement will occur in a H_2 environment below 573 K. Thin films of palladium alloys can be produced to prevent the membrane from rupturing in H_2. This can also enhance the hydrogen permeability if the correct alloying component is used. Silver is commercially used as an alloying constituent. The composition and thickness of films that were prepared by Uemiya (1991a) are summarised in **Table 2.3**. **Table 2.4** shows the

effect of the heat treatment temperature on the hydrogen permeation rate of a supported palladium-silver membrane. The film was of thickness 5.8 microns and had a silver content of 23 wt %. To form an alloy with palladium, the film had to be heat treated. The membrane treated at 1173 K exhibited a 2.7 times greater rate of hydrogen permeation than the film heat treated at 773 K. It was suggested that heat treatment at temperatures above 1073 K is necessary to form a miscible alloy. However, there is still great uncertainty about which conditions work best for heat treating thin Pd films (Keuler, 2000). Keuler (2000) employed different heat treatment methods to improve the hydrogen permeance of a Pd-Ag film. In all tested gas environments the films weakened at and above 590 °C. Defects in the film were caused by hydrogen at a moderate rate at 550 °C and at a fast rate at 590 °C. Continuous thermal cycling contributed towards film defection.

Table 2.3 Composition and thickness of supported palladium-silver alloy membranes (Uemiya, 1991a)

Membrane	Amount of Pd ($mg.cm^{-2}$)	Amount of Ag ($mg.cm^{-2}$)	Content of Ag (wt %)	Thickness (μm)
Pd	5.47	-	-	4.5
Pd-Ag	5.26	0.65	11.0	5.0
Pd-Ag	5.11	1.14	18.2	5.3
Pd-Ag	5.16	1.55	23.1	5.8
Pd-Ag	5.08	1.80	26.2	5.9
Pd-Ag	5.11	2.24	30.5	6.4

Table 2.4 Effect of heat treatment temperature on the hydrogen permeation rate of supported palladium-silver membrane (Uemiya, 1991a)

Treatment temperature (K)	Rate of hydrogen permeation [$mol/m^2.s$]
773	0.163
1173	0.434

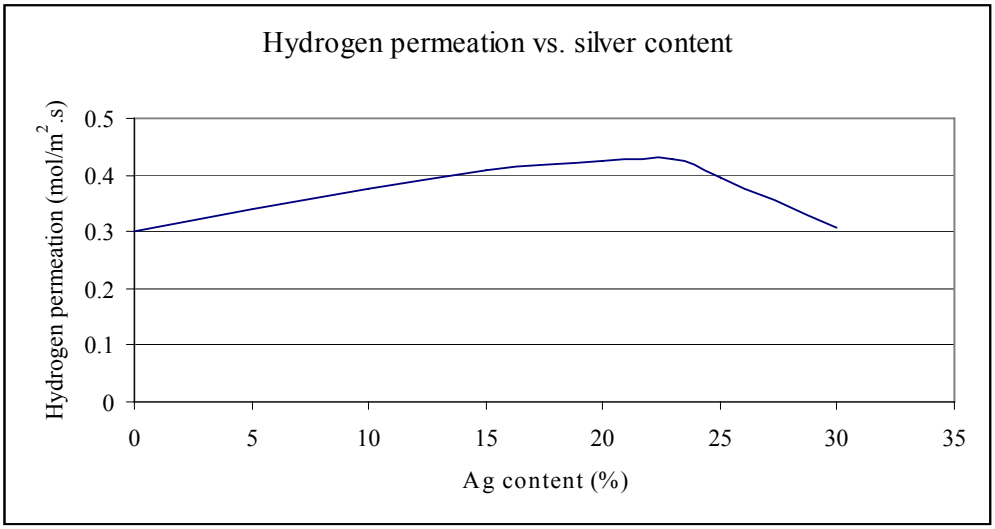

Figure 2.1 Hydrogen permeation through palladium-silver as a function of silver content (Uemiya, 1991a)

Figure 2.1 shows that the rate of hydrogen permeation increased with silver content and reached a maximum at 23 wt % of silver. These results were in agreement with those reported for palladium-silver alloy membranes thicker than 100 microns (Holleck, 1970; Goto, 1970).

The applications of palladium membrane reactors can be separated into three possible situations:

i) to feed hydrogen to the reactants for hydrogenation or hydrogenolysis reactions (Uemiya, 1991a&b),
ii) to extract hydrogen from the products of dehydrogenation or dehydrocondensation reactions (Shu, 1991; Jayaraman, 1995), and
iii) to transfer hydrogen from a compound which is dehydrogenated on one side of the membrane to another compound which is hydrogenated on the other side of the membrane (Buxbaum, 1993; Itoh, 1997).

2.4.1 Hydrogenation

For this kind of reaction, hydrogen forms part of the feed. When hydrogen and the reactants are co-fed into a reactor (**Figure 2.2**), they will compete for adsorption sites on the catalyst and the conversions reached will be limited by the mass transfer resistance of the catalyst. The concentration of hydrogen will be much lower in the adsorbed layer if hydrogen permeates through a membrane as shown in **Figure 2.3**. Thus, the hydrogenation rate per unit surface area is often much higher for **Figure 2.3** than that in the situation where hydrogen and the reactant contact the same surface (**Figure 2.2**).

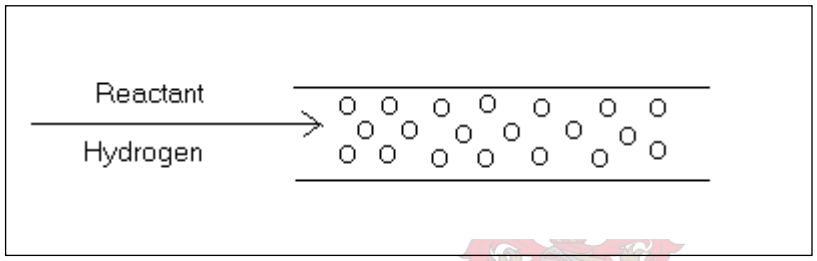

Figure 2.2 Hydrogen and the reactants co-fed into a reactor

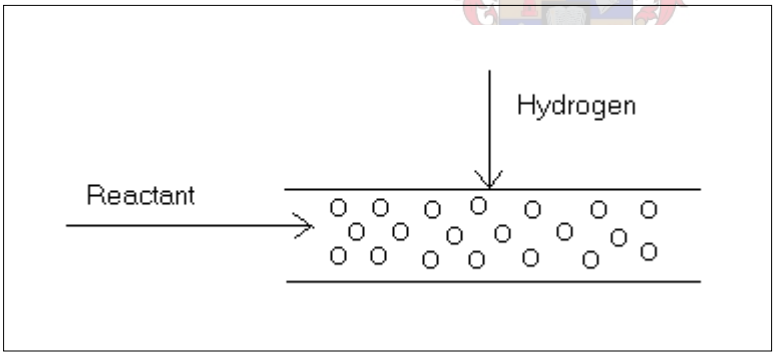

Figure 2.3 Hydrogen permeating through a membrane

In the chemical and pharmaceutical industries the selectivity in hydrogenation is very important. Hydrogenation is usually done in the liquid phase (Shu, 1991) and it involves the dissolution of hydrogen in the reactant. An advantage of the membrane reactor is that the only transfer of hydrogen is through the membrane. The dissolution of molecular hydrogen into the solvent is not necessary. This process has been successfully introduced into the production of chemicals (Gryaznov and Smirnov, 1974) and pharmaceuticals (Gryaznov, 1986), where the liquid phase operation is usually utilised. This technique can

avoid the difficult separation of products and excessive H_2 and reduce contamination of the residual catalyst by unwanted side reactions (Shu, 1991).

2.4.2 Dehydrogenation

The dehydrogenation of hydrocarbons is endothermic and the equilibrium constants increase with temperature. At low temperatures, the dehydrogenation conversion is low due to the equilibrium restrictions. Selective permeation of hydrogen through a membrane will displace the equilibrium and increase the conversion. High purities of hydrogen can be obtained on the permeation side of the membrane or hydrogen can be used to perform other reactions.

Dehydrogenation of paraffins or cycloparaffins of more than six carbon atoms is industrially important leading to valuable aromatic hydrocarbons (Wood, 1968). Shindo et al. (1989) obtained a benzene yield of close to 100% from the dehydrogenation of cyclohexane over a Pd-23 wt % Ag membrane at 200 °C. It is much higher than the equilibrium conversion of only 18.2% at 200 °C. This is due to the continuous removal of hydrogen produced in the reaction by permeation through the palladium-based membranes. On the negative side, high conversions in the membrane reactor usually occur at low feed flow rates, which results in low reaction rates.

2.5 General modelling principles applied to cyclohexane dehydrogenation

Kokugan et al. (1998) discussed the performance of membrane reactors for the dehydrogenation of cyclohexane.

$$C_6H_{12} \surd C_6H_6 + 3H_2 , \quad \Delta H = 206.2 \text{ kJ/mol} \qquad (2.1)$$

The rate of the *i*-th component flowing through the reaction side of a membrane reactor can be expressed by following equation:

$$\frac{d\left[\frac{F_i}{F_o}\right]}{d\left[\frac{L}{L_o}\right]} = \frac{L_o \cdot r_i}{F_i} - \frac{A_r \cdot J_i}{F_i \cdot S} \tag{2.2}$$

The performance of the membrane reactor will depend on the reaction rate term (the first term of the right hand side) and the flux of the component leaving the reaction side (the second term of the right hand side.)

The relation between the rates of reaction of each component is given by:

$$r_H = 3r_B = -3r_C \tag{2.3}$$

The reaction rate for the dehydrogenation of cyclohexane over Pt/Al_2O_3 can be expressed as follows (Itoh et al., 1988)

$$r_C = \frac{k_C\left[\frac{K_{eq}P_C}{P_H{}^3} - P_B\right]}{1+\left[\frac{K_B K_{eq} P_C}{P_H{}^3}\right]} \tag{2.4}$$

In **equation (2.4)** the units of K_{eq} is Pa^3.

2.5.1 Permeability of gases

The hydrogen flux through dense Pd films can be expressed by Sievert's Law:

$$J_H = d(P_H{}^n) \times \frac{P_{er}}{l} \tag{2.5}$$

$$P_{er} = D \times S \tag{2.6}$$

For microporous membranes with Knudsen diffusion pores (2-40 nm) the permeate flux of the *i*-th component can be expressed by the Knudsen diffusion equation:

$$J_i = k_{Knud} \times \frac{dP_i}{l} \tag{2.7}$$

$$k_{Knud} = a_i \times \frac{4\varepsilon d_M}{4\tau\sqrt{2\pi RTM_i}} \tag{2.8}$$

2.5.2 The effect of the Damkohler number on conversion

The Damkohler number (*Da*), which represent the extent of the reaction, is defined by:

$$Da_i = \frac{k_i L_o P_t}{F_i} \tag{2.9}$$

The units of *k* in **equation (2.9)** are mol/m.s.Pa. Experiments performed by Kokugan et al. (1998) showed that the conversion increased with an increasing *Da* number. As defined by **equation (2.9)**, the increase in *Da* number means an increase in residence time. Both *Da* and the residence time increases with a decrease in flow rate (F_i). The time the atoms spent in the reactor is called the residence time of the atoms in the reactor. This is also true for conventional fixed-bed reactors. This effect of increasing *Da* on conversion in a membrane reactor is almost negligible.

2.6 The dehydrogenation of 2-propanol

Industrial 2-propanol dehydrogenation processes are performed over heterogeneous catalysts above 300 °C, since the change in the standard Gibbs free energy becomes negative at high temperatures.

$$C_3H_7OH \square CH_3COCH_3 + H_2 \tag{2.10}$$

(P) (A) (H)

According to Langmuir-Hinshelwood mechanisms, there are three consecutive steps which can be rate limiting for the dehydrogenation of 2-propanol, namely: adsorption, surface reaction and desorption. The corresponding equations obtained by Jeylakshmi et al. (1990) are given below:

Adsorption:

$$r = k \frac{P_P - \left[\frac{P_A P_H}{K_{eq}}\right]}{1 + \left[\frac{K_P P_A P_H}{K_{eq}}\right] + K_A P_A + K_H P_H} \tag{2.11}$$

Surface reaction:

$$r = kK_P \frac{P_P - \left[\frac{P_A P_H}{K_{eq}}\right]}{(1 + K_P P_P + K_A P_A + K_H P_H)^n} \tag{2.12}$$

In **equation 2.12** the units for k are mol/m^3.s.

Desorption:

$$r = kK_{eq} \frac{\left[\frac{P_P}{P_A}\right] - \left[\frac{P_H}{K_{eq}}\right]}{1 + K_P P_P + K_A P_A + \left[\frac{K_{eq} K_H P_P}{P_A}\right]} \tag{2.13}$$

Jeylakshmi et al. (1990) showed that the reaction followed first order kinetics and the dual site surface reaction was found to be rate controlling.

The dehydrogenation of 2-propanol can be catalysed with different catalysts. The dehydrogenation of 2-propanol over zinc oxide was investigated by Teichner et al. (1967), who concluded that the dissociation of the methine C-H bond is rate determining. Krylov (1970) later discussed the reaction mechanism according to different catalysts. The dissociation of 2-propanol into isopropoxide and hydrogen surface species on zinc oxide, followed by enforced desorption of acetone with the absorbed isopropoxide species, was revealed by Tamaru et al. (1980).

Kemball et al. (1960) studied the desorption process of 2-propanol from the zinc oxide surface at temperatures of up to 300 °C. If the hydrogen was immediately removed from the reaction medium, the reaction could proceed at low temperatures for example 82 °C.

Aramendia et al. (1996) studied the dehydrogenation of 2-propanol over magnesium oxides. The dehydrogenation of the alcohol was found to follow first-order kinetics described by the Basset-Habgood equation (see Aramendia, 1996). The activation energies for 2-propanol dehydrogenation with magnesium oxide catalysts were calculated from the Arrhenius **equation (2.14)**.

$$k = A\exp\left[\frac{-E_a}{RT}\right] \qquad (2.14)$$

where k is the kinetic constant, A is the pre-exponential factor, R is the gas constant, T is the temperature and E_a is the activation energy. The results obtained are shown in **Table 2.5** (Aramendia et al., 1996). The different catalysts were produced from $Mg_5(OH)_2(CO_3)_4{\cdot}H_2O$ and $Mg(OH)_2$, namely MgO(I)AIR, MgO(I)VAC and MgO(II)AIR. They were calcined either in air or in a vacuum.

Table 2.5 Pre-exponential factors (ln A) and Activation Energies (E_a) obtained from the Arrhenius equation for the dehydrogenation of 2-propanol (Aramendia et al., 1996)

Catalyst	E_a (kJ/mol)	ln A
MgO(II)AIR	18.56±1.15	-4.91±0.34
MgO(I)VAC	17.95±2.02	-4.89±0.25
MgO(I)AIR	27.36±1.7	-5.21±0.63

2.7 Catalysts

2.7.1 Copper on γ-alumina

In recent years, copper-based catalysts have attracted considerable interest because of their selective properties in reactions involving hydrogen. The water shift reaction and the synthesis of methanol use catalysts that contain copper. Pepe et al. (1985) studied the decomposition of 2-propanol. They investigated the activity and selectivity towards dehydrogenation as a function of the copper concentration and oxidation state. Copper on alumina catalysts have to be pre-treated and conditioned before use. **Figure 2.4** (Pepe et al., 1985) illustrates the various conditioning treatments in a schematic way. The freshly prepared catalysts calcined in air are denoted as state 1. Results that were obtained from these catalysts are as follows:

The γ-Al_2O_3 support exhibited only dehydrating activity in the temperature range 443-523 K. At about 500 °C, the conversion was 100%. The copper containing samples exhibited dehydrogenating activity below 443 K and dehydrogenating and dehydrating activity above 443 K. It was confirmed that oxidation and reduction treatments did not produce variations in either activity levels or selectivity.

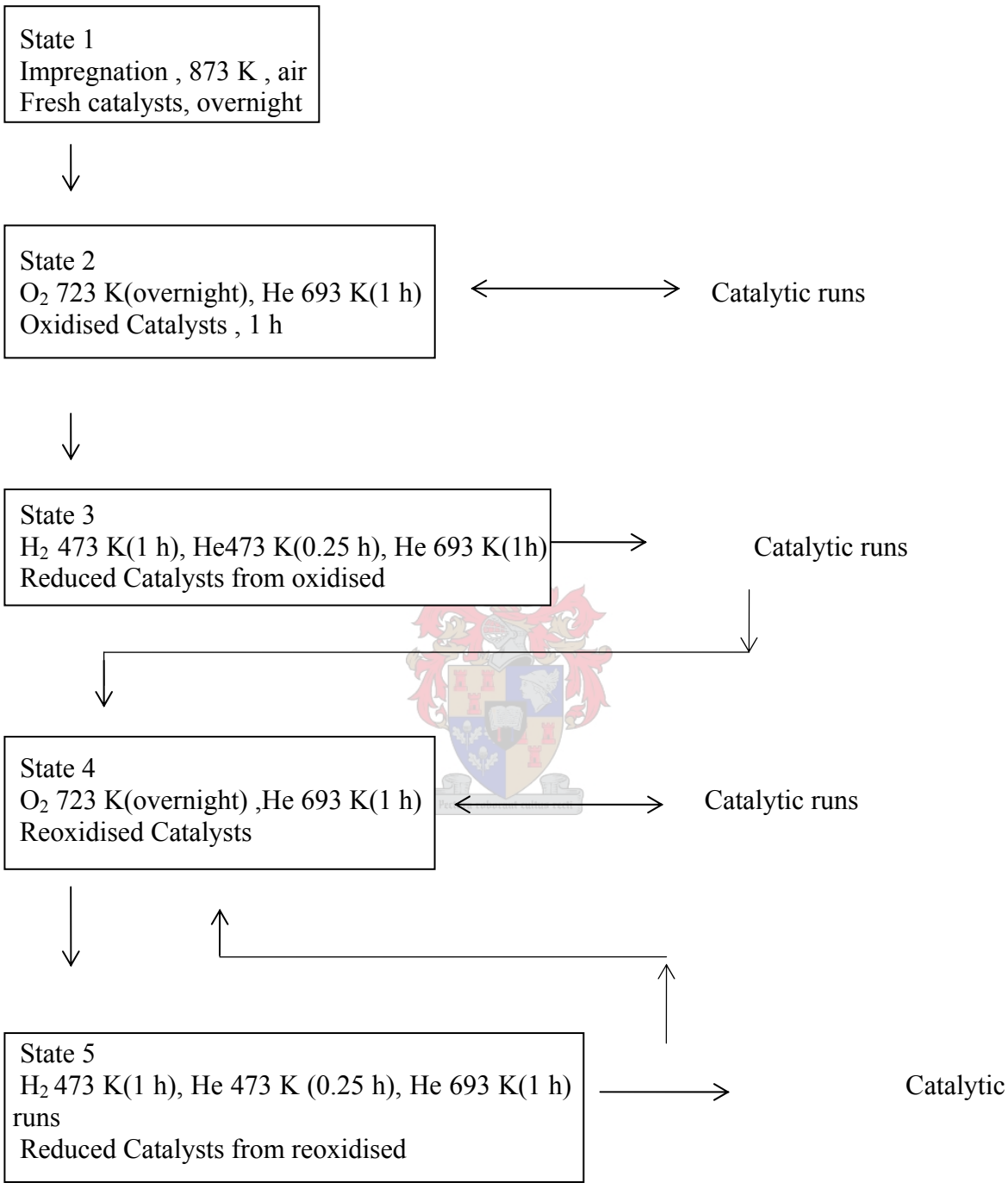

<u>Figure 2.4</u> Scheme of pre-treatments and catalytic sequence

Results also showed that reduction treatments provoked an increase in the dehydrogenation activity. The increase depended on the copper concentration and the history of the sample. It could be deduced that Cu(0) and Cu(I) were responsible for the large difference in activity between oxidised and reduced samples. The activities of the oxidised samples could be explained due to the presence of a small concentration of Cu(0). It can be noted that:

(i) there was an increase in activity under reaction conditions of the deoxidised copper on γ-Al_2O_3,
(ii) oxygen exerted a poisoning effect, and
(iii) the values of E_a for oxidised and reduced samples were comparable.

It was concluded that the Cu(0) species was the only one responsible for the dehydrogenation (Pepe et al., 1985).

2.7.2 Copper on α-alumina catalysts

In recent years, the catalytic dehydrogenation of cyclohexanol has gained much importance. Sivaraj et al. (1988) reported results for the dehydrogenation of cyclohexanol to cyclohexanone over Cu-ZnO-Al_2O_3 catalysts, prepared by a deposition precipitation method. Chang et al. (1993) investigated the performance of copper/α-alumina catalysts for the dehydrogenation of cyclohexanol.

An electroless copper plating method, a precipitation method and an impregnation method were used in the preparation of the Cu/α-Al_2O_3 catalysts. The effects of the different preparation methods on the dehydrogenation of cyclohexanol were investigated. The dehydrogenation reaction of cyclohexanol is:

$$C_6H_{11}OH \rightarrow C_6H_{10}O + H_2 \qquad (2.15)$$

$$-r_A = kP_H \qquad (2.16)$$

which is pseudo first order.

Results from Chang (1993) showed that the dehydrogenation activity increased as the copper loading increased up to a certain limit and then declined with further copper loading. The selectivity to cyclohexanone also increased as the copper loading increased up to a certain limit, then decreased as the copper loading increased for the catalysts prepared by the impregnation method. The selectivity stayed almost constant for the catalysts prepared by the electroless plating method. The selectivity was poor for the catalysts prepared by the precipitation method. Results showed that the catalysts prepared by the electroless plating method performed the best.

2.7.3 Magnesium oxides

The dehydrogenation and the dehydration of 2-propanol can also be performed over magnesium oxide catalysts.

Isothermal gas-phase reactions were used by Aramendia et al. (1996) to calculate kinetic data for the dehydration-dehydrogenation of 2-propanol in the temperature range 200 to 500 °C. The magnesium oxides used by Aramendia et al. (1996) were prepared from two different precursors, namely:

(a) $Mg_5(OH)_2(CO_3)_4 \cdot H_2O$, which produced MgO(I)AIR and MgO(I)VAC, and
(b) $Mg(OH)_2$ which produced MgO(II)AIR.

These were obtained from calcination in a ceramic crucible, either in air or in a vacuum (hence AIR and VAC), by heating from room temperature to 600 °C at a rate of 4 °C/min and then keeping the support at the final temperature for 2 hours.

A quartz reactor was used which had a length of 20 cm and an inner diameter of 1 cm. It was placed inside a furnace with a temperature controller which adjusted the temperature

to within 1 °C. A new and unused catalytic bed was used for every isothermal reaction and a nitrogen stream, flowing at a rate of 120 ml/min, was used as the carrier gas. The reactant (2-propanol) was injected at a controlled rate of 12 ml/min. The catalyst mass used was 50 mg, the temperature stabilisation time 20 minutes and the reaction time 150 minutes in every case.

Table 2.6 shows the conversion of 2-propanol to acetone (dehydrogenation) and propene (dehydration) obtained with all the catalysts tested after a reaction time of 60 min. **Table 2.6** reveals the effect of in vacuo calcination. MgO(I)AIR had a very low dehydrogenation activity relative to MgO(I)VAC. The better performance of the vacuum-calcined solid, MgO(I)VAC, in the dehydrogenation reaction could be ascribed to its higher surface basicity relative to the air-calcined solid.

Table 2.6 Conversion of 2-propanol to acetone using MgO catalysts (Aramendia et al., 1996)

	T (K)													
	200		250		300		350		400		450		500	
Catalyst	X_A	X_{PR}	X_A	X_{PR}	X_A	X_{PR}	X_A	X_{PR}	X_A	X_{PR}	X_A	X_{PR}	X_A	X_{PR}
MgO(II)AIR	9.5	10.8	11.3	12.2	13.9	13.4	15.5	11.7	21.4	10.1	28.5	9.4	36.7	8.6
MgO(I)VAC	9.2	10.7	11	11.4	12.7	11.3	15.5	10.8	20.4	8.7	24.4	7.7	31	7.1
MgO(I)AIR	5.3	5.9	5.7	5.8	6.4	6.2	7.7	6.3	12.3	7.2	17.5	6.6	22.1	5.9

2.7.3.1 Influence of temperature on the selectivity

The selectivity towards acetone (S_A) and propene (S_{PR}) was calculated from the following equations:

$$S_A = \left[\frac{\% \, conversion \, acetone}{\% \, total \, conversion} \right] \times 100 \qquad (2.17)$$

$$S_{PR} = 100 - S_A \qquad (2.18)$$

S_A increased and S_{PR} decreased with an increase in temperature for all the magnesium oxide catalysts. It could be explained bearing in mind that the dehydration is widely accepted to take place via acid sites and the dehydrogenation through basic sites (Aramendia et al., 1994; Aramendia et al., 1995). The number of basic sites (those favouring dehydrogenation) increased, whereas the number of acidic sites (those responsible for dehydration) decreased with increasing temperature. The result was an increase in S_A and a decrease in S_{PR}, respectively.

2.7.4 Amorphous Cu-Ti and Cu-Zr alloy catalysts

The development of the melt quenching method led to amorphous alloys becoming available from the beginning of the 1980s and a large number of studies have reported on their unique physical properties (Katona et al., 1990). These alloys exhibited very good catalytic properties in many cases. Katona et al. (1990) studied the dehydrogenation of 2-propanol over $Cu_{61}Zr_{39}$ catalysts. Results showed that the amorphous alloy catalyst had higher catalytic activity than the crystalline catalyst used for comparison. Cu-Zr metallic glasses have been found to be excellent catalysts for the dehydrogenation of 2-propanol.

The dehydrogenation of 2-propanol occurred selectively to acetone at 573 K over Cu-Zr and Cu-Ti alloys. The formation of 4-methyl-2-pentanone, a condensation product of acetone, was detected only over Cu-Zr catalysts prepared from amorphous precursors. The selectivity of this by-product was always less than 5%. A small amount of propene was formed over Cu-Ti. The catalytic performances of Cu-Ti alloys were weaker than those of the corresponding Cu-Zr alloys. The activity vs. time-on-stream curves exhibited maxima during the first 5 hours of the run.

2.7.5 CaO and SrO

A comparative study of 2-propanol decomposition over CaO and SrO was done by Szabo et al. (1975). CaO and SrO were prepared by the same procedure from hydroxides purified by recrystallization from conductivity-water. Only dehydrogenation occurred on

each of these catalysts. The catalytic activity was measured in a flow microreactor combined with a Carlo-Erba gas chromatograph in a stream of pure nitrogen. Experiments were carried out at various temperatures and different partial pressures of the alcohol. **Table 2.7** shows the kinetic parameters of the reaction, determined from the relation $k = A.\ e^{-Ea/RT}.P^n$ (Szabo et al., 1975) with the units of k as $mol/m^3.s$.

Table 2.7 Kinetic parameters of 2-propanol decomposition (Szabo et al., 1975)

Catalysts	A ($mol.m^{-3}.s^{-1}\ Pa^{-1}$)	E_a ($kJ.mol^{-1}$)
CaO	6.17E4	156.1
SrO	8.91E3	135.9

The reaction order was zero in each case.

With CaO and SrO oxides, it was the acetone that adsorbed strongly to the catalyst, blocking a considerable amount of originally active surface (which itself is a smaller part of the total surface only). With other catalysts, such as MgO, it is usually the alcohol that adsorbs strongly to the active surface of the catalyst (Szabo et al., 1975).

2.8 Electroless plating

The electroless plating technique is based on the controlled autocatalysed reduction of metastable metallic salt complexes on target surfaces. Electroless metal deposition refers to the chemical deposition of an adherent metal coating on a conductive, semiconductive or non-conductive substrate in the absence of an external electric source. Palladium is usually used as a catalysing agent to provide catalytic nucleating centres on the substrate. After pre-treatment, the desired material can be deposited on the catalysed surface with a salt of the appropriate metal plus a reducing agent. Electroless plating has become commercially important for finishing steel, aluminium, copper, plastics and many other materials. In the field of electronic devices, the application of electroless plating is increasing rapidly. Major reasons for applying electroless plating in preference to electrolytic plating include:

- uniform deposits over irregular surfaces - many applications are related to this capability,
- direct plating on non-conductors,
- deposition on isolated metal areas,
- less porous, more corrosion-resistant deposits,
- unique deposit properties, and
- bulk plating and "semi-bulk" racking.

2.8.1 Electroless deposits

2.8.1.1 Ni-P plating

Ni and Ni-P alloys are very different from each other. The Ni-P alloy has many unique characteristics and advantages. This difference is due to the co-deposited phosphorus content in the electroless alloy that ranges from about 3 to 12 percent depending upon bath composition and operating parameters. The hardness of electroless Ni-P is about 500 to 600 kg/mm^2, which is harder than conventionally electrodeposited nickel. Hardness of the plated alloy can be increased by heat treatment. For example, the Ni-P alloy can be hardened to 1000 kg/mm^2 by heat treatment for 1 hour at 400 °C.

Several mechanisms have been proposed to explain the electroless nickel deposition process. Lukes (1964) proposed a hydride transfer theory represented by the following equation:

$$H_2PO_2^- + H_2O \xrightarrow{\text{catalytic surface}} HPO_3^- + 2H^- + H^- \qquad (2.19)$$

The hydride ion (H^-), on the catalytic surface, can react with available nickel ions by electron transfer to produce a nickel deposit and hydrogen gas:

$$2H^- + Ni^{2+} \longrightarrow Ni^0 + H_2 \qquad (2.20)$$

The overall reaction can be represented by:

$$2H_2PO_2^- + 2H_2O + Ni^{2+} \longrightarrow Ni^0 + H_2 + 4H^+ + 2H_2PO_3^{-2} \quad (2.21)$$

2.8.1.2 Copper plating

It was not until the mid-1950s that electroless copper plating was commercially used (Cahill, 1957). It was developed for the manufacture of plated-through-hole printed circuit boards. A fast electroless copper plating method was developed in the late 1960s (Schneble et al., 1967). This method produced more ductile and thicker films. By 1980, automated, analytically based replenishment controllers were used in many large volume production lines (Shipley, 1984).

Electroless copper baths in commercial use are formaldehyde based. The baths are usually operated at pH above 12 because the reduction potential of formaldehyde increases with alkalinity. To prevent copper hydroxide precipitation it is necessary to use a complexing agent. Commonly used complexing agents include Ethylenediaminetetraacetic Acid (EDTA), Quadrol and alkanolamines (Atkinson, 1964). Copper is deposited on the substrate surface by an oxidation-reduction reaction. The copper ion in the electroless copper plating solution diffuses to and is adsorbed at the nucleating centres of the substrate. Formaldehyde then reduces the copper ion to metallic copper. The further deposition reaction continues autocatalytically. This reaction can be represented by:

$$Cu^{2+} + 2HCHO + 4OH^- \xrightarrow{\text{Catalytic surface}} Cu^0 + H_2 + 2HCOO^- + 2H_2O \quad (2.22)$$

Chang et al. (1993) used a plating solution indicated in **Table 2.8** to plate alumina with copper. The following plating procedure was employed. The plating bath temperature was maintained at 70 °C and the pH was adjusted to 12.5, with constant agitation for 30 minutes. The plated alumina was separated by filtration and then washed several times with distilled water.

Saubestra (1959) also investigated the use of hydrazine, hypophosphite and hyposulfite as reducing agents. In his investigation it was concluded that these are good reducing agents for electroless copper deposition.

Table 2.8 The components and concentrations of a copper plating solution (Chang et al. 1993)

Component	Concentration
$CuSO_4 \cdot 5H_2O$	0.04 M
EDTA·4Na	0.08 M
HCHO	0.08 M
Pyridine	5 ppm

2.8.1.3 Palladium plating

Amine complexes such as $Pd(NH_3)_4(NO_3)_2$, $Pd(NH_3)_4Br_2$ or $Pd(NH_3)_4Cl_2$ can be used to deposit thin Pd films in the presence of a reducing agent, typically hydrazine or sodium hypophosphite. In 1959, Rhoda developed a process for the deposition of palladium by means of electroless plating. The tendencies for a homogeneous reduction of palladium ions and a high degree of solution instability were overcome by using the disodium salt of EDTA as a stabiliser. The plating solution employed by Rhoda, consisted of a palladium-amine complex, a reducer and a stabilising agent as basic ingredients. Palladium deposition occurs according to the following two simultaneous reactions:

anodic reaction:

$$N_2H_4 + 4OH^- \rightarrow N_2 + 4H_20 + 4e^- \quad (2.23)$$

cathodic reaction:

$$2Pd^{2+} + 4e^- \rightarrow 2Pd^0 \quad (2.24)$$

autocatalytic reaction:

$$2Pd^{2+} + N_2H_4 + 4OH^- \rightarrow 2Pd^0 + N_2 + 4H_2O \quad (2.25)$$

Frequently used substrates such as porous glass, ceramics and even stainless steel are not active enough to initiate this reduction reaction. The substrate needs to be modified by palladium nuclei in order to activate the surface and reduce the possible long induction period at the beginning of deposition. Shu et al. (1993) used the pre-treatment solutions in **Table 2.9**. Before deposition, the specimens were pre-treated by successive dipping in two activation solutions of Sn^{2+} and Pd^{2+} ten times at ambient temperatures, the compositions of which are reported in **Table 2.9**. Each dip lasted five minutes and was followed by rinsing under deionised water. Then they were dried at 120 °C. **Figure 2.5** (Shu et al., 1993) shows the amount of palladium deposited as a function of time on activated substrates compared with unactivated ones. For the unactivated ones, a long induction period was needed to initiate the reduction of palladium species. Only a short induction period was needed when the activated substrates were used.

Table 2.9 Composition of activation solution

Tin chloride solution	
$SnCl_2 \cdot 2H_2O$	1 g/l
HCl(37%)	1 ml/l
Palladium salt solution	
$Pd(NH_3)_4(NO_3)_2$	0.168 g/l
HCl(37%)	1 ml/l

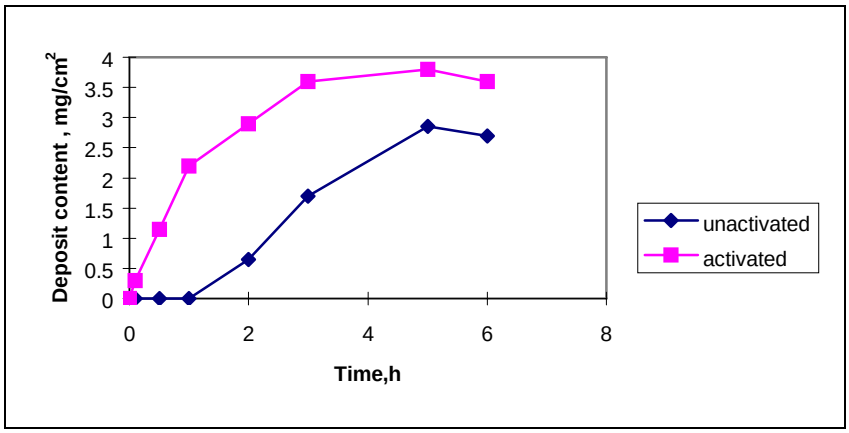

Figure 2.5 Palladium deposited as a function of time on activated substrates compared with unactivated ones (Shu et al., 1993)

Shu et al. (1993) plated porous stainless steel with palladium. They studied the plating procedure with SEM images. These images indicated that the deposition was essentially a growth process on the pre-deposited palladium nuclei. After half an hour of deposition, the palladium particles became about 5000 Å in diameter. A three hour deposition resulted in a relatively uniform palladium covered substrate. Li et al. (1996) used the plating bath composition in **Table 2.10** to deposit α-Al_2O_3 membranes with palladium.

Table 2.10 Palladium plating bath (Li et al., 1996)

Electroless plating bath	
$Pd(NH_3)_4Cl_2$	4 g/l
EDTA.2Na	67.2 g/l
$NH_3.H_2O$(28%)	350 ml/l
N_2H_4(0.1M)	50 ml/l
pH	11.2
Temperature	50 °C

2.8.1.4 Silver plating

Shu et al. (1993) used hydrazine as reducing agent for the plating of silver on porous stainless steel. Dilute silver solutions were used because EDTA has a small complexing ability for silver. The following reactions took place:

anodic reaction:

$$N_2H_4 + 4OH^- \longrightarrow N_2 + 4H_20 + 4e^- \quad (2.26)$$

cathodic reaction:

$$4Ag^+ + 4e^- \longrightarrow 4Ag^0 \quad (2.27)$$

overall reaction:

$$4Ag^+ + N_2H_4 + 4OH^- \longrightarrow 4Ag^0 + N_2 + 4H_20 \quad (2.28)$$

The electroless plating of silver must be initiated by palladium nuclei. **Figure 2.6** (Shu et al., 1993) compares silver deposition with and without activation of the substrate.

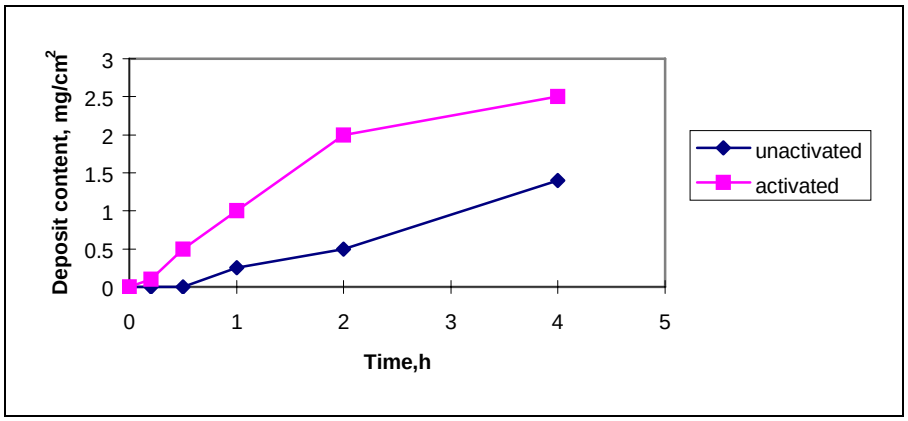

Figure 2.6 Silver deposited as a function of time on activated substrates compared with unactivated ones (Shu et al., 1993)

2.9 Hydrogen diffusion through palladium

The diffusion of hydrogen in Pd and Pd alloys is of great interest because of its fundamental importance as one of the best-defined examples of interstitial diffusion in transition metals. From a theoretical prospective, several other metals should be more permeable to hydrogen than palladium. These metals are not used for hydrogen extraction because, until recently, the experimental fluxes fell far short of the predicted values. Pd membranes are widely used for the separation and purification of hydrogen gas. The permeation of hydrogen through palladium can be described by the following three steps:

i) reversible chemisorption of hydrogen on the membrane surface,
ii) reversible dissolution of surface atomic hydrogen in the bulk layers of the metal, and
iii) diffusion of atomic hydrogen in the membrane.

Numerous authors (Silberg and Bachman, 1958; Holt et al., 1913; Lombard and Eichner, 1933a) have investigated the diffusion of hydrogen through palladium membranes with quite divergent results. Observations have generally been expressed in the form:

$$J = \frac{P_{er}}{l}\left[{P_{H,high}}^{n} - {P_{H,low}}^{n}\right] \qquad (2.29)$$

where J is the flow rate per unit surface area, P_{er} the permeability coefficient, l the membrane thickness, $P_{H,high}$ and $P_{H,low}$ the high and low pressure side of the membrane and n the pressure exponent. For hydrogen transport through a Pd membrane of several micron thickness, bulk diffusion is reported to be the rate controlling step (Lombard and Eichner, 1933b; Lewis, 1967). In the case of bulk diffusion limitations, the value of n has been calculated by many researches (Silberg and Bachman, 1958; Holt et al., 1913; Lombard and Eichner, 1933a; Lewis, 1967) and found to be about 0.5.

Takata and Suzuki (1993) have conducted exhaustive theoretical and experimental studies on hydrogen permeation through vanadium, showing a deviation from Sievert's law at low temperatures. Sievert's law can be expressed as follows:

$$C_H = k_S({P_H}^{n}) \qquad (2.30)$$

Probably the least understood mechanism is the transport of hydrogen through ultrathin palladium and palladium based alloy membranes (thickness < 2 μm). Hydrogen permeates through palladium films via a solution-diffusion mechanism. For very thin films, hydrogen adsorption and desorption (and not diffusion) will become more rate limiting.

Pure palladium membranes cannot be used below a temperature of 298 °C in H_2 due to hydrogen embrittlement. Hydrogen embrittlement is a phenomenon in which dissolved hydrogen result in lattice expansions in the metal, eventually causing it to fracture on repeated pressure and temperature cycling. When a pure palladium membrane is operated below 298 °C in a hydrogen atmosphere, increasing the hydrogen concentration leads to reduction of membrane selectivity, since β-phase palladium hydride is formed under these conditions. The phase transformation from α to β hydride is accompanied by hydrogen embrittlement. This phase change leads to the development of pinholes and

consequently the selectivity for hydrogen separation is reduced. By alloying palladium with group 1b metals such as silver, the resistance of the film against embrittlement can be increased. Group 1b metals suppress the formation of the β-phase hydride. It has been reported that the addition of group 1b metals to palladium suppresses the formation of the β-phase hydride, that is, Pd alloys containing a group 1b metal of more than 30 wt % are not transformed from α- to β-phase at 0 °C (Axelrod and Makrides, 1964; Makrides, 1964; Goto, 1970).

Decreasing the film thickness can increase the permeation rate of hydrogen through diffusion limited Pd-Ag alloys. Because of the low mechanical strength of palladium foils, palladium foils cannot be reduced in thickness below about 50 µm. Plating thin Pd-Ag layers on several supports such as polymers or ceramics will provide mechanical strength to the film and thus very thin films can be prepared. Jayaraman et al. (1995) plated ultrathin (<500 nm) Pd-Ag alloys on a porous α-alumina disc with a γ-alumina top layer. The hydrogen and nitrogen permeation rates were determined from experimental measurements. **Figures 2.7 to 2.9** from Jayaraman et al. (1995) show the hydrogen and nitrogen gas permeances at different temperatures as a function of average pressure across the composite membrane.

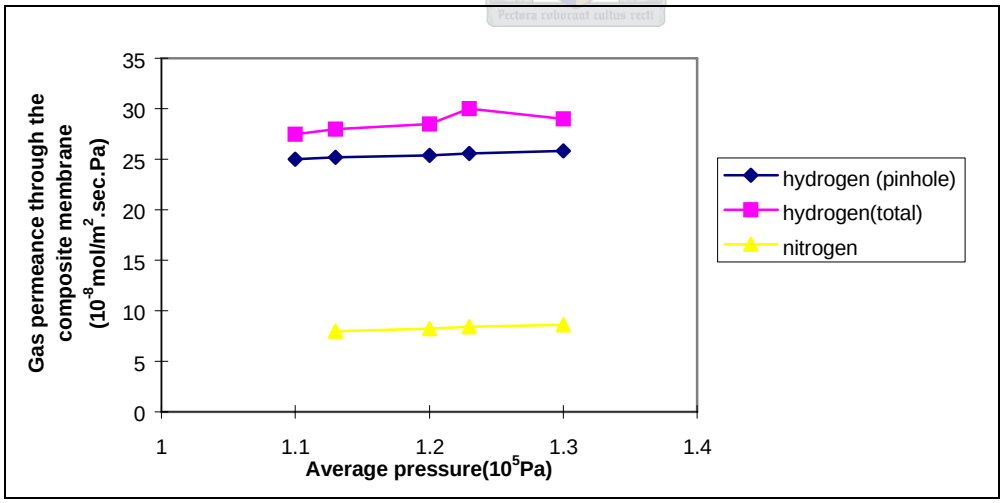

Figure 2.7 Gas permeance as a function of the average pressure across the membrane at a temperature of 100 °C. The hydrogen flow through the pinholes is also calculated and represented.

The total hydrogen permeance in **Figure 2.7** at an average pressure of 1.2×10^{5} Pa is 28×10^{-8} mol/m^2.s.Pa. The total hydrogen permeance in **Figure 2.9** (which is at a higher temperature) at an average pressure of 1.2×10^{5} Pa is 14×10^{-8} mol/m^2.s.Pa. This is much lower than the hydrogen permeance at the lower temperature. According to the Arrhenius equation (**equation 2.14**) the hydrogen permeance through thick solid films should increase with increasing temperature. According to Knudsen diffusion theory (**equation 2.7**) the hydrogen permeance should decrease with increasing temperature. This suggests that Knudsen diffusion occurred and that the hydrogen mainly permeated through defects in the film and not through the solid film.

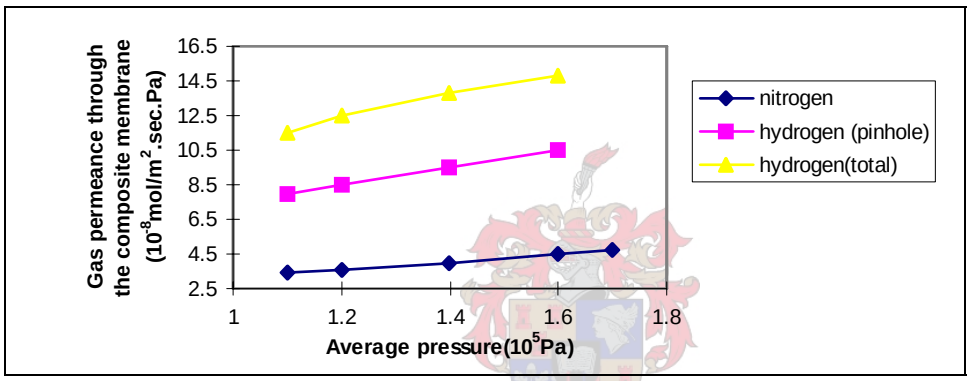

Figure 2.8 Gas permeance as a function of the average pressure across the membrane at a temperature of 200 °C. The hydrogen flow through the pinholes is also calculated and represented.

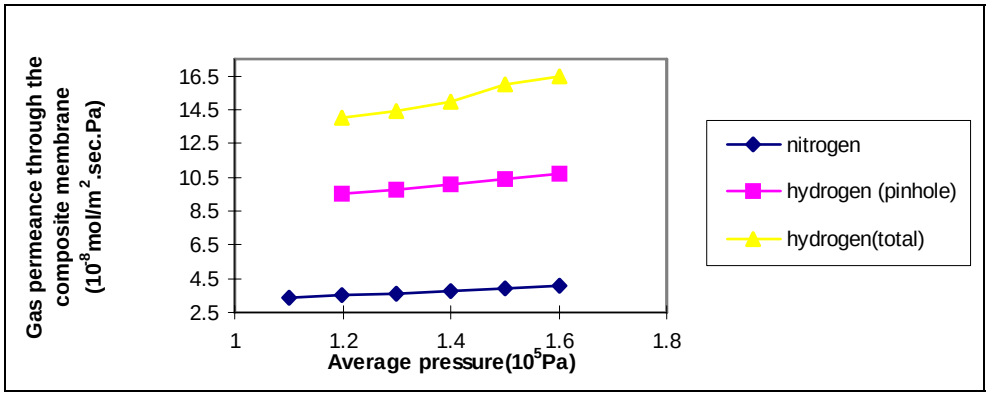

Figure 2.9 Gas permeance as a function of the average pressure across the membrane at a temperature of 250 °C. The hydrogen flow through the pinholes is also calculated and represented.

In **Figures 2.8** and **2.9**, both the gas flows increased with increasing pressure. There were some pinholes in the plated membrane. Due to those pinholes there was a notable flow of nitrogen gas through the membrane, resulting in lower selectivity. Since nitrogen gas permeates only through the pinholes and not through the Pd metal, the N_2 permeance is an indication of amount pinholes. The data were used to calculate the net hydrogen flow through pinholes at each temperature. The nitrogen permeance data were measured as a function of average pressure across the membrane, and fitted to the equation:

$$\frac{dJ}{d(\Delta P)} = \alpha_{av} + \beta_{av} P_{av} \tag{2.31}$$

where $dJ/d(\Delta P)$ equals the permeance per unit length, α_{av} is a measure of the Knudsen flow through the composite membrane, β_{av} is a measure of the viscous flow through the composite membrane and P_{av} is the average pressure across the membrane. The coefficients α_{av} and β_{av} are correlated to the gas properties and the membrane characteristics by the following equations:

$$\alpha_{av} = 1.06\left[\frac{1}{L_o}\right] v\left[\frac{\varepsilon}{\tau}\right](RTM)^{-0.5} \tag{2.32}$$

$$\beta_{av} = 0.125\left[\frac{1}{L_o}\right]\left[\frac{\varepsilon}{\tau}\right] v\left[\frac{v^2}{\mu RT}\right] \tag{2.33}$$

It can be seen that for a membrane with fixed dimensions (v,L_o) and at a given permeation temperature, α is inversely proportional to the square root of the molecular weight of the permeating gas. Consequently $\alpha(H_2)$ and $\beta(H_2)$ can be calculated using the formula:

$$\alpha(H_2) = \alpha(N_2) \cdot \left[\frac{M_{N_2}}{M_{H_2}}\right]^{-0.5} \tag{2.34}$$

$$\beta(H_2) = \frac{\beta(N_2)\mu(N_2)}{\mu(H_2)} \tag{2.35}$$

where ε and τ are the porosity and tortousity factors respectively, v is the average pore size of the composite membrane, T is the temperature in K, M is the molecular weight of the gas and μ is the viscosity of the gas. Jayaraman et al. (1995) used the values of $\alpha(H_2)$ and $\beta(H_2)$ to determine the extent of hydrogen gas flow through pinholes. Knowing the total hydrogen flow through the membrane and the hydrogen flow through the pinholes, the net hydrogen flow through the dense metal part could be calculated by

$$J_{H2(metal)} = J_{H2(total)} - J_{H2(pinhole)} \tag{2.36}$$

Equations (2.31) to **(2.36)** were obtained from Jayaraman et al. (1995). The hydrogen permeance in the investigation of Jayaraman et al. (1995) was found to be proportional to the hydrogen pressure. Jayaraman et al. (1995) concluded that the surface reaction played a dominant role in hydrogen permeance through ultrathin metallic films in the temperature range they investigated.

2.10 Permeability of acetone and 2-propanol vapours through a porous alumina membrane

The production of membranes with an average pore size in the region of 4 nm has been very successful. Such membranes can be used for high temperature gas separation in membrane reactors. Jia et al. (1994) studied the separation of a hydrogen-methanol mixture through ceramic-zeolite composite membranes. Separation factors of up to 1000 were obtained, which proved that the process could be used to recover solvents from industrial streams.

Keizer et al. (1988) impregnated silver into γ-alumina membranes to enhance the diffusion of oxygen and impregnated MgO into γ-alumina to enhance the diffusion of carbon monoxide. The fact that a membrane can serve as a separator and as a reactor can

be used to shift the equilibrium conversion. The performance of membrane reactors has been studied both by experiment (Assabumrungrat and White, 1998) and by computer simulation (Assabumrungrat and White, 1998). An accurate model describing the permeability rates of products and reactants can be solved using computer simulation. It is therefore important to develop models to describe the transport rate through membranes. Assabumrungrat and White (1998) studied the permeability of acetone and 2-propanol vapours through a porous alumina membrane with average pore diameter of 4 nm.

2.10.1 Modelling of the process

When surface diffusion becomes one of the rate limiting steps in gas transport through a porous membrane, the total gas flow rate per unit length of membrane can be expressed as the combination of flows from the gas phase and the adsorbed phase:

$$\left[\frac{F_i}{L_o}\right]_{total} = \left[\frac{F_i}{L_o}\right]_g + \left[\frac{F_i}{L_o}\right]_s, \tag{2.37}$$

where F_i is the molar flow rate of component i and L_o is the axial length of the membrane. The subscript g refers to the gas flow and s is the surface flow. The gas phase flow is the contribution of Knudsen diffusion and viscous bulk flow. The expression of the gas phase flow rate of component i per unit length of membrane was developed before (Assabumrungrat and White, 1996), for the case of a mixture between nitrogen gas and an alcohol vapour. Mathematically it can be expressed by:

$$\left[\frac{F_i}{L_o}\right]_g = \left[\frac{a(1-\omega)^3(P_{High}x_i - P_{Low}y_i)}{(M_iT)^{0.5}}\right] + \left[\frac{b(1-\omega)^4 x_i(P_{High}^{\ 2} - P_{Low}^{\ 2})}{2\mu T}\right] \tag{2.38}$$

$$\omega = \lambda_{alc}P_{High}x_{alc}(1+E_{alc}P_{High}x_{alc}) \tag{2.39}$$

and

$$\lambda_{alc} = \frac{2E'_{alc} V_{t\,alc}}{S_t d_o} \tag{2.40}$$

where a and b are Knudsen and viscous parameters. P_{High} is the feed side pressure, P_{Low} is the permeate side pressure , x_i and y_i are molar fraction of species i on feed side and permeate side, respectively, T is the operating temperature, E_i and E'_i are parameters in a Langmuir isotherm, d_o is the membrane pore diameter, μ is gas viscosity, V_t is the specific volume of the adsorbed phase and S_t is the membrane specific surface area. The subscript alc refers to alcohol. For the permeability of ethanol and methanol through the same membrane, it was found that the permeability at all temperatures were less than those predicted from the nitrogen gas permeability. It should be noted that **equations (2.37)** to **(2.40)** considered only the contribution of gas-phase flow and assumed that the blockage of membrane pores was the cause of change from the predicted values. **Table 2.11** (Assabumrungrat and White, 1998) presents the results of the two fitting parameters, λ and E.

Table 2.11 Fitting parameters of gas-phase flow model for the permeability of isopropanol (Assabumrungrat and White, 1998)

T(°C)	$\lambda\times10^6$(Pa^{-1})	E$\times10^6$(Pa^{-1})	Standard deviation
160	1	0	1.3×10^{-9}
180	0.8	0	3.4×10^{-9}
200	0.6	0	6×10^{-9}

Fick's law can be used as a model to describe the surface diffusion as follows:

$$J_{s,i} = \left[\frac{-\rho_{app} D_{s,i}}{\tau_s}\right] \cdot \left[\frac{dq_i}{dP_i}\right] \cdot \left[\frac{dP_i}{d(d/2)}\right] \tag{2.41}$$

and

$$D_{s,i} = D_{s,i}^{\,o} \exp\left[\frac{-E_{s,i}}{RT}\right] \tag{2.42}$$

where $J_{s,i}$ is the surface flux of species i, ρ_{app} is the apparent density of the membrane, $D_{s,i}$ is the surface diffusivity of species i, $D_{s,i}^{\,o}$ is a constant, $E_{s,i}$ is the activation energy of surface diffusion of component i, q_i is the amount of species i adsorbed, τ_s is the tortousity factor for surface flow and d_M is the membrane diameter. It is assumed that the surface diffusivity is constant within the Henry's law region. Henry's law in its most general form can be expressed by:

$$\hat{f}_i = x_i h_i \tag{2.43}$$

Equation (2.43) must be valid as $x_i \rightarrow 0$ and h_i is Henry's law constant for component i (Perry, 1984). By assuming that the adsorption isotherm follows Henry's law, the total surface flow rate through a cylindrical membrane $(F_i)_s$ is given by Fick's law model:

$$(F_i)_s = -\left[\frac{\pi d L_o \rho_{app} D_{s,i} E_i'}{\tau_s}\right] \cdot \left[\frac{d}{d(d/2)}\right] \cdot P_i \tag{2.44}$$

Integrating this equation with respect to the boundary condition that at distance $(d/2)_{in}$ (inner side of the membrane) the partial pressure is $P_{High}x_i$ and at distance $(d/2)_{out}$ (outer side of the membrane) the partial pressure is $P_{Low}y_i$ gives Fick's law model:

$$\left[\frac{F_i}{L}\right]_s = D_{F,i}(P_{High}x_i - P_{Low}y_i) \tag{2.45}$$

where

$$D_{F,i} = \frac{2\pi\rho_{app} D_{s,i} E_i'}{\tau_s \ln\left[\frac{d_{in}}{d_{out}}\right]} \qquad (2.46)$$

The total flow rate can then be calculated as follows by Fick's law model:

$$\left[\frac{F_i}{L}\right] = \left[\frac{a_{av}(1-\omega)^3 (P_{High} x_i - P_{Low} y_i)}{(M_i T)^{0.5}}\right] + \left[\frac{b_{av}(1-\omega)^4 x_i (P_{High}^{\ 2} - P_{Low}^{\ 2})}{2\mu T}\right] + D_{F,i}(P_{High} x_i - P_{Low} y_i) \qquad (2.47)$$

Assabumrungrat and White (1998) used **equation (2.47)** to fit experimental results of pure isopropanol vapour permeabilities and the fitting parameters of the Fick's law model are shown in **Table 2.12**.

Table 2.12 Fitting parameters with the Fick's law model for the permeability of isopropanol (Assabumrungrat and White, 1998)

T(°C)	$\lambda \times 10^6$ (Pa^{-1})	$D_F \times 10^8$ (mol/m.s.Pa)	Standard deviation
160	4	3	7×10^{-10}
180	3.3	2.8	7.5×10^{-10}
200	1.8	2	9.7×10^{-10}

2.10.2 The permeability of 2-propanol and acetone

The permeability of isopropanol vapour through the alumina membrane with pore diameter of 4 nm was measured at 160, 180 and 200 °C by Assabumrungrat and White (1998). The results are shown in **Figure 2.10** to **2.13**. The permeability at all temperatures were found to be less than those predicted from the nitrogen gas permeability experiments. The Fick's law model was checked with the results from the experiments with mixtures of isopropanol vapour and nitrogen gas. The results of the

predicted values and the measured values of the nitrogen-isopropanol mixture flow rate per unit length are plotted in **Figure 2.11** (Assabumrungrat and White, 1998).

Assabumrungrat and White (1998) performed permeability testing with pure acetone vapour at the same temperature levels as the tests done on the isopropanol vapour. The permeability results are given in **Figure 2.12**. The permeability of acetone at some data points was higher than predicted from the nitrogen permeability experiments. Assabumrungrat and White (1998) concluded that surface diffusion may be one of the transport mechanisms.

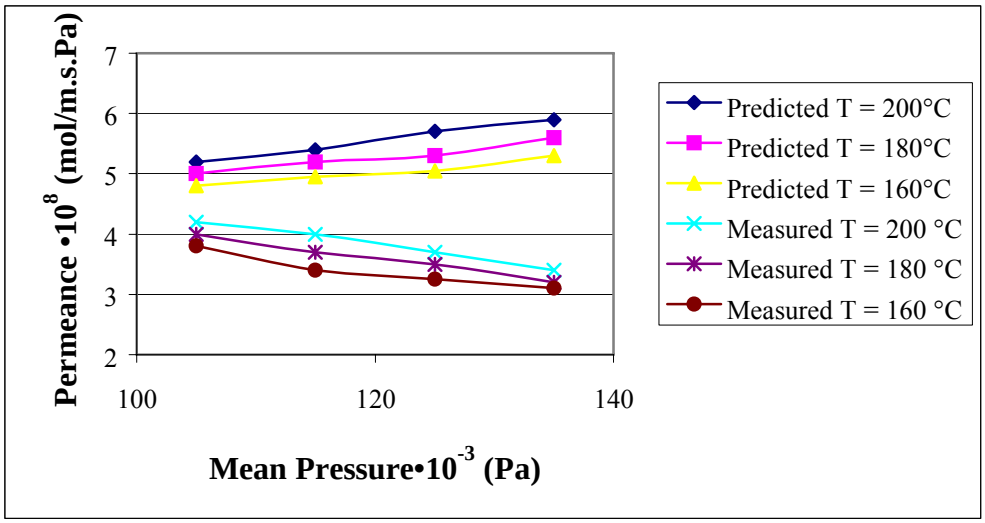

Figure 2.10 Permeability of pure isopropanol through the alumina membrane with 4 nm pore size (Assabumrungrat and White, 1998)

Assabumrungrat and White (1998) tested the model by doing experiments with mixtures of acetone and nitrogen gas as shown in **Figure 2.13.** The experimental and calculated values agreed to a large extent. At 160 °C, however, the deviation increased. Assabumrungrat and White (1998) concluded that this may be due to a deviation from Henry's law when the operating temperature is low.

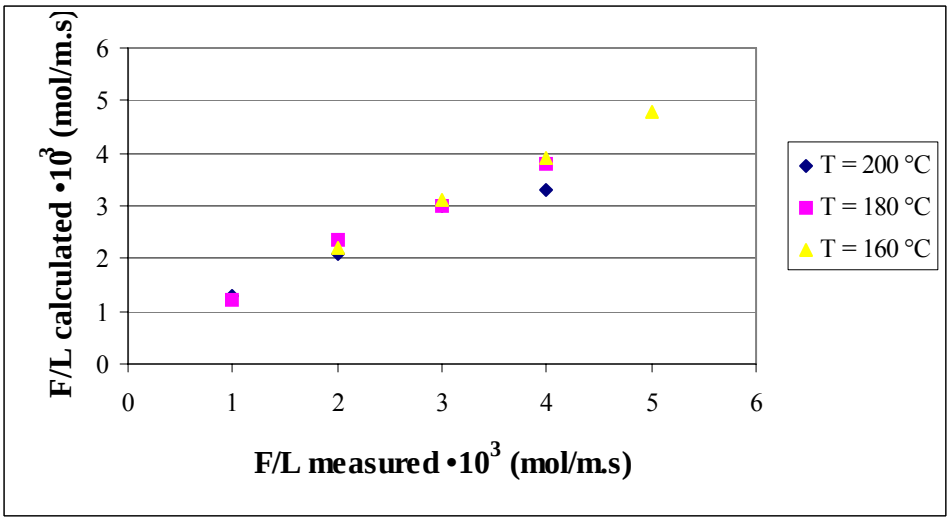

Figure 2.11 Experimental results of the flow rate per unit length of a nitrogen-isopropanol gaseous mixture through the membrane with 4 nm pore diameter (Fick's law model) (Assabumrungrat and White, 1998)

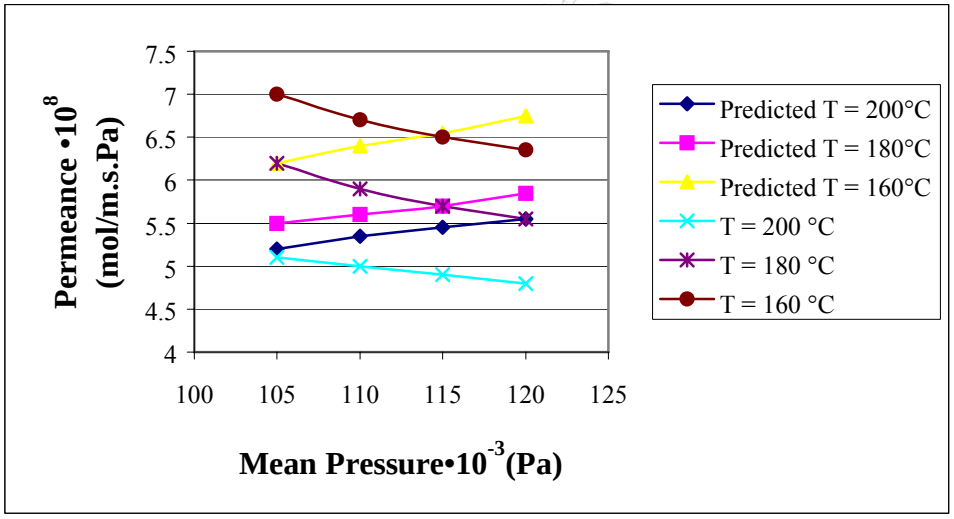

Figure 2.12 Permeability of pure acetone through the alumina membrane with 4 nm pore diameter(Assabumrungrat and White, 1998)

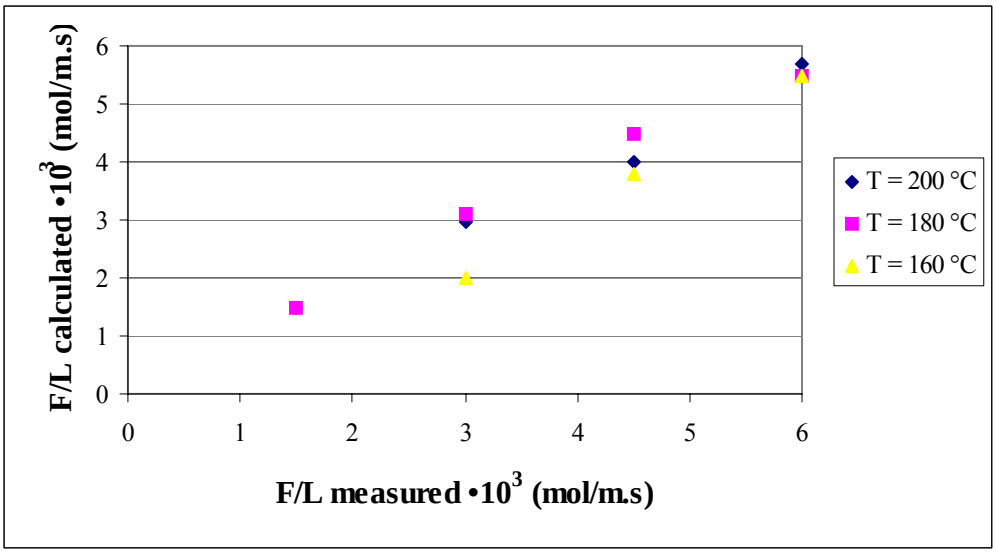

Figure 2.13 Experimental results of the flow rate per unit length of a nitrogen-acetone gaseous mixture through the membrane with 4 nm pore diameter (Fick's law model) (Assabumrungrat and White, 1998)

2.11 Summary

This chapter introduced the background for the remaining section of this thesis. Different membrane processes as well as different types of membranes were discussed. The theory and applications of electroless plating (a process to coat alumina membranes with different metals) was described. In this study α-Al_2O_3 membranes were plated with palladium. The usage of these type of membranes as catalytic membrane reactors for dehydrogenation and hydrogenation reactions was explained. Thereafter the appropriate catalyst to use for these type of reactions were presented. The embrittlement of palladium in a hydrogen atmosphere below 300 °C as well as hydrogen diffusion through palladium films were also explained.

3. Experimental Work

3.1 Introduction

In this chapter the experimental work will be discussed in detail. All of the experimental work, except the X-ray diffraction analysis (XRD), proton induced X-ray emission (PIXE) and scanning electron microscopy (SEM) experiments, was conducted at the Department of Chemical Engineering (University of Stellenbosch). The first part of the project focussed on building the membrane reactor setup. This setup was used for the dehydrogenation reactions, the heat treatments and the selectivity tests of the plated alumina membranes. A list of chemicals used in this study is found in appendix A.

3.2 Manufacture of catalysts

Al_2O_3, SiO_2 and MgO were used as supports. The supports were impregnated with different Cu percentages. The Al_2O_3 (product code, AL-3996 R) and the SiO_2 (product code, C500-234) were obtained from Engelhard, Chemical Catalysts Division, The Netherlands. $Cu(NO_3)_2{\cdot}3H_2O$ (purity > 99%; supplier: ACE) was used to impregnate the supports with copper. **Table 3.1** lists the different copper loadings investigated. The particle sizes of all the catalyst except those noted in **Table 3.1** were 850-1180 µm. The following equation was used to calculate the mass of $CuNO_3{\cdot}3H_2O$ needed to obtain the desired Cu % on the support.

$$Mass_{Cu(NO_3)_2\cdot 3H_2O} = \frac{Mass_{Support}}{\left[\frac{\%Cu + 1.5}{100}\right]} \cdot \frac{Mr_{Cu(NO_3)_2\cdot 3H_2O}}{Mr_{Cu}} \qquad (3.1)$$

The procedure for preparing 5 g of catalyst was:

- Pour 12 ml of warm distilled water in a container and heat the water to 90 °C,
- Slowly add the required amount of $CuNO_3{\cdot}3H_2O$ to the water until it is fully dissolved (stir the mixture while adding),

- Add the support particles in the container,
- Stir the mixture until all the water evaporated,
- Heat the mixture at 150 °C for 2 hours, and
- Oxidise the mixture at 475 °C for 5 hours.

Table 3.1 Different copper loadings investigated (Particle sizes = 850-1180 µm)

Alumina support	MgO support	Silica support
18.5% Cu	0% Cu	0% Cu
24% Cu	10.3% Cu	4.2% Cu
8.8% Cu	16.9% Cu	9.2% Cu
13.2% Cu	24.9% Cu	11.7% Cu
30.7% Cu		0% Cu
		9.2% Cu
		18.6% Cu
		27.7% Cu
		4.2% Cu
		11.7% Cu
		15% Cu
		9.2% Cu (150-300 µm)
		9.1% Cu (850-1180 µm)
		9.1% Cu (3 mm)

3.3 Catalytic investigation for the dehydrogenation of isopropanol

Figure 3.1 shows the reactor setup, which was used for the catalytic investigation of 2-propanol dehydrogenation to acetone. The 2-propanol was fed to the system with a Braun Perfuser VI syringe pump. Nitrogen was used as a carrier gas. The nitrogen flow rate was controlled by a Hastings flow controller (HFC 202C). A nitrogen to 2-propanol molar ratio of 4 to 1 was employed, with 2-propanol flow rates of 1.6, 3.2 and 6.4 ml/h.

Temperatures ranging from 240 to 390 °C were tested. One gram of catalysts was placed inside a quartz tube and the quartz tube was sealed inside a stainless steel reactor. The different catalysts listed in **Table 3.1** were used for catalytic testing. The inner and outer diameter of the quartz tube was 8 mm and 10 mm respectively. The reactor system was such that the N_2 and the 2-propanol flowed together to the reactor, which was heated with heating wire. Heating wires were also used to heat the exit lines to keep the products in the gas phase. The reactant mixture of 2-propanol and nitrogen passed through a 1 meter coil, which was placed in a pre-heating oven and connected to the inlet of the reactor. The pre-heating oven ensured that the reactant mixture entered the reactor at the reaction temperature. Gas samples were taken at the sample point. A heated syringe (120 °C) was used for taking the samples and injecting them into a GC. The products were analysed using a gas chromatograph (GS) with an electron ionisation detector. A capillary BP1-PONA column (50 m by 0.15 mm by 0.5 μmdf) was employed for analyses.

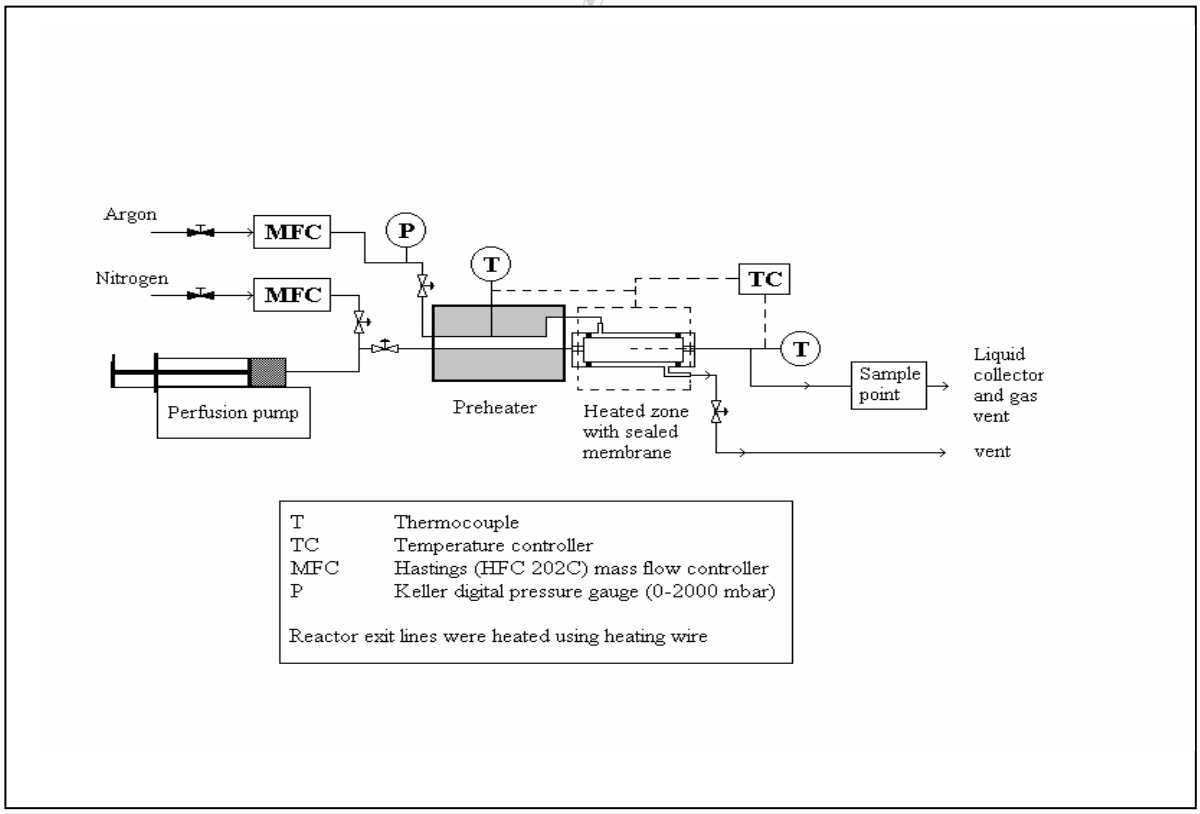

Figure 3.1 Reactor setup for catalytic testing

3.4 Electroless plating

3.4.1 Membrane pre-treatment

Two types of membranes were used in this study. The first type was purchased from Atech (Germany) and the second type purchased from SCT (Societé des Céramiques Techniques, France). The membranes with their different specifications are listed in **Table 3.2 to 3.4**. **Figure 3.2** shows the structure of membrane B. The 90 cm length membranes (A) were cut into sizes of 30 mm with a diamond saw. The 30 mm membrane A samples were then electroless plated and characterised using SEM, XRD and PIXE. The membrane B samples were electroless plated and used for dehydrogenation reactions in the membrane reactor.

Table 3.2 Specifications of membrane A (Atech)

Membrane A	
Pore diameter (nm)	100
Type	α-Al_2O_3
Outside diameter (mm)	10
Inside diameter (mm)	8
Length (cm)	90

Table 3.3 Specifications of membrane B (SCT)

Membrane B	
Type	α-Al_2O_3
Inside diameter (mm)	7
Outside diameter (mm)	10
Length (cm)	25

Table 3.4 Membrane layer characteristics of a SCT membrane (Membrane B) (Keuler, 2000)

	Pore diameter (μm)	Layer thickness (μm)
Layer 1	11	1500
Layer 2	0.64	40
Layer 3	0.2	20

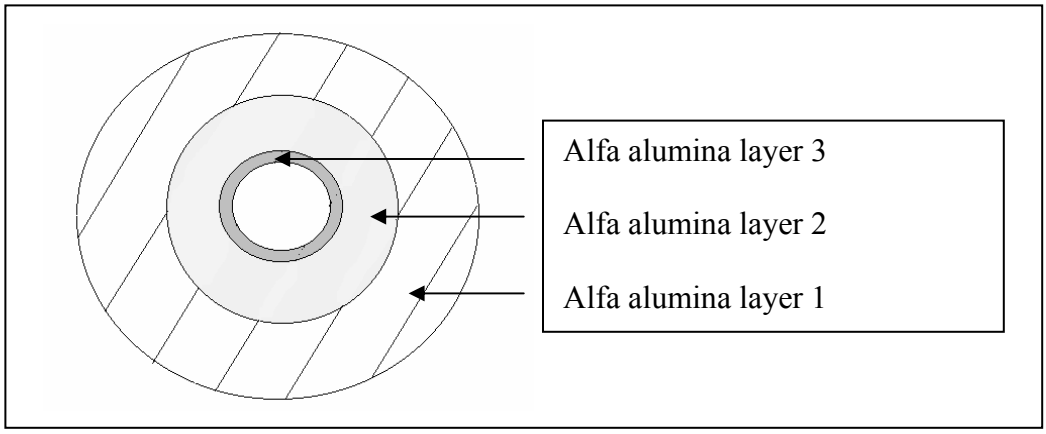

Figure 3.2 SCT membrane structure (Membrane B) (Keuler, 2000)

Table 3.5 Composition of pre-treatment solution used for surface activation

Tin chloride solution	
$SnCl_2 \cdot 2H_2O$	1 g/l
HCl(37%)	1 ml/l
Palladium salt solution	
$Pd(NH_3)_4(NO_3)_2$	0.168 g/l
HCl(37%)	1 ml/l

Table 3.5 shows the composition of the pre-treatment solution. Three cylindrical tubes, with diameter of 3 cm and length of 30 cm, were used for the pre-treatment of the alumina membranes. The tin chloride solution was poured into one tube, the palladium salt solution into another one and distilled water into the third tube. The outside surface of the membrane tubes was wrapped with PTFE tape. Only the inside of the membrane would then be catalysed. The clean membrane was first dipped into the tin chloride solution for two minutes then dipped into the distilled water for ten seconds and then dipped into the palladium salt solution for two minutes. This was repeated twenty times. After pre-treatment, the PTFE tape was removed from the membranes. The pre-treated membranes were stirred in distilled water for half an hour to remove residual solution in their pores. The set-up is shown in **Figure 3.3**. Finally, the membranes were dried

overnight at 200 °C. A uniform brown layer was deposited on the white alumina membrane supports after pre-treatment.

For testing of the membranes, it is important to obtain a good seal between the membrane and the reactor. The outside surface of the membrane was sealed with an enamel to prevent gas leakage between the membrane and a compression fitting (graphite ring). The enamel was supplied by SCT. Both ends of the membranes were dipped about 15 mm into an enamel slurry to coat that part of the membrane. The enamelled membranes were then cured by a procedure recommended by SCT as indicated in **Figure 3.4**. This was done in a high temperature furnace from Vecstar Furnaces. Two or three layers of enamel were applied on the membrane ends to obtain good sealing.

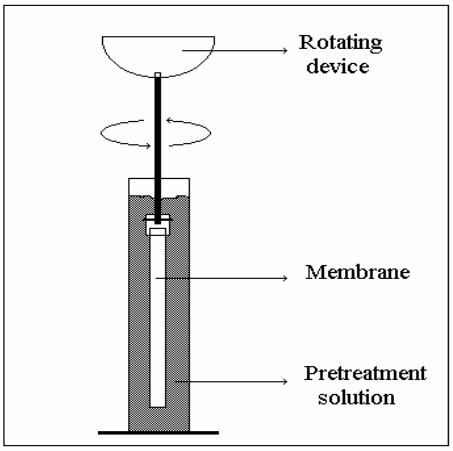

Figure 3.3 Stirrer used for cleaning pre-treated membranes (Keuler, 2000)

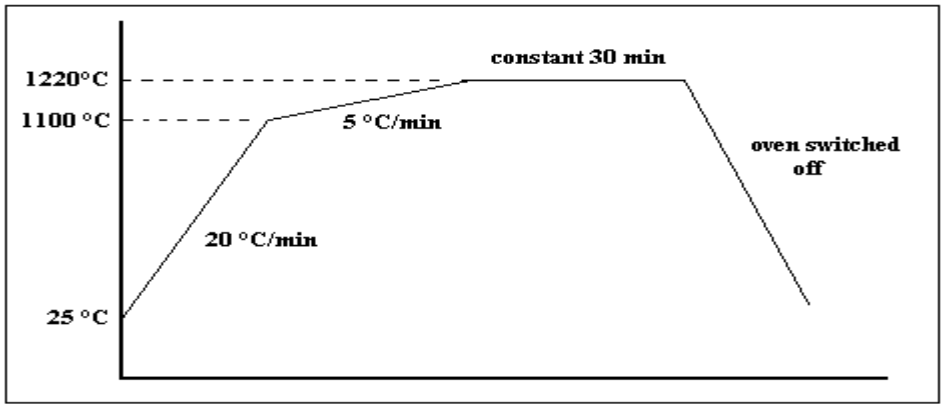

Figure 3.4 Curing process for enamelled membranes

3.4.2 Electroless palladium plating

The plating bath used in this study was based on a recipe developed by Collins (1993). The concentration of the disodium EDTA was doubled to improve bath stability at relatively high plating temperatures. A palladium amine complex was formed by adding ammonium hydroxide to acidified palladium chloride solution. **Table 3.6** shows the recipes used to prepare the complex solution and the plating bath.

Table 3.6 Plating bath recipe (Collins, 1993)

Solution description	Recipe
Plating bath	- add 1.75 g of disodium EDTA to 25 ml of Pd-ammine solution - allow solution to sit for at least two hours
$PdCl_2$ stock solution	- add 20 ml of concentrated HCl (37 wt %) to 980 ml of deionised H_2O - add 10 g of $PdCl_2$ to the acidic solution - allow solution to sit for several hours to dissolve the $PdCl_2$
Pd- ammine complex solution	- add 120 ml of deionised H_2O to 1000 ml of Pd stock solution - slowly add 715 ml of NH_4OH (28 wt % NH_3) - allow solution to sit for two to three days to redissolve precipitate - filter the clear solution

Two methods were used to determine the amount of palladium deposited on the membrane supports. The mass of the membrane to be plated was determined before and after plating. After plating refers to the mass after heat treatment of the membrane. The difference between the initial mass and final mass was taken as the amount of palladium deposited. The concentration of palladium in the palladium stock solution was

determined using atomic adsorption before and after plating. Since the initial mass of the plating solution was known, the mass of the deposited palladium could be calculated. With these values the thickness of the palladium film could be calculated.

The plating procedure was relatively simple. The membrane was sealed in a tubular teflon plating reactor that had two caps with ends that screwed onto the container. This container was placed inside a water bath, which was kept at a temperature of 71 °C. The plating setup is shown in **Figure 3.5**. Just before plating commenced, 5 ml of 0.04 M hydrazine was added to 60 ml of the palladium stock solution. The 60 ml of this plating solution was sucked into a syringe. The syringe was connected with tubing to the membrane inlet. About 12 ml of plating solution was introduced into the membrane tube to wet the entire inside surface. The solution was kept there for 10 minutes and 12 cm^3 of unused plating solution was pressed in again. After that, 12 cm^3 of plating solution was pressed in every 10 minutes until the syringe was empty. When the syringe was empty, the membrane was taken out of the teflon container, rinsed with deionised water and put back for further plating. One run was then completed.

Before starting with the second run, another 5 ml of 0.04 M hydrazine was added to the initial 60 ml solution. No more hydrazine was added for the next four runs. For both the seventh and the eighth runs, five drops of concentrated hydrazine (35% hydrazine) was added to the solution to reduce the remaining Pd ions. The whole procedure thus consisted of eight runs. **Table 3.7** lists how the hydrazine was added to the palladium solution.

Hydrazine is very hazardous, therefore special safety procedures were followed when it was handled. The hydrazine was used in a fume hood with an extractor fan, while wearing a respirator, lab coat and rubber gloves.

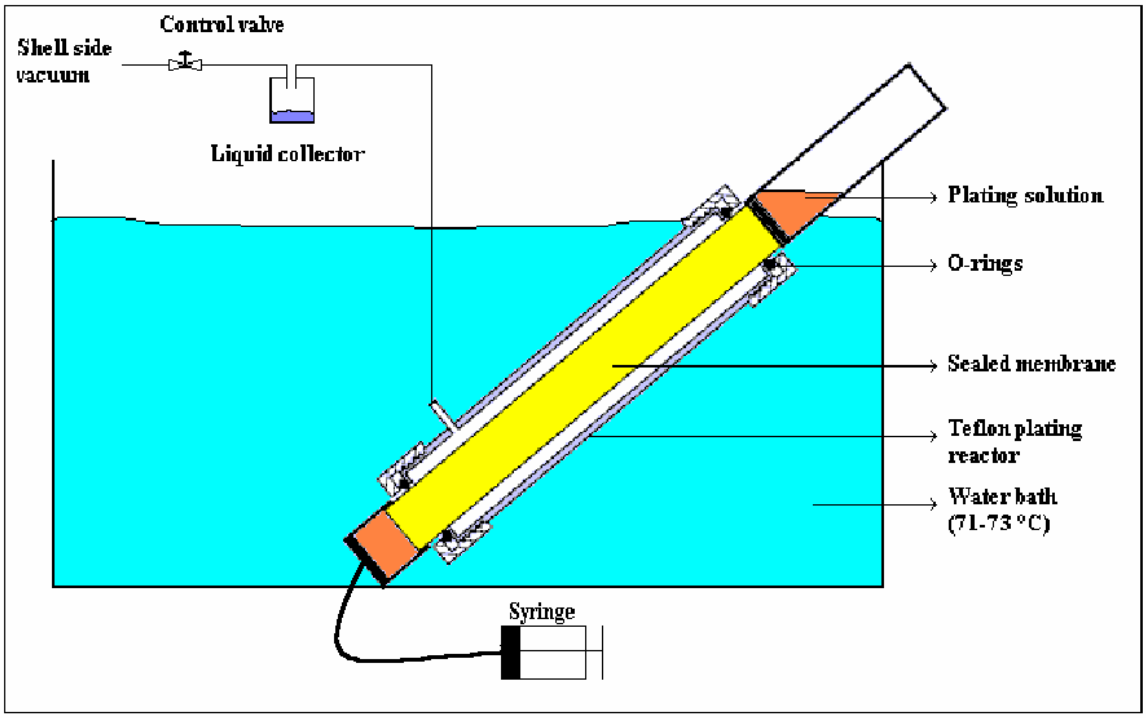

Figure 3.5 Electroless plating setup

Table 3.7 Plating procedure for producing Pd films

Run	Reaction time for 60 cm^3 plating solution (min)	Vol. 0.04 M hydrazine added for 60 cm^3 solution (ml)
1	50	5
2	50	5
3	50	0
4	50	0
5	50	0
6	50	0
7	50	5 drops of 35% hydrazine
8	50	5 drops of 35% hydrazine

3.4.3 Electroless copper plating

When preparing palladium-copper composite membranes, the palladium was first plated and then the copper. The same equipment used for the electroless palladium plating was used for the electroless copper plating. **Table 3.8** shows the plating bath composition. The amount of copper stock solution required to deposit a certain film thickness was calculated. Before plating commenced, 5 ml of 0.04 M hydrazine was added to every 60 ml of the copper stock solution. Again 60 cm^3 of the plating solution was sucked into the syringe and the same procedure followed as for the palladium plating. Before the second run, another 5 ml of 0.04 M hydrazine was added to the plating solution. However, in this case 1 ml of concentrated hydrazine (35%) was added before the third and fourth runs. Only four runs were performed. **Table 3.9** lists how the hydrazine was added to the copper solution.

Table 3.8 Copper plating bath composition

Solution description	Recipe
Plating bath	- add 10.2 g of disodium EDTA to 50 ml of copper stock solution - allow solution to sit for at least 6 hours - add 10 cm^3 concentrated hydrazine for every 50 ml of copper stock solution just before membrane is added to plating bath
Copper stock solution	- add 1.494 g $CuSO_4$ to 32.8 ml NH_3 (28%)

Table 3.9 Plating procedure used for producing Cu films

Run	Reaction time for 60 cm^3 plating solution (min)	Vol. 0.04 M hydrazine added for 10 cm^3 solution (ml)
1	50	5
2	50	5
3	50	1 ml concentrated hydrazine (35%)
4	50	1 ml concentrated hydrazine (35%)

3.5 Pd-Cu alloying

Permeabilities for palladium copper alloys have been reported by Shu et al. (1991). The permeability of a Pd-Cu membrane reaches a maximum value at 40 wt % Cu, as illustrated in **Figure 3.6**. At this composition the alloy forms an equilibrium phase having a bcc structure with a simultaneous increase in diffusivity by two orders of magnitude. The aim of this study was to produce a Pd-Cu alloy with 40% Cu.

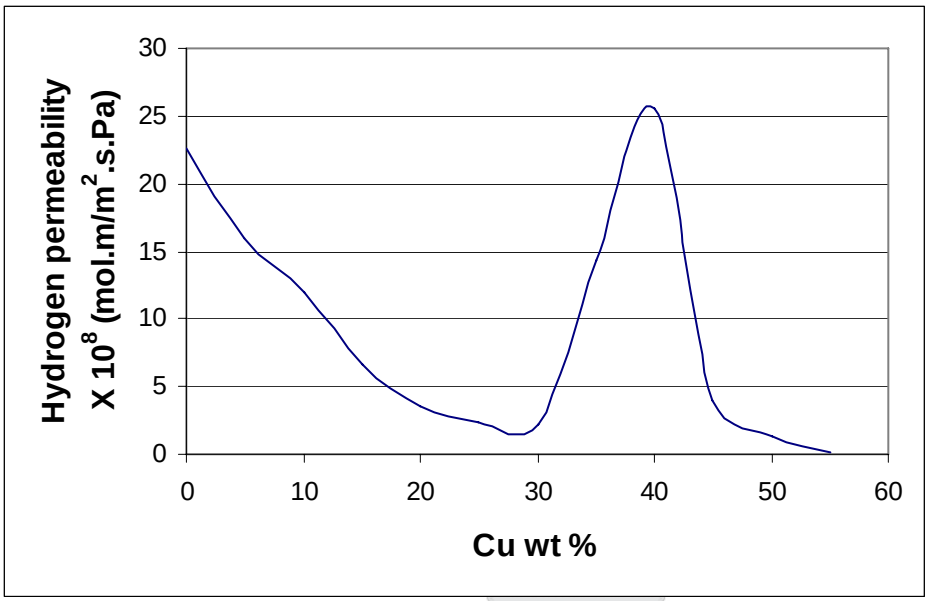

Figure 3.6 Permeability of hydrogen through a Pd-Cu membrane at 350 °C and 2.2 MPa (Shu, 1991)

3.6 Membrane testing

The same setup that was used for the catalytic testing was used to test the membrane permeance. The membrane reactor employed for permeance testing is shown in **Figure 3.7**. The complete testing setup is shown in **Figure 3.8**. A plated membrane was placed in the stainless steel reactor, the reactor was wrapped with the heating wire and the system insulated. Graphite rings were used to obtain an effective membrane to reactor seal. These graphite rings had dimensions of 10.4 by 17.9 mm, the density was 1.6 g/cm^3 and they had a thickness of 5 mm. They were purchased from Coltec Industries (Le Carbone

Loraine). Nuts that turned into the membrane reactor ends pushed two fittings onto the graphite rings. Those fittings slid over the membrane ends and were cut with an angle at the bottom edge to be able to wedge into the graphite. When the nuts were tightened, the fittings forced the graphite rings sideways, pressing them against the enamelled membrane endings.

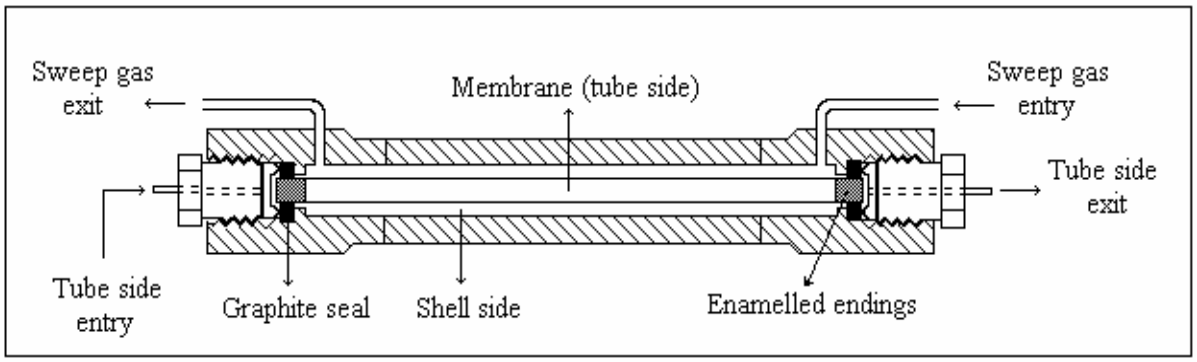

Figure 3.7 Membrane reactor used to test the membrane permeance (Keuler, 2000)

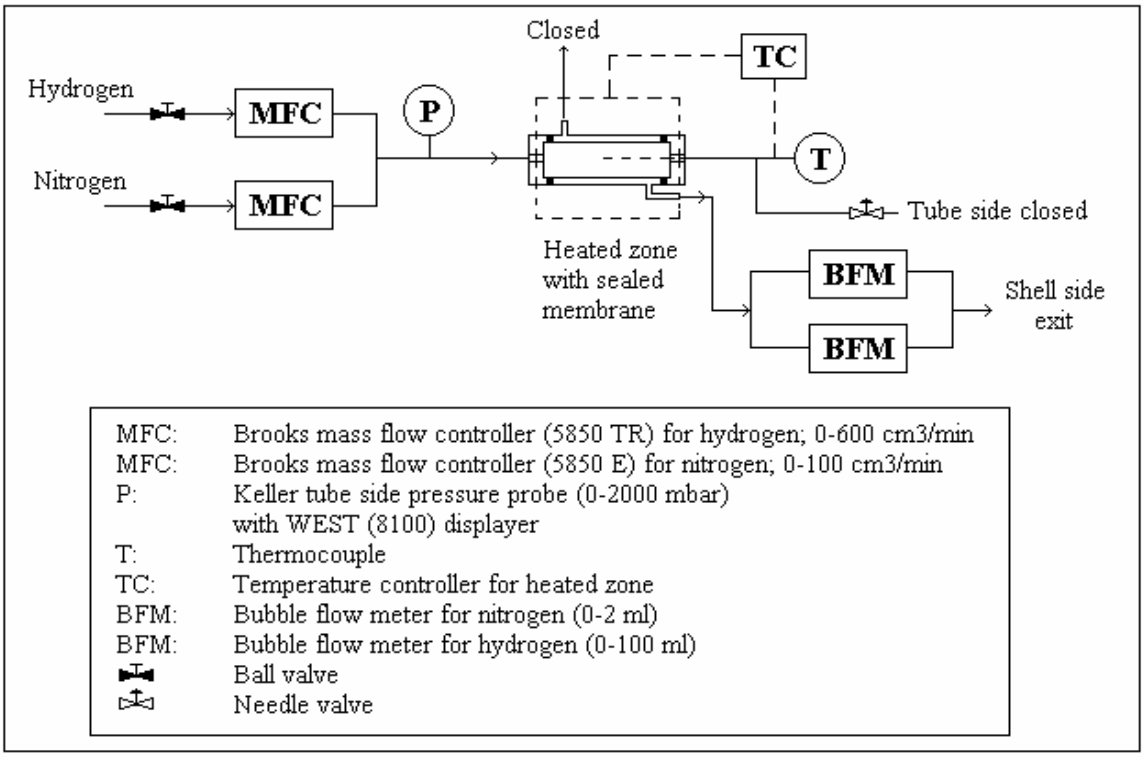

Figure 3.8 Set-up used for high temperature (> 300 °C) hydrogen and nitrogen permeation testing (Keuler, 2000)

The membrane was thoroughly sealed to ensure that the feed gas could only permeate through the Pd film or defects in the film. The feed gas entered the membrane on the tube side. The flow of the gases was measured by using a flow controller. The pressures of the inlet gases were fixed and the flow rates of the permeated gases recorded. The nitrogen and hydrogen permeances were used to determine the selectivity of the palladium films. The flow rate of the permeated gas was measured using two bubble flow meters as indicated in **Figure 3.8**. The temperature was varied with a temperature controller. The selectivity at different temperatures could be calculated as follows:

$$H_2 \text{ to } N_2 \text{ Selectivity} = \frac{\text{Flow rate of } H_2 \text{ through membrane}}{\text{Flow rate of } N_2 \text{ through membrane}} \qquad (3.2)$$

3.7 Heat treatment

The plated membranes were heat treated before testing. A membrane was placed in a stainless steel reactor that was wrapped with heating wire. The temperature regulator heated the membrane to 450 °C at a rate of 3 °C/min, kept the temperature at 450 °C for 5 hours and then decreased the temperature at a rate of 2 °C/min to room temperature. Prior to heat treatment the system was purged with nitrogen to remove oxygen. Nitrogen was fed through the membrane at a flow rate of 40 cm^3/min with a Hasting flow controller (HFC 202C) until 450 °C was reached. Then hydrogen was introduced to remove all the nitrogen. Hydrogen was fed at a flow rate of 50 cm^3/min through the membrane for five hours. Nitrogen was pumped through the system, during the cooling stage.

3.8 Reactor temperature profiles

Temperature profiles across the length of the reactor were determined at various oven temperatures. The number of windings of the heating wire around the reactor and the distance between them were adjusted until satisfactory profiles were obtained. A constant temperature over the length of the reactor was necessary to assume isothermal conditions. The final profiles are presented in **Figure 3.9.**

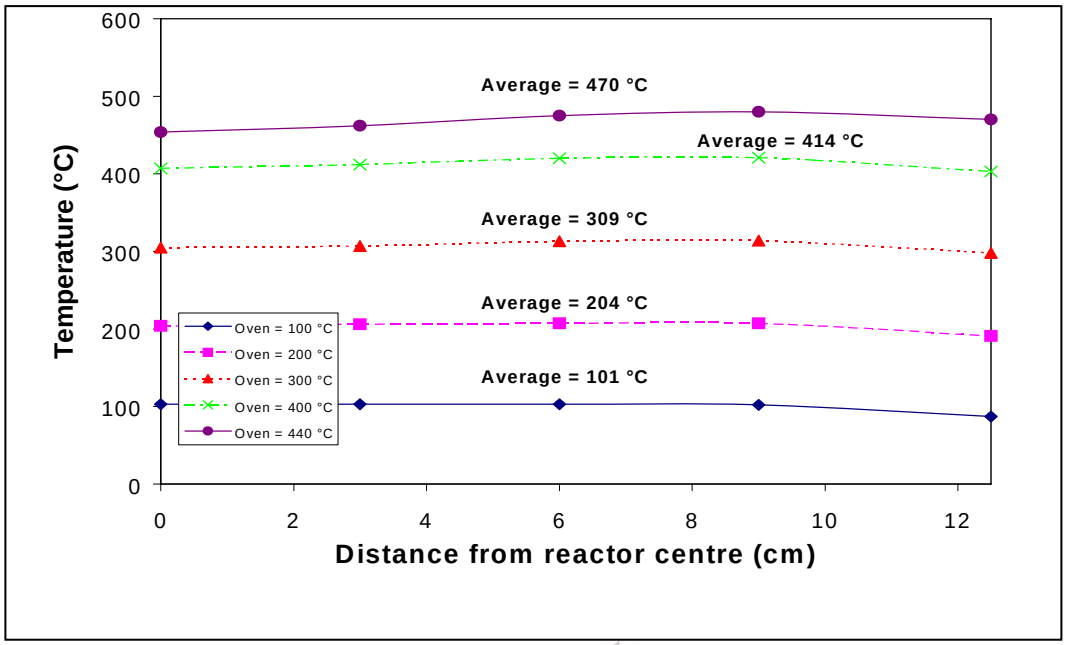

Figure 3.9 Reactor temperature profiles at different oven temperatures (Keuler, 2000)

Two thermocouples were used for measuring temperature. One was located on the outside of the reactor and one was located inside the membrane tube. The temperature controller was connected to the thermocouple on the outside of the reactor wall. To control the reaction temperature at for example 300 °C, the oven was adjusted by the difference according to **Figure 3.9** and set at 291 °C. As illustrated in **Figure 3.9**, the temperature profiles at 300 °C and below were very good from the centre of the reactor up to a distance of 9 cm from the centre.

3.9 Membrane reactor experiments

The dehydrogenation of 2-propanol with a 9.2 wt % Cu on SiO_2 catalyst was performed in a membrane reactor. Two types of alumina membranes were used as indicated in **Table 3.10**. The same reactor setup as in **Figure 3.1** was utilised for the dehydrogenation of 2-propanol in the membrane reactor. In this case, the quartz tube was replaced with a membrane tube. There was an entry point for sweepgas to flow through the shell side of

the membrane reactor as shown in **Figure 3.7**. Argon was employed as a sweepgas and the flow was co-current to the feed. Nitrogen was used as carrier gas of the 2-propanol to the membrane reactor. Two Argon to nitrogen flow rate ratios of 1 to 1 and 2 to 1 were used, with 2-propanol flow rates of 1.6 and 3.2 ml/h. Two Argon to 2-propanol ratios of 4:1 and 8:1 were employed. Temperatures ranging from 240 to 320 °C were tested.

Table 3.10 Different types of alumina membranes used for the dehydrogenation of 2-propanol

	Membrane B	
	Type 1	Type 2
Film type	Pd	Pd
Pd film thickness (microns)	5	4
Alloying component	-	Cu
Alloying content (wt %)	-	40

3.10 Analytical techniques

3.10.1 Scanning electron microscopy (SEM)

Samples were prepared by cutting the membranes into smaller pieces. Scanning electron microscopy (SEM) was performed at the Microscope Unit, University of Cape Town, with a Cambridge Stereoscan 440. The samples were mounted on aluminium stubs and gold plated to obtain top view SEM images. For cross section views, the samples were mounted on their sides in round cups with a diameter of about 30 mm. These cups were filled with a quick setting resin that hardened within five minutes. To obtain good images, the resin disks were polished with sanding paper of different mesh sizes. The final step was to polish the disk on a polishing wheel with 0.3 and 0.05 μm alumina slurries.

3.10.2 X-ray diffraction (XRD)

The crystal phases of the membranes were investigated using X-ray diffraction (XRD) analysis. The analyses were done at the Geology Department, University of Stellenbosch.

A Phillips vertical X-ray diffractometer adapted using Difftech-122D digital control, with Cu Kα radiation and a graphite monochromator, was used to record the spectra.

3.10.3 Proton induced X-ray emission (PIXE)

The concentration profiles for palladium and copper (across the metal coating) were constructed using micro-PIXE (Proton induced X-ray emission). These experiments were conducted at the South African National Accelerator Centre (Faure) with a Van der Graaf Generator. Line scans were taken from the outside to the inside of the membrane's cross-section. Measurement depths of up to 30 microns were studied. Gupix software was used to analyse the data.

3.10.4 Atomic adsorption (AA)

A Varian spectroflame 250 plus atomic adsorption apparatus was used to determine the concentration of palladium ions in the plating solution. The AA with flame detector was first calibrated using different solutions containing 10, 20, 40, 70, 100 and 120 ppm palladium.

3.10.5 BET (Brunauer-Emmett-Teller) and Chemisorption

A micromeritics ASAP 2010 apparatus was used to determine the total surface area of the catalysts. Samples were dried in situ at 300 °C for 12 to 16 hours before analyses. Chemisorption was performed to determine the copper surface area of the catalysts. A typical procedure for chemisorption was as follows:

Sample weight:	0.248 g
Free space:	17.5916 cm^3
Analysis gas:	H_2
Analysis temp:	35 °C
Equilibrium interval:	30 seconds

Low pressure dose: None

Smoothed pressures: No

A typical options report is listed in **Table 3.11.**

Table 3.11 Options report for the determination of Cu surface area using chemisorption

Task number	Task name	Start time (hr:min)	Gas	Furnace temp. (°C)	Sample temp. (°C)	Time (min)	Pressure (mmHg)
1	EVAC	0:10	HE	101	100.9	60	
2	FLOW	1:28	HE	263	260.3	60	777.181
3	EVAC	2:53	HE	263	260.7	10	
4	FLOW	3:06	H_2	263	258.8	120	800.646
5	EVAC	5:08	H_2	263	260.5	60	
6	EVAC	6:09	H_2	33	35.3	60	
7	LEAK	7:42		33	35.2	0	
8	EVAC	7:46	H_2	33	35.2	20	
9	ANL	8:06	H_2	33	34.9	361	618.981

3.11 Summary

This chapter covered all the experimental work performed for this investigation. All the experimental setup used including, the reactor used for catalytic testing, the electroless plating setup, membrane testing and the membrane reactor, were illustrated. The operating procedure for doing experiments and permeability tests on the membranes were explained. Copper impregnated on Al_2O_3, SiO_2 and MgO support were used as catalysts for the dehydrogenation of isopropanol. The pre-treatment and electroless plating of copper and palladium on two types of alumina membranes were investigated and discussed. The dehydrogenation of isopropanol was performed in a fixed-bed and membrane reactor.

4. Electroless plating

4.1 Introduction

In a liquid medium metals can be deposited on a support by electrolysis or by electroless plating. Metal alloys can also be deposited on a support with co-deposition. Usually deposition is on metals, but by appropriate pre-treatment methods, a wide range of plastics can be metallised.

Electroless plating is a process whereby dense uniform coatings can be deposited on both conducting and non-conducting surfaces. It is a relatively inexpensive process, requiring simple equipment. This process is much cheaper for producing palladium membranes than other techniques. High metal recovery can easily be achieved to further reduce the manufacturing costs. With electroless plating, the metal film can be made both continuous and very thin. Such deposits form only on certain catalytically active sites. The electrons needed to reduce the metal ions are provided by the reducing agent (R^{n+}). The reduction and oxidation equations are:

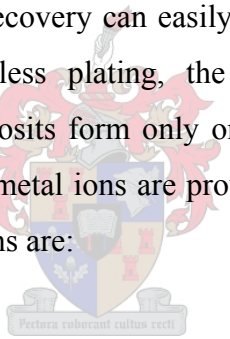

$$R^{n+} \rightarrow R^{(n+z)} + ze \qquad (4.1)$$

$$Me^{z+} + ze \rightarrow Me \qquad (4.2)$$

where,

Me = metal,
R = Reducing agent,
z = electrons, and
n = valence

In this chapter, the results of copper and palladium electroless plating on α-alumina membranes will be explained and discussed. The procedures and chemicals mentioned in Chapter 3 were used for the plating of copper and palladium.

4.2 Electroless palladium plating

4.2.1 Process variables

Palladium, palladium-nickel and palladium-silver alloys have been used primarily for separable connectors and printed wiring board figures (Abys, 1998). Palladium has been found to be a satisfactory replacement for gold in most applications, but since the palladium price is currently three times as much as the gold price this is not relevant anymore. Palladium coated iron foils have been used in the construction of gas probes to detect hydrogen generated by corrosion reactions (Lyon and Fray, 1984), electroplating and cathodic protection (Lyon and Fray, 1984).

The use of inorganic membranes for gas separation and catalytic reactions has become feasible at high temperatures. For dehydrogenation reactions, the removal of hydrogen is very important to manipulate the reaction equilibrium conversion. By plating a thin film of palladium on porous inorganic membranes, hydrogen molecules can be separated from the reaction products, resulting in a shift in the reaction equilibrium. As explained in chapter 3, the plating process consists mainly of four components:

(i) reducing agent (0.04 M hydrazine),
(ii) temperature bath,
(iii) stabilised source of metal ions, and
(iv) support membrane (α-alumina).

Keuler (1997) investigated the first three variables. Tetra ammine palladium nitrate was found to be the best salt to give maximum palladium conversion with an alkaline solution (pH buffer of 9-11). A palladium ion to palladium metal on the substrate conversion of 90% was achieved using alumina-zirconia membranes.

4.2.2 Discussion of results

4.2.2.1 Rate of electroless palladium plating

Electroless plating of palladium is an autocatalytic, electrochemical reaction. The process occurs on the solid-liquid interface between the plating surface and the solution. To determine the rate of plating on the alumina membranes, different membranes were plated and the concentration of palladium in solution after a specific time was determined using atomic adsorption (AA) as explained in chapter 3. All the experimental data are shown in appendix B. The true concentration of palladium in the stock solution could be calculated using the results from the AA. The following figures **(Figure 4.1** to **4.5)** show the results obtained from plating experiments. The membranes used were purchased from Atech with specifications as indicated in **Table 3.2**. For some samples, the plating time was increased to obtain thicker films. More palladium stock solution was also added to some samples to increase the thickness of the palladium film. The plating procedure for producing Pd films was indicated in **Table 3.7**. Other electroless plating parameters that were varied are indicated in **Table 4.1**. The membranes were also named as shown in **Table 4.1**.

The purpose of this study was not to minimise the film thickness. Thicker films were made to study the diffusion of Cu into Pd during heat treatment. With PIXE it is easier to construct concentration profiles of elements across the film thickness for slightly thicker films (about 5 microns).

Table 4.1 Membranes used for electroless plating

Membrane name	Volume of Pd stock solution used (ml)	Length of membrane plated (mm)
Membrane A1	110	110
Membrane A2	108	300
Membrane A3	259.4	300
Membrane A4	275	300
Membrane A5	275	300

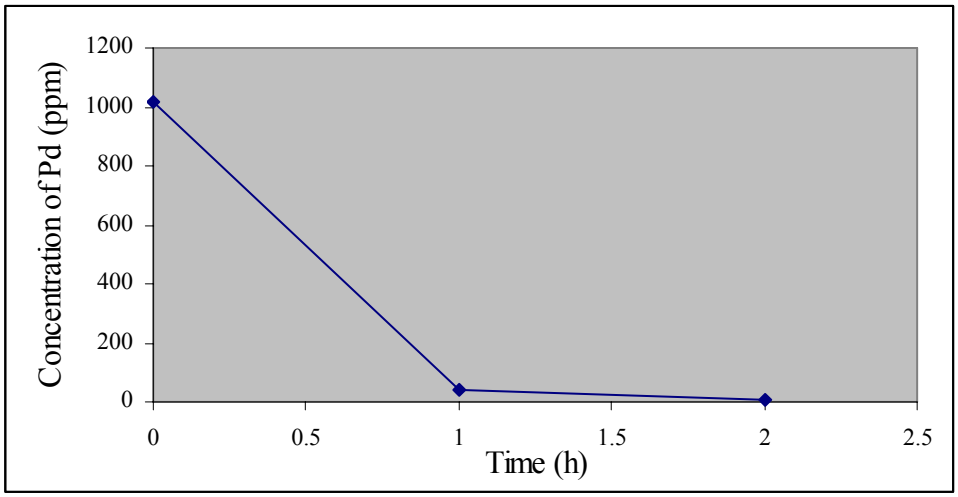

Figure 4.1 Decrease of Pd concentration in the stock solution as a function of time (Membrane A1)

As can be seen in **Figure 4.1**, most of the plating took place in the first hour of plating. In that period the concentration of the palladium decreased from 1014 ppm to 42 ppm. In the second hour of plating the concentration decreased from 42 ppm to 9 ppm. A palladium film thickness of 4.4 μm was obtained on this membrane.

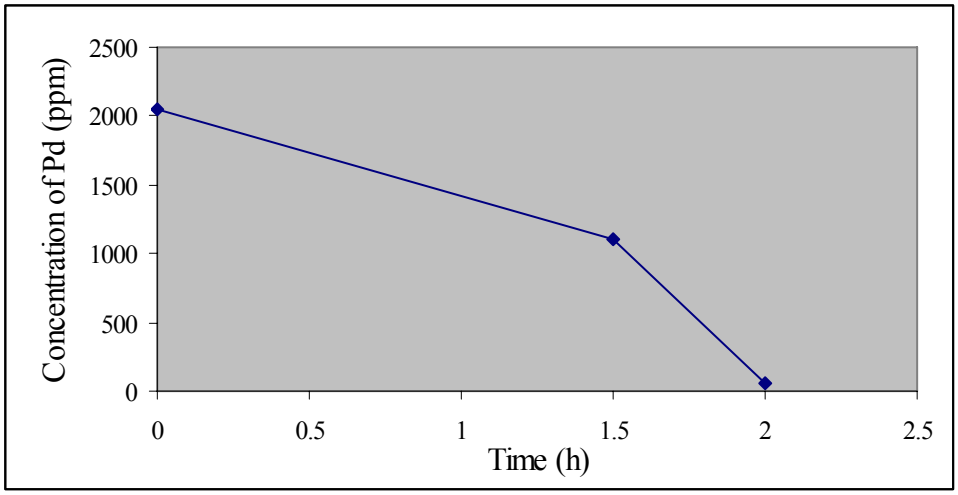

Figure 4.2 Decrease of Pd concentration in the stock solution as a function of time (Membrane A2)

For the sample in **Figure 4.2** the starting concentration was chosen as 2045 ppm palladium. After 2 hours of plating most of the palladium ions in solution were reduced and deposited as Pd metal. In this case the rate of plating increased after 1.5 hours. A film thickness of 2.7 μm was obtained for this sample.

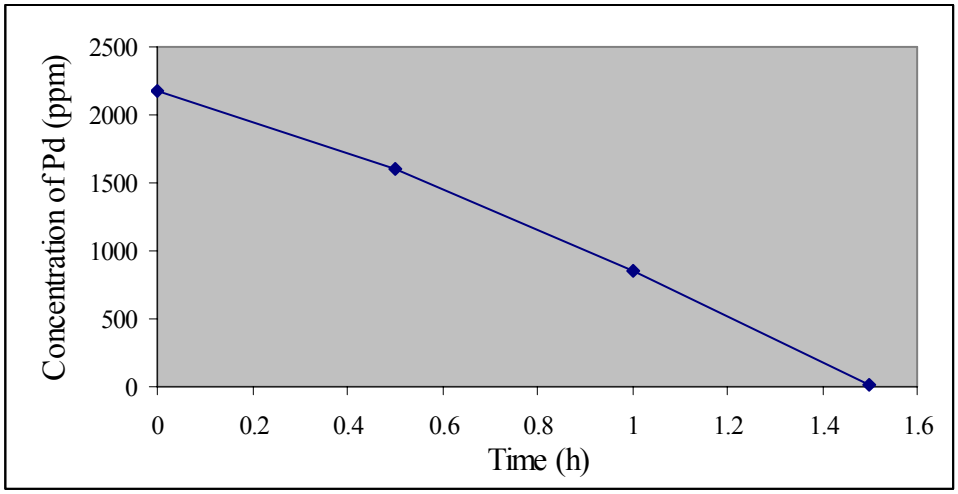

Figure 4.3 Decrease of Pd concentration in the stock solution as a function of time (Membrane A3)

The rate of plating for the sample in **Figure 4.3** stayed constant throughout the whole plating time. A film thickness of 8.2 μm was produced from this experiment. For this sample (membrane A3) the plating time is less than for the previous sample (membrane A2). In **Figure 4.2** the plating rate also increases after 1.5 hours. This can not be explained and it is expected that there were experimental errors with the plating of membrane A2.

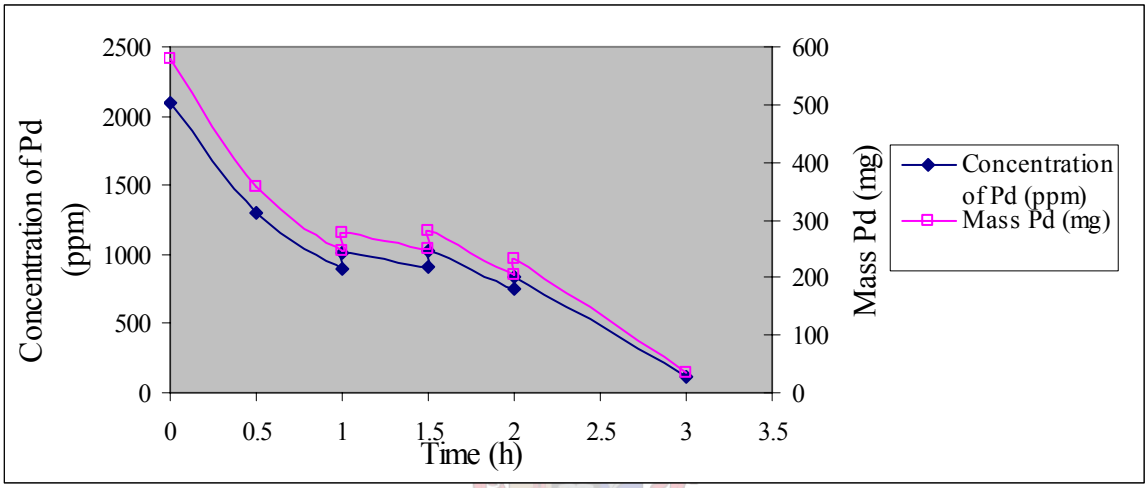

Figure 4.4 Decrease of Pd concentration in the stock solution and the mass of Pd as a function of time (Membrane A4)

In the first part of the curve in **Figure 4.4** (0-1 h) the plating rate seemed to be the same as for the previous samples (membrane A1 and A3). For both membrane A4 and membrane A5, 20ml of palladium stock solution was added to the plating solution after 1, 1.5 and 2 hours. The concentration from 1 hour until 2 hours declined only slightly because extra plating solution was added and then after 3 hours the stock plating solution had almost no palladium left. That means that during 1 and 2 hours all the palladium that was added was plated on the support membrane. Adding palladium stock solution after a time, rather than starting with a lot of stock solution in the beginning could thus produce a thicker film. Between 1 and 3 hours the concentration of Pd did not decrease to the extent of 0-1 hour where it decreased from 2100-900 ppm. Between 0 and 1 hour, 330 mg of Pd was plated on the membrane and only 245 mg was plated during 1 and 3 hours.

It was also noticed that starting with a high concentration of Pd could lead to a bad quality of the coating because the reaction is not stable and takes place to quick. The same experiment was done with a different sample and the same results were observed as in **Figure 4.5**.

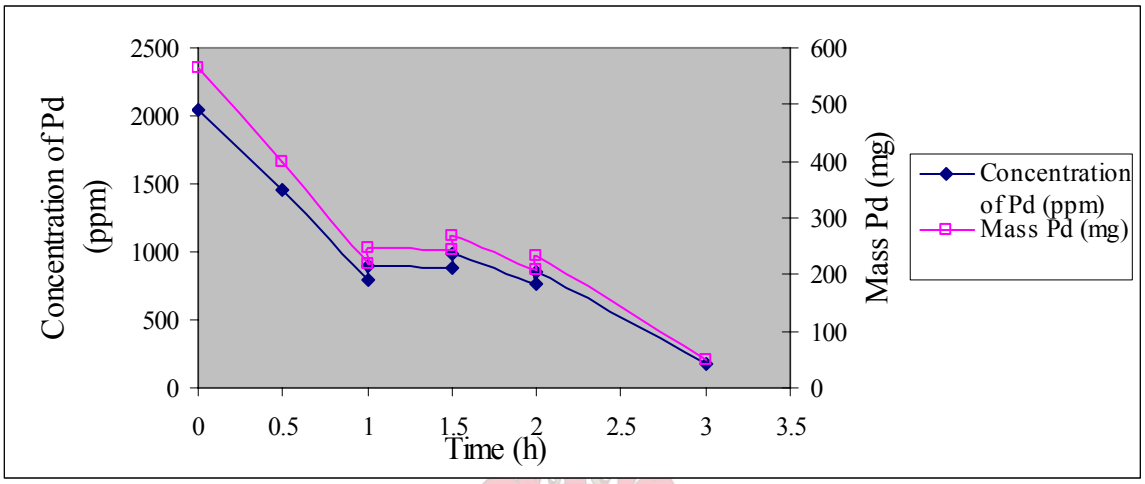

Figure 4.5 Decrease of Pd concentration in the stock solution and the mass of Pd as a function of time (Membrane A5)

4.2.2.2 Properties of electroless palladium deposits

Three membrane samples were prepared for copper plating. All three samples were Pd plated in exactly the same manner. Thereafter, Cu was plated on the Pd layer. One of the membrane samples was plated to a palladium thickness of 4.8 microns and the others were plated to a thickness of 4.6 microns. The texture and strength of these layers were studied. The following information is of importance:

1. The properties of electroless palladium deposits depend on the deposition mechanism, the film thickness and microstructure.
2. The H_2:N_2 selectivity varied for membranes that were prepared in the same way.
3. After deposition, a composite structure of deposit and substrate is formed with a new set of properties that differ considerably from the original substrate.

4.2.2.2.1 Appearance

The palladium deposits had a bright silvery colour. In terms of colour, the different samples that were prepared did not differ. The outside (the side that was attached to the membrane) of the coating seemed brighter than the inside of the coating

4.2.2.2.2 Adhesion

The usefulness of a composite material (like a palladium coated ceramic substrate) is restricted to the extent that adhesion of the deposit is unimpaired. Such an unimpaired coating implies, in the case of ceramic substrates, that a true metal-to-ceramic bond must form between metal deposit and ceramic base. In such cases, adhesion, as measured by the pull-off test, is of the same order of magnitude as the tensile strength of the weaker of the two materials. The adhesion of palladium on alumina membranes thus depends on mechanical keying with associated Van der Waals and heteropolar binding forces (Saubestre, 1965).

Adhesion strength (in the case of electroless plating) is around one order of magnitude lower than for metal-to-metal bonding (Mallory, 1985). In both cases, however, the adhesion strength is mainly dependent on the pre-treatment of the substrate. For some of the experiments, the palladium film came apart from the support easily, thus the adhesion was not good. This was for palladium coatings on alumina membranes with 5 nm pores (α,γ-alumina, SCT). The adhesion of the film was found to be much better with membranes with 200 nm pores (membrane B, **Table 3.3** and **3.4**) and when the rate of plating was decreased.

The difference in the thermal expansion coefficient between the γ-alumina and palladium may also be responsible for the poor adhesion between palladium and γ-alumina.

4.2.2.2.3 Ductility

One of the most important mechanical properties of a palladium film is its ductility. Electroless deposits are usually less ductile than electrodeposit metals (Riedel, 1980). Some electroless deposits can be so brittle that it limits their usefulness. This is the case where a palladium film is in contact with hydrogen under 300 °C. Once the film is damaged (even a small defect), the selectivity of the film will decrease drastically. Thus, is it important not to heat treat the palladium plated membrane in a hydrogen atmosphere under 300 °C. The palladium film is also not very hard. A scratch can damage the coating.

4.3 Electroless copper plating

4.3.1 Process variables

In industry, electroless copper plating is used in the fabrication of printed circuit boards and other electronic applications (Shipley, 1984). In general, formaldehyde is used as reducing agent for electroless copper plating. In the beginning of this investigation formaldehyde was used, but the results that were obtained were not good. The reaction rate was extremely slow and conversions were low. It was decided to use hydrazine as reducing agent. The copper plating bath and plating procedure indicated in **Tables 3.8** and **3.9** were used.

Electroless deposition of copper has been studied by investigating the solution composition, substrate type (different supports that were used) and process kinetics. Two types of alumina membranes were used as explained in chapter 3. The process used in this study is believed to proceed through the following reactions:

Anodic reaction:

$$N_2H_4 + 4OH^- \rightarrow N_2 + 4H_2O + 4e^- \qquad (4.3)$$

Cathodic reaction:

$$2Cu^{2+} + 4e^- \rightarrow 2Cu \qquad (4.4)$$

Overall reaction:

$$N_2H_4 + 2Cu^{2+} + 4OH^- \rightarrow N_2 + 4H_2O + 2Cu \qquad (4.5)$$

The anodic and the cathodic reactions proceed simultaneously in accordance with the mixed-potential theory (Stern and Geary, 1957). This is a simple correlation between polarisation resistance and corrosion rate at the free corrosion potential. Using this theory the corrosion rate can be estimated from the gradient of the current density-potential curve (polarisation resistance).

A suitable copper plating solution composition was determined with electroless plating experiments on 10 mm pieces of membranes. The solution feeding mechanism to the inside of the membrane tube was determined on 30 cm membranes in the following manner:

-the speed of pumping the plating solution through the inside of the membrane tube was varied from 9.9 to 19.9 mm/s,
-the amount of times the plating solution was pumped through the inside of the membrane were varied, and
-the hydrazine concentration was increased after different plating times.

The optimum plating conditions were found to be a pumping speed of 30 cm^3/min (linear velocity of 9.9 mm/s), the same solution should be pumped through the membrane four times and after the second throughput the hydrazine concentration must be increased by 10%. The temperature was kept constant at 70 °C.

These conditions were used to make palladium-copper membranes of different Cu percentages. Palladium films of thicknesses of 4.8, 4.6 and 4.6 microns were plated on

three different membranes of type A as indicated in **Table 3.2**. The required amount of copper plating solution was determined and attempts were made to produce three membranes of 20, 30 and 40% copper. The actual copper thicknesses were determined to be 0.72 (15%), 1.40 (30%) and 1.78 (38%) microns. These membranes were characterised using SEM, XRD and PIXE. The results will be discussed in chapter 5.

4.3.2 Texture and appearance of copper coating

The use of high concentrations of hydrazine and copper in the stock solution resulted in patchy plating. The film was not evenly distributed and some pieces of the membrane had no copper on it. Using the correct concentrations, the copper film was evenly distributed all over the inside of the membrane.

The copper film that was formed during the plating process had a reddish colour and had an uneven texture. If the film was heated in an oxygen atmosphere, the colour of the film turned grey. The heating of all copper plated membranes was done in a vacuum oven to prevent oxidisation. The colour of the copper film stayed reddish using the vacuum oven. The adhesion of the copper film was stronger than the palladium film and did not peel of easily. This might be because the copper was plated on top of the palladium and the metal to metal bond was stronger than the Pd to ceramic bond. In chapter 5 it will be seen that the copper penetrated into the pores of the membranes and that may attribute to the fact that the copper film is more adhesive to the support.

4.4 Summary

In this chapter, the electroless plating process for coating the alumina membranes with palladium and copper was discussed. The rate of the palladium plating and the properties in terms of the appearance and adhesion of both the palladium and copper films were presented. The process variables used for the different electroless plating procedures were explained. It was also explained how the membranes were prepared for XRD, PIXE and SEM studies. For these purposes, thicker films of up to 5 microns were produced. It

was mentioned that the adhesion of the palladium films was much better on the α-alumina than on the α,γ-alumina membrane.

5. Characterisation of copper-palladium films on alumina support membranes using SEM, XRD and PIXE.

5.1 Introduction

In this chapter a discussion will be given about the characterisation of copper–palladium coatings on alumina membranes. Electroless plating was used to coat the membranes. Three different copper percentages were plated on palladium coated membranes. For each percentage, two membranes were prepared and one of each percentage was heat treated in a H_2 atmosphere at 450 °C for six hours. These six membranes were characterised using SEM, PIXE and XRD.

5.2 Results of scanning electron microscopy (SEM)

For the SEM analysis, side view and top view images of the membrane samples were taken to study the surface structure and thickness of the metal layers. All images were taken at 10 000 magnification. The membranes were named as indicated in **Table 5.1**. The calculated thicknesses of the palladium and copper layers on the alfa alumina support are also shown in **Table 5.1**.

Table 5.1 Membranes characterised with SEM, XRD and PIXE.

Percentage Copper	Name	Pd thickness (μm)	Cu thickness (μm)
15 wt %	Membrane 1	4.8	0.7
15 wt % heat treated	Membrane 1h	4.8	0.7
30 wt %	Membrane 2	4.6	1.4
30 wt % heat treated	Membrane 2h	4.6	1.4
38 wt %	Membrane 3	4.6	1.8
38 wt % heat treated	Membrane 3h	4.6	1.8

Side view images

Membrane 1 and 1h

The membrane was plated with 20 wt % of copper. Clearly identifiable films were formed on the membrane support during the electroless plating process. In **Figure 5.1 (a)** the bright white layer in the middle of the picture is the film. The dark part above the film is the resin. The structure below the film is the alumina support. An even film was formed. Only one layer is visible on the alumina support. It can be seen that the film has not become detached from the alumina support. The film adhesion to the support was reasonable. From **Figure 5.1 (b)** it can be seen that in some areas on the support the film is very thin. There are also some holes, of size 1 micron, in the film on this image. It shows that the plating did not occur very well in those areas. One reason can be that the alumina support had irregularities in some areas. From this image it can be seen that the coating is dense.

Membrane 2 and 2h

The unevenness of the film can again be noticed in **Figure 5.2 (a)**. The black spots in the thick films indicate holes in the films where the plating did not form a defect free film. **Figure 5.2 (b)** shows a gap between the layer and the membrane support. A large gap is visible between the film and the support, which suggests poor adhesion to the support. The support could have deficiencies in this area and therefore the layer is not anchored very well to the support. It is important to note that irregularities in the support will cause irregularities in the coated film.

Membrane 3 and 3h

Figures 5.3 (a) and **(b)** show the same effect caused by the heat treatment that was observed for the previous two samples. The coating is also dense.

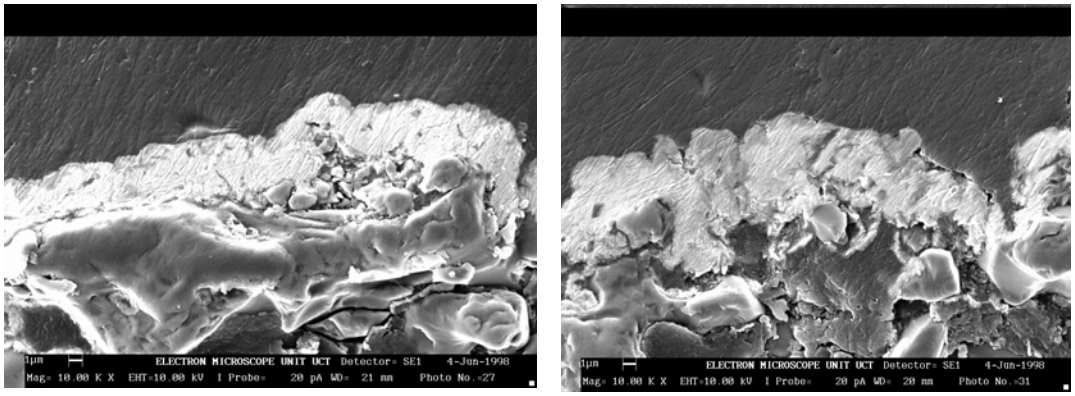

(a) **(b)**

<u>Figure 5.1 (a) and (b)</u> Side view image of membrane 1 (a) and 1h (b)

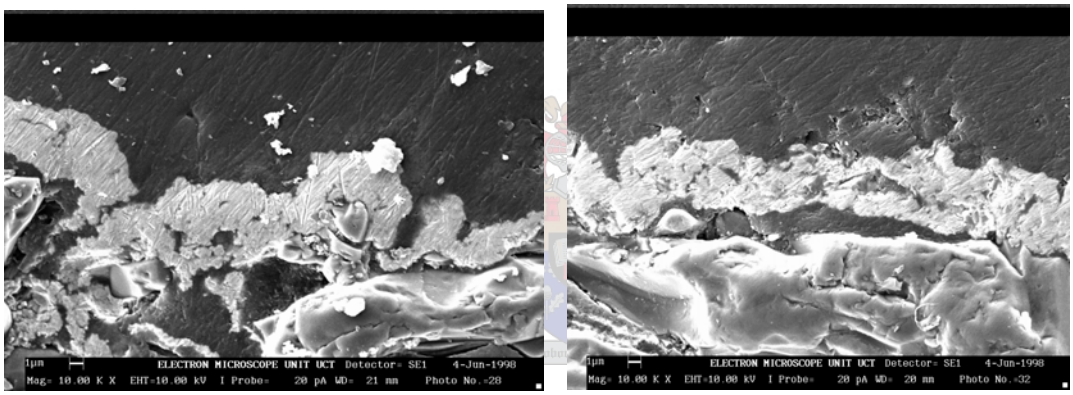

(a) **(b)**

<u>Figure 5.2 (a) and (b)</u> Side view image of membrane 2 (a) and 2h (b)

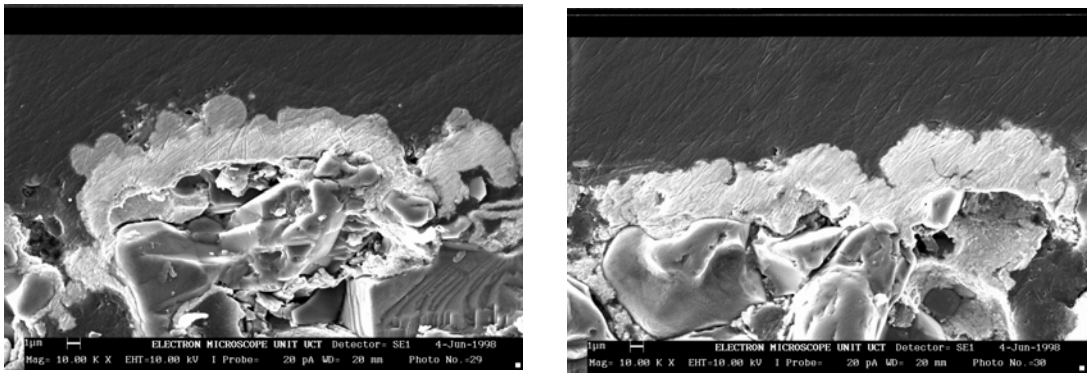

(a) **(b)**

<u>Figure 5.3 (a) and (b)</u> Side view image of membrane 3 (a) and 3h (b)

Top view images

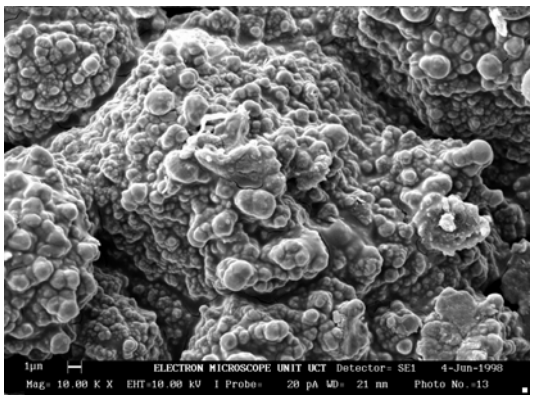

(a)

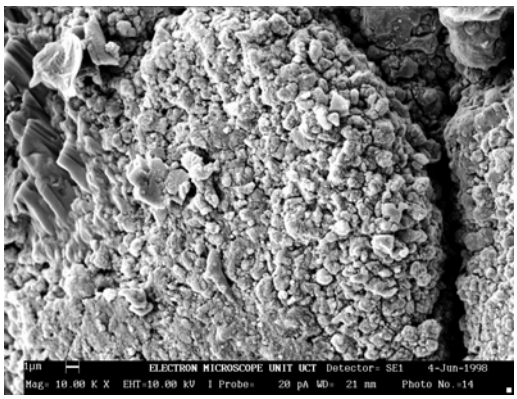

(b)

<u>Figure 5.4 (a) and (b)</u> Top view image of membrane 1 (a) and 1h (b)

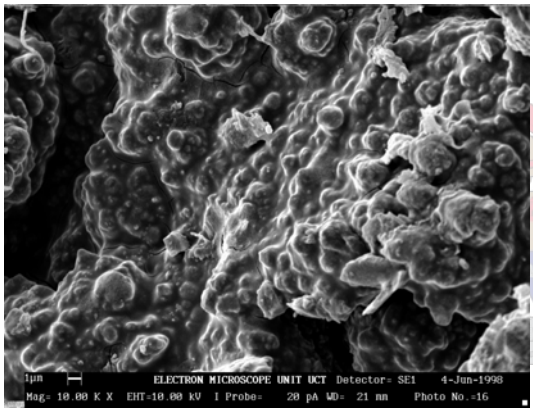

(a)

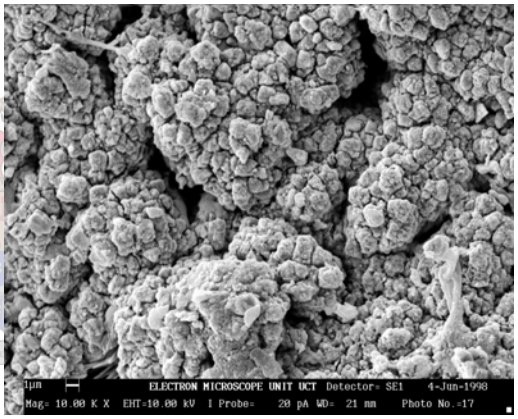

(b)

<u>Figure 5.5 (a) and (b)</u> Top view image of membrane 2 (a) and 2h (b)

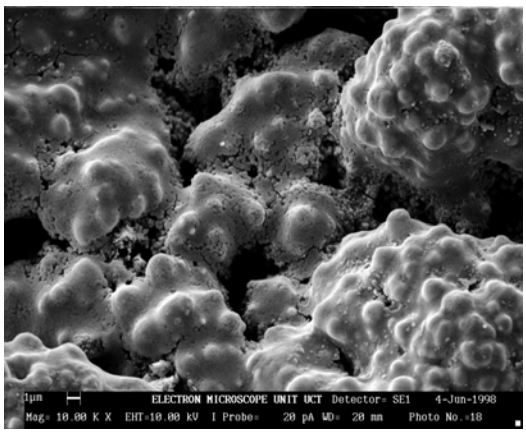

(a)

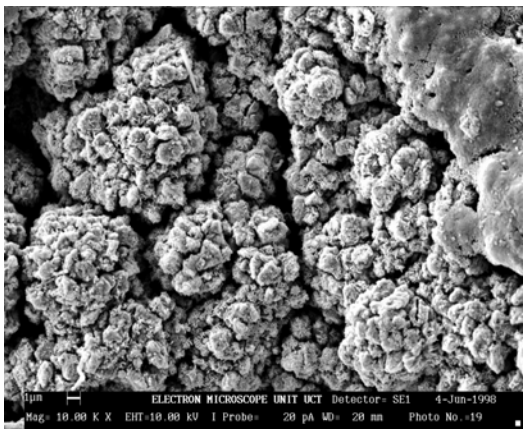

(b)

<u>Figure 5.6 (a) and (b)</u> Top view image of membrane 3 (a) and 3h (b)

Membrane 1 and 1h

From **Figure 5.4 (a)** it seems as if the nuclei agglomerate (groups) in certain areas with holes (gorges) in between. The plating reaction occurs on the surface of the activated support, and preferentially around the palladium seeds. The palladium metal is deposited onto the nuclei resulting in film growth. From **Figure 5.4 (b)** it can be seen that dense metal clusters formed on the membrane. This area of the support seems to be unevenly plated with the palladium and copper. There is a hole on the right hand side of the image. After heat treatment the palladium-copper layer seems very fragile (crisp). It almost seems as if the metal-nuclei embrittles during the heating. Tiny crystals were formed during the heating.

Membrane 2 and 2h

The same pattern as in the 20 wt % copper sample is observed in **Figure 5.5 (a)**. This heated sample in **Figure 5.5 (b)** shows the same agglomerates of the copper and the palladium nuclei. The holes, which suggest the deficiencies in the support, can also clearly be seen.

Membrane 3 and 3h

More and larger copper nuclei can be seen in **Figure 5.6 (a)**. In this image it looks like the bigger copper nuclei grows on each other. The heating effect can again be very well observed in **Figure 5.6 (b)**. The surface of this sample looks porous with defects. The sizes of the clusters are almost the same with the gorges in between. From a catalytic point of view this situation is favourable, because the surface area of the catalysts is increased, but membrane selectivity will most likely be very poor.

Figures 5.1 to **5.6** show the coatings on Atech membranes (**Table 3.2**). From these results it can be seen that the film quality was poor. The pore diameter of the membranes were never theoretically determined. The specifications of the membranes indicated that

the pore diameter was 100 nm. This is unlikely, because SEM images show the presence of very large alumina crystals, which can not lead to membranes with very small pores.

Keuler (2000) plated palladium on SCT membranes (**Tables 3.3** and **3.4**). **Figure 5.7** shows the cross-section view of a SCT membrane. The three layers are clearly visible on the picture. It can be seen that the top layer of this membrane is very smooth, which is favourable for electroless plating. **Figure 5.8** shows a very dense and even layer on top of a SCT membrane. The palladium film is the thin layer on top of the 200 nm alumina support. The more even structure of the support can clearly be seen in **Figure 5.9**. The top part of the picture is the resin with a 1.45 micron palladium film above the support. From **Figures 5.8** and **5.9** it can be seen that the film adhesion to the SCT membranes was very good.

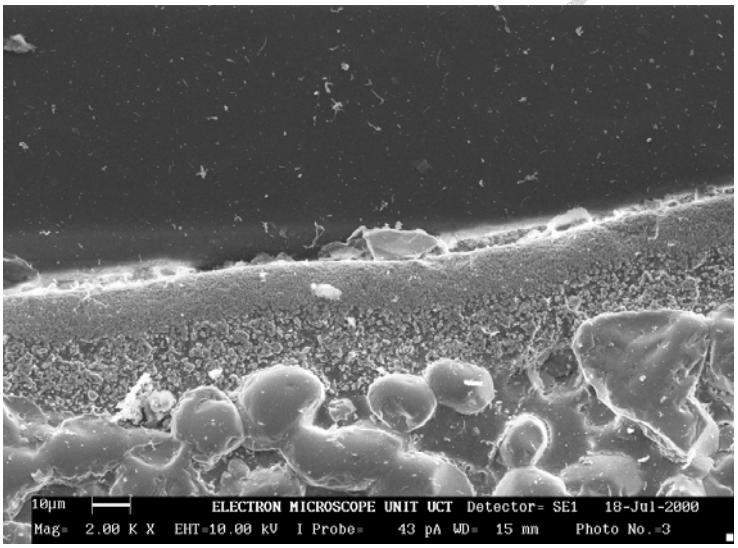

<u>Figure 5.7</u> Side view of a three layer SCT membrane (2000×)

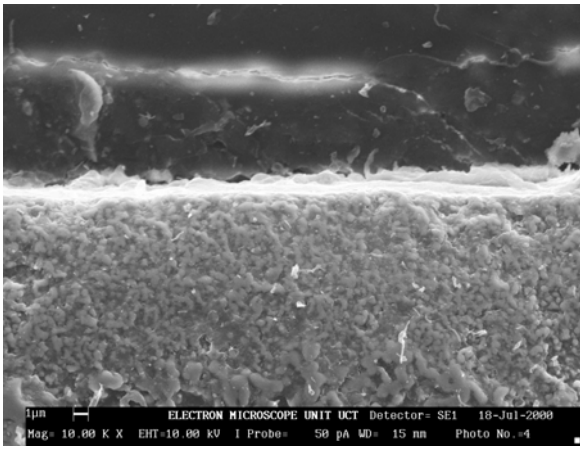

Figure 5.8 Side view of SCT membrane (10 000×)

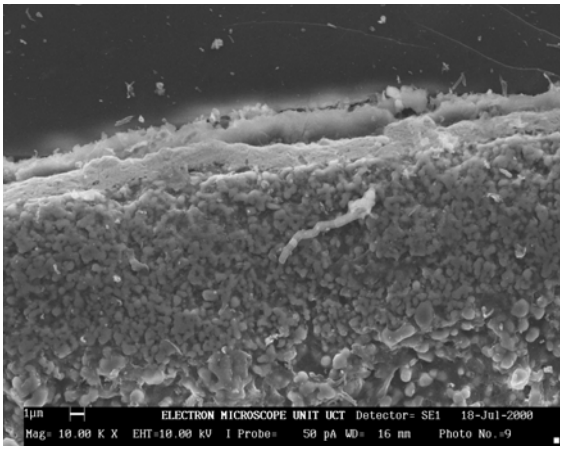

Figure 5.9 Side view of a heat treated SCT membrane (10 000×)

Figures 5.10 and **5.11** show the top view images of a SCT membrane that was coated with a palladium film of thickness 1.45 microns. These top view images confirmed a dense structure without any defects. Good permeability results were achieved for these membranes (Keuler, 2000).

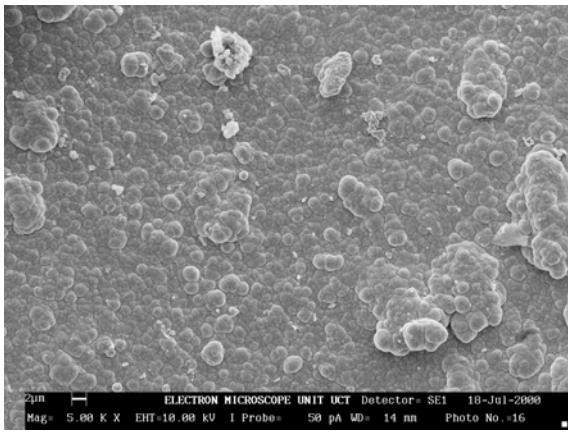

Figure 5.10 Top view of SCT membrane (5000×)

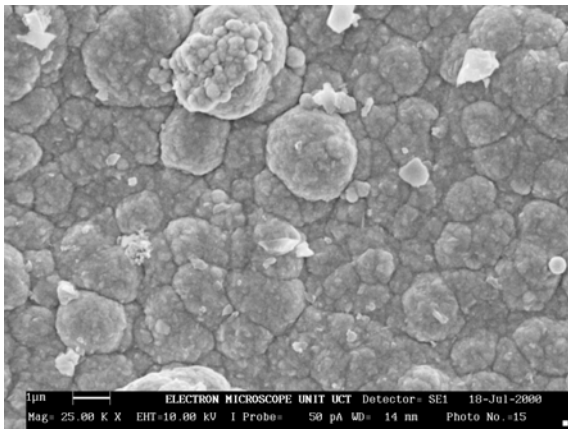

Figure 5.11 Top view of SCT membrane (25 000×)

5.3 X-Ray Diffraction (XRD)

5.3.1 X-Ray structure determination

The structure of a crystal can be determined by analysing the diffraction pattern of a single crystal. By knowing the position and the relative intensities of the X-ray diffraction peaks, the symmetrical elements, coordinates and the temperature factors of each atom can be determined.

5.3.2 Results of XRD

The different elemental peaks were determined using DIFFTECH XRD Automation and PCPDFWIN software. The program Traces V3.0 was used. The XRD patterns were studied to detect the difference in crystal structure between the heated and the non-heated samples. The peak intensity is a relative measure of the amount of X-Rays diffracted for a certain configuration. **Tables 5.2** to **5.7** present the structural data for Pd-Cu deposits on the membranes.

Membrane 1

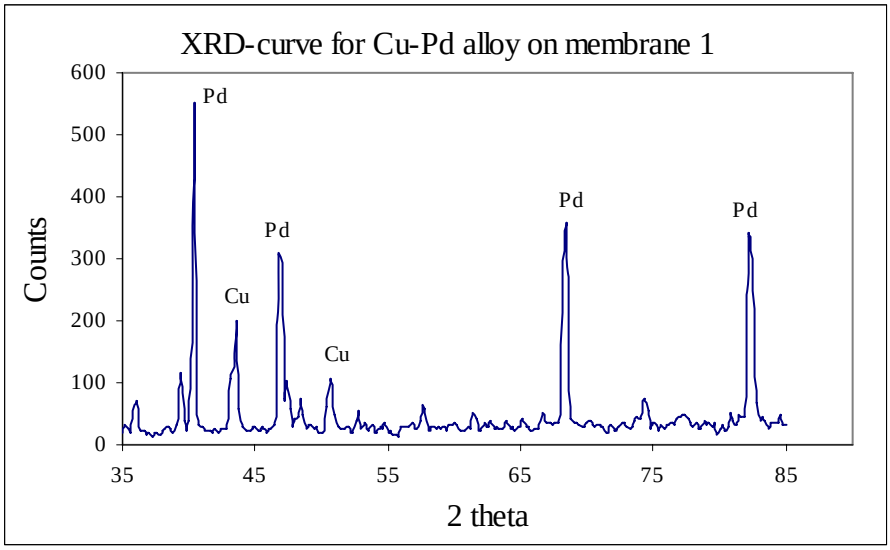

Figure 5.12 XRD pattern for a Cu on Pd film (membrane 1)

Table 5.2 Structural data for Pd-Cu deposit (membrane 1)

Angle	Counts	d space Å	Relative intensity
39.4	115	2.287	21
40.4	552	2.233	100
43.6	199	2.076	36
46.8	308	1.941	56
68.4	356	1.372	64
82.2	335	1.173	61

Before heat treatment, the separate peaks could clearly be seen in **Figure 5.12**. High palladium counts were observed. The copper peaks were small because only a small concentration of copper was plated on the palladium for this sample. The other small peaks were the alumina support peaks.

Membrane 1h

After heat treatment, the counts for the palladium were not as much as before heat treatment according to **Figure 5.13**. The palladium peaks got broader. This indicates that smaller crystallites were formed. Heat treatment led to smaller palladium and copper crystallites being formed, which is in agreement with the results obtained by the SEM images. The crystal structure of the film definitely changed due to the heat treatment.

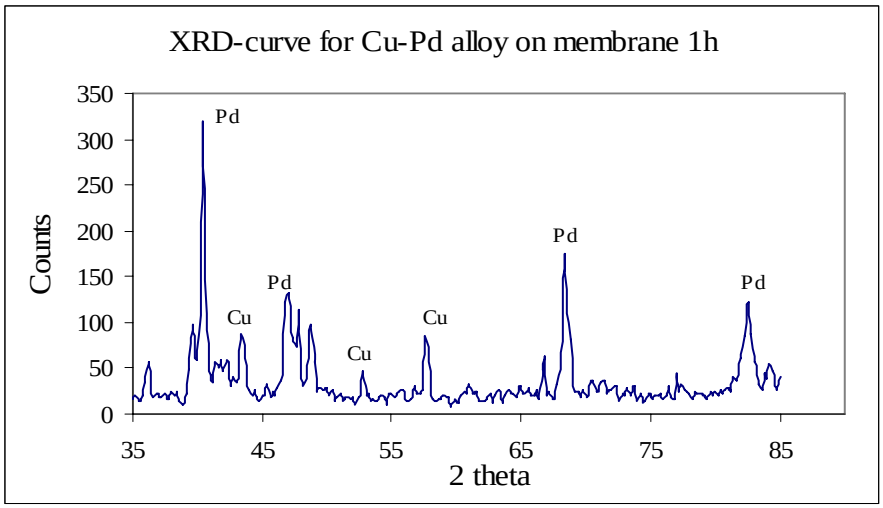

Figure 5.13 XRD pattern for a Cu on Pd film (membrane 1h)

Table 5.3 Structural data for Pd-Cu deposit (membrane 1h)

Angle	Counts	d space Å	Relative intensity
40.4	320	2.233	100
47.0	133	1.933	42
48.8	97	1.866	30
68.4	175	1.372	55
82.6	122	1.168	38

Membrane 2

The peak broadening effect after heat treatment can again be noticed in **Figures 5.14** and **5.15**. The same explanation can be given as in the case of membranes 1 and 1h.

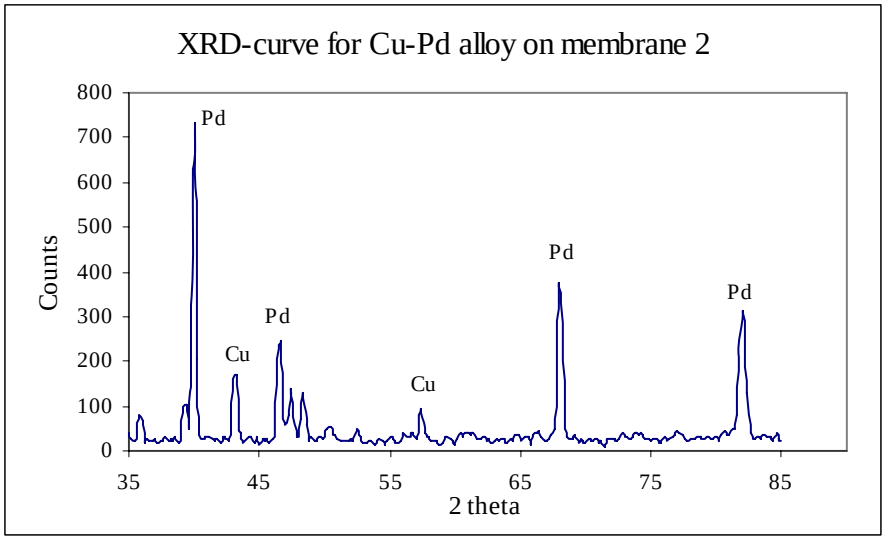

Figure 5.14 XRD pattern for a Cu on Pd film (membrane 2)

Table 5.4 Structural data for Pd-Cu deposit (membrane 2)

Angle	Counts	d space Å	Relative intensity
40.4	467	2.233	100
43.4	216	2.085	46
46.8	261	1.941	56
68.4	348	1.372	75
82.2	347	1.173	74

Membrane 2h

Table 5.5 Structural data for Pd-Cu deposit (membrane 2h)

Angle	Counts	d space Å	Relative intensity
40.4	300	2.233	100
43.4	154	2.085	51
46.8	151	1.941	50
68.4	162	1.372	54
82.6	142	1.168	47

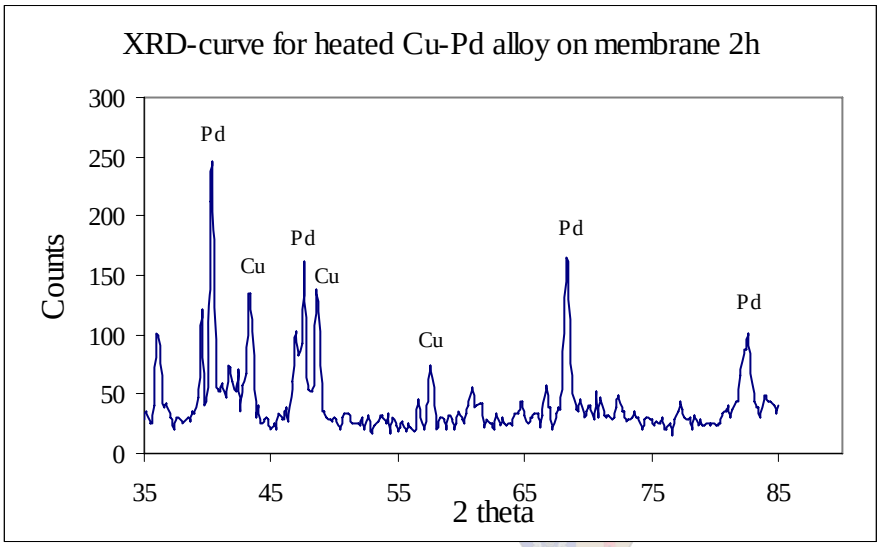

Figure 5.15 XRD pattern for a Cu on Pd film (membrane 2h)

Membrane 3

The copper intensity relative to the palladium intensity in **Figure 5.16** was higher for membrane 3 as compared to membranes 1 and 2, because of the higher copper concentration in the deposit. Again, after heat treatment alloying took place. After heat treatment, the intensities of the peaks are lower. This can be noticed in **Figure 5.17**. However, for this sample the peaks look broader than for the other heat treated samples. This is because the copper concentration for this sample is higher, which leads to additional small copper crystallites being formed and more peak broadening.

Table 5.6 Structural data for Pd-Cu deposit (membrane 3)

Angle	Counts	d space	Relative

		Å	intensity
40	731	2.254	100
43.2	171	2.094	23
46.6	243	1.949	33
68	376	1.379	51
82	311	1.175	43

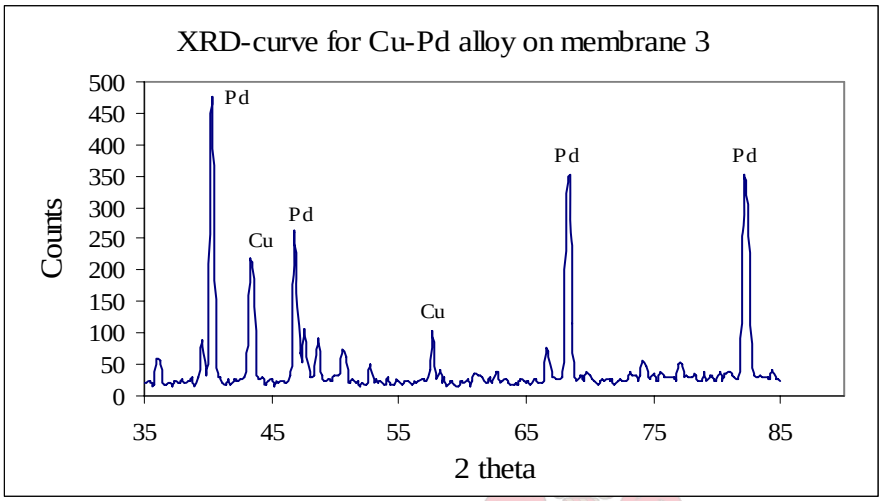

Figure 5.16 XRD pattern for a Cu on Pd film (membrane 3)

Membrane 3h

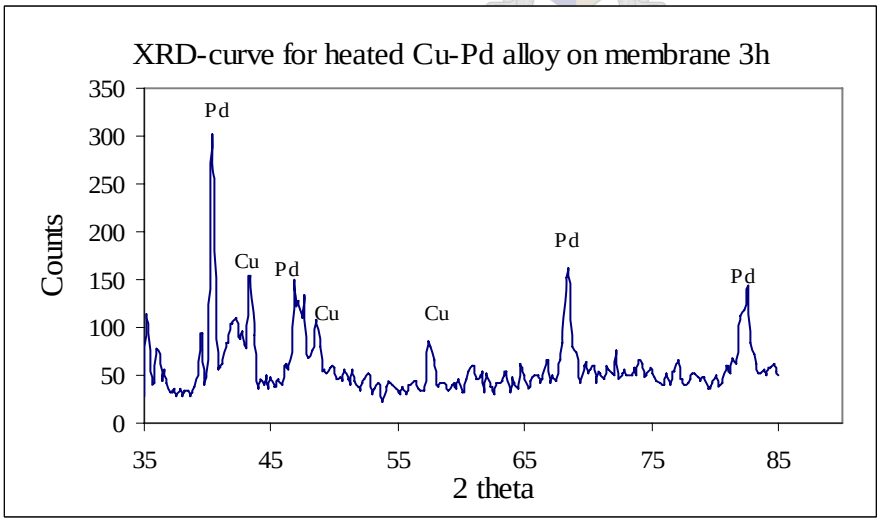

Figure 5.17 XRD pattern for a Cu on Pd film (membrane 3h)

Table 5.7 Structural data for Pd-Cu deposit (membrane 3h)

Angle	Counts	d space Å	Relative intensity

36	99	2.495	41
40.4	242	2.233	100
43.4	135	2.085	56
47.6	162	1.91	67
48.6	138	1.873	57
68.2	164	1.375	68
82.6	101	1.168	42

5.4 Particle-induced X-Ray emission (PIXE)

5.4.1 Results

Due to the length of time it took for one sample to be analysed and the cost of the analyses, it was decided to look at the concentration profiles of the heat treated samples and only one sample that was not heat treated. The 30 wt % Cu on Pd sample was analysed with and without heat treatment. The data are shown in appendix C.

Membrane 1h

Figure 5.18 shows the concentration profiles of the palladium and the copper on membrane 1h. **Figure 5.18** indicates a film thickness of 5 microns. The theoretical thickness of this film was 4.8 microns. The palladium concentration starts to decline rapidly from a thickness of 2.5 microns and stabilises after 6 microns. During the preparation of the disk for PIXE experiments the film could get smeared. This can lead to the formation of tails after a depth of 6 microns. From these graphs it is assumed that the film thickness can be determined at the point where the concentration of palladium reaches 100 000 ppm.

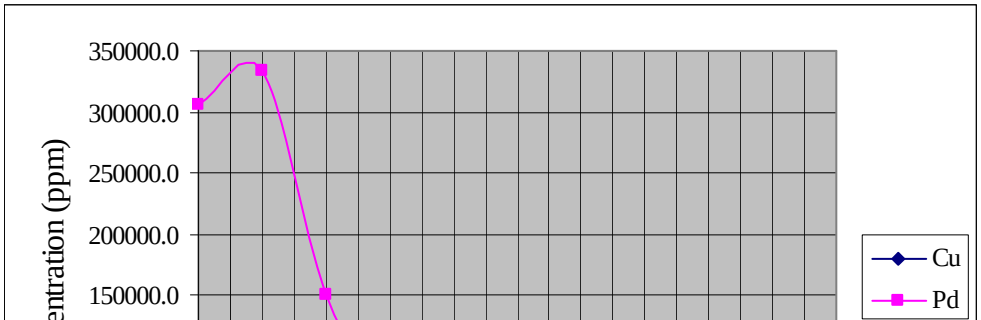

Figure 5.18 Concentration profile for Cu-Pd film (membrane 1h)

Membrane 2

From **Figure 5.19** it can be seen that the film thickness is 7 microns. This does not compare well with the theoretical value of 4.6 microns.

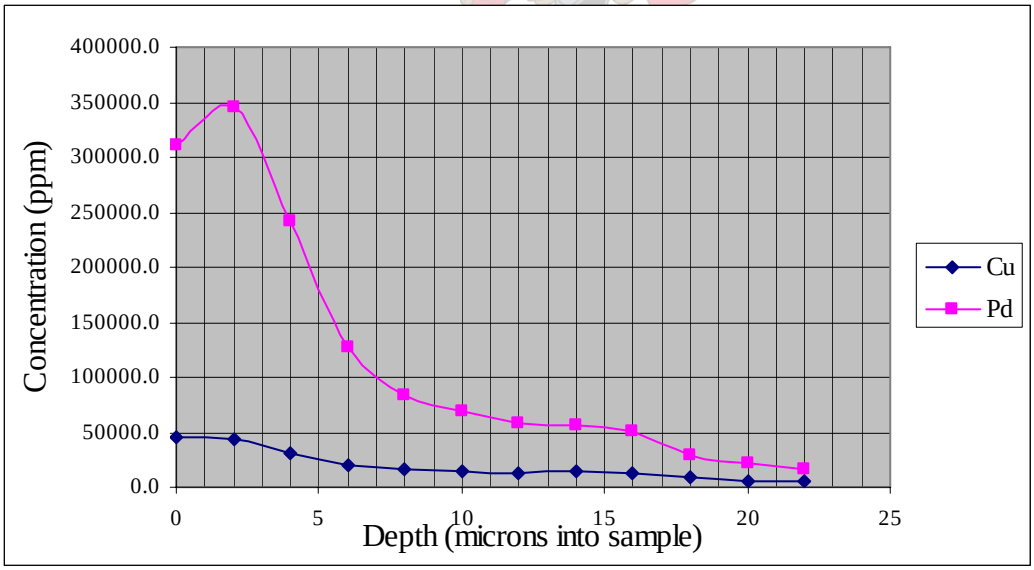

Figure 5.19 Concentration profile for Cu-Pd film (membrane 2)

Membrane 2h

From **Figures 5.19** and **5.20** it can be seen that the copper and palladium diffused deep into the pores of the membrane support. For the heat treated sample 40 000 ppm Pd and 10 000 ppm Cu is still present at a depth of 28 microns. Impregnation of metal deep into the pores of the support can occur during the plating process. This could also take place during the pre-treatment of the supports.

According to the concentration profile (**Figure 5.20**) the measured thickness is 6.5 microns. This also does not correlate well with the theoretical thickness of 4.6 microns. This indicates that the film thickness was not totally uniform in thickness across the membrane support, because the theoretical value assumes a uniform and dense film thickness, and no penetration into the pores. **Figures 5.1** to **5.3** confirmed these defects in the film.

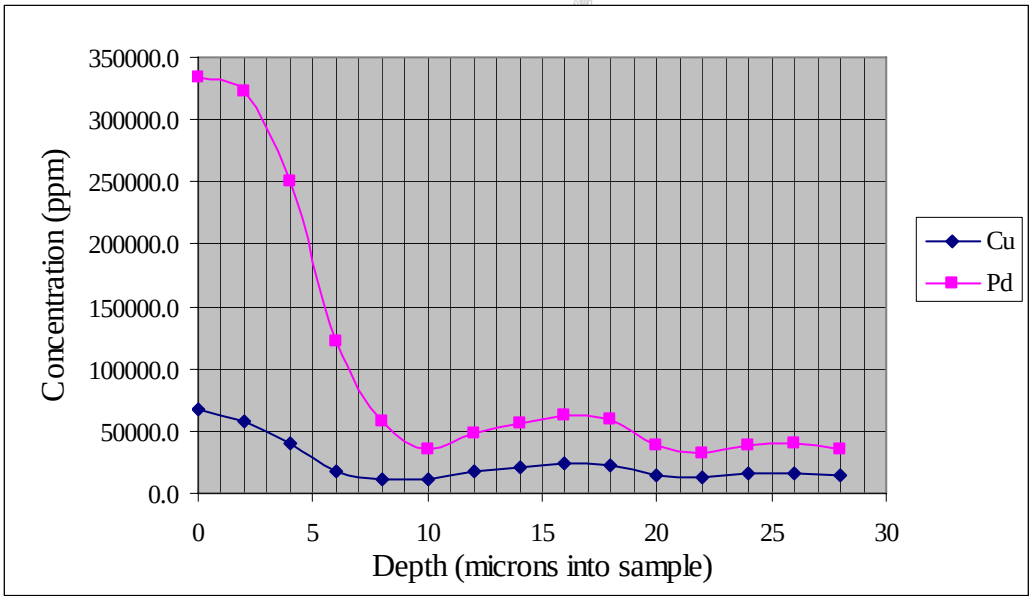

Figure 5.20 Concentration profile for Cu-Pd film (membrane 2h)

Membrane 3h

The film thickness, according to **Figure 5.20**, is about 4.8 microns. This correlates well with the theoretical film thickness is 4.6 microns. The high concentration of the copper on the surface can be seen in **Figure 5.20**. From about 2 microns the palladium

concentration starts declining and at the outer surface of the film the copper concentration already starts declining. At a depth of 8 microns depth the palladium concentration is 10 000-20 000 ppm.

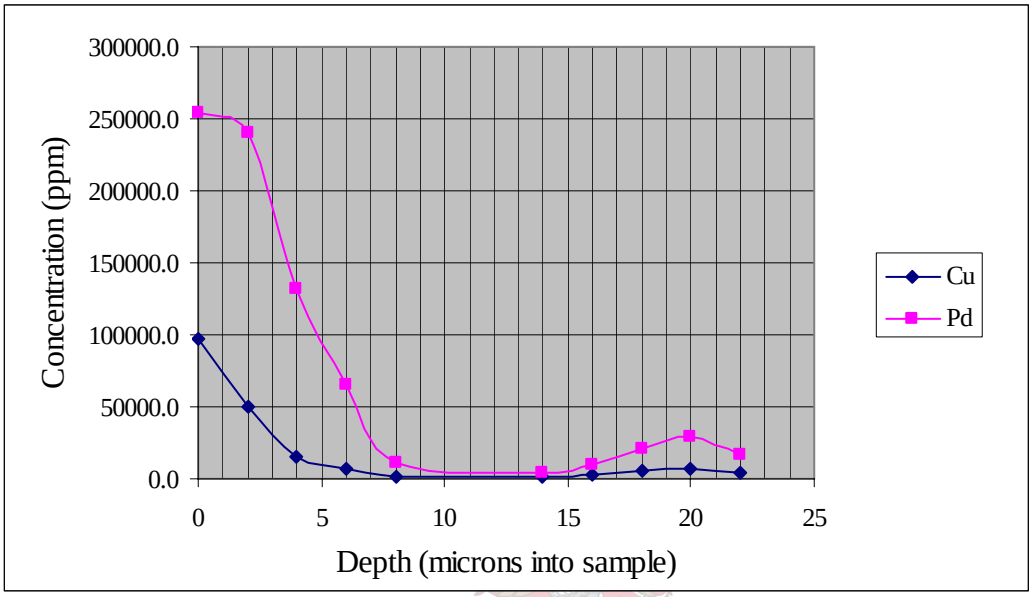

Figure 5.21 Concentration profile for Cu-Pd film (membrane 3h)

5.5 Summary

This chapter focused on the characterisation of copper-palladium films deposited on alumina membrane supports supplied by Atech. SEM photographs showed that the films were not of a dense nature and that the pore size of the Atech membranes was doubtful. These photographs were compared to coatings on SCT membranes, which showed a much more even film structure than for the Atech membranes. SEM results also illustrated that the films on Atech supports were not of uniform thickness across the membrane support. This characteristic was confirmed by the PIXE results. From the PIXE results it can be seen that the copper and palladium atoms penetrated deep into the pores of the membrane during film preparation. XRD results revealed that the heat treating process led to smaller palladium and copper crystallites being formed.

6. Catalytic investigation of the dehydrogenation of 2-propanol

6.1 Introduction

The dehydrogenation of 2-propanol to acetone in a fixed-bed reactor over different catalysts was investigated. The fixed-bed reactor was used to find the most suitable catalyst for the dehydrogenation of isopropanol in an alumina membrane reactor. The performance of the fixed-bed reactor will be presented. A short discussion of the properties of 2-propanol and acetone will also be given.

6.2 Properties of isopropanol

Isopropanol takes part in reactions typical of an active secondary alcohol. It can be dehydrogenated, oxidised, etherified, aminated and halogenated. Secondary alcohols are more active than primary alcohols. Isopropanol can be catalytically dehydrogenated by a wide variety of catalysts at high yields (75-95 mol %) in an endothermic vapour-phase process. At high operating temperatures and moderate pressures (2 atm.), acetone yields of up to 90 mol % can be achieved (Kirk-Othmer, 1978). The best catalysts usually contain Cu, Cr, Zn, and Ni either alone, as oxides, or in combinations on inert supports (Addy, 1961). Small amounts of by-products, e.g. propylene, diisopropyl ether, mesityl oxide, acetaldehyde and propionaldehyde, form by dehydration, condensation and oxidation. Even though these by-products are formed, the selectivity remains high.

The production of 2-propanol in the U.S. in 1981 was $1\ 285\times10^3$ tons (Directory of Chemical Producers, 1981). As an alcohol, 2-propanol was second in commercial production to methanol. The boiling point of isopropanol is 4 °C higher than ethanol and isopropanol possesses similar solubility properties, which accounts for the competition between these two products in many solvent applications. Isopropanol is widely used as a chemical intermediate, for example in reductive amination to produce monoisopropyl amine (for herbicide and pesticide production) and as a source of isopropyl acetate.

The use of 2-propanol to manufacture acetone has decreased dramatically in recent years. There is only one acetone plant using this process left in the United States (Ullman, 1993). However, since the cumene route to phenol provides equal amounts of phenol and acetone, a strong demand for acetone relative to phenol can increase the need for acetone production from 2-propanol.

6.3 Properties of acetone

Acetone shows the typical reactions of saturated aliphatic ketones. Acetone can be reduced to 2-propanol and pinacol if it is exposed to a reducing agent. It is also subjected to many condensation reactions.

Of the aliphatic ketones, acetone is the most important one. It is applied as an intermediate in the synthesis of methyl methacrylate, bisphenol A, diacetone alcohol and other products. It is also widely used as a solvent for paints, varnishes and lacquers. It is used as a component in thinners and as a spinning solvent in the manufacture of cellulose acetate. Feeds consisting of either cumene, isopropanol or propene account for over 95% of the acetone produced worldwide. **Table 6.1** shows the world acetone capacity (Kirk-Othmer, 1978).

Table 6.1 Acetone World Capacity (in kilotons), (Kirk-Othmer, 1978)

Location	1975 (estimated)	1980(predicted)
United States	1149	1302
Remainder of Western Hemisphere	89	196
Eastern Europe	215	243
Western Europe	902	1003
Japan	276	396
Remainder of Asia	31	34

6.4 Discussion of results

Figures 6.1 to **6.26** show the experimental results of the dehydrogenation of 2-propanol in a fixed-bed reactor. The reactions were performed at different temperatures and with different feed flow rates. The apparatus described in the experimental section was used for all reactions (section 3.3). Al_2O_3, MgO and SiO_2 supports were used with different copper percentages impregnated on these supports. Detailed results for all catalysts are shown in appendix E. The particle size of all the supports used was in the range of 850-1180 microns. For the Al_2O_3 and SiO_2 supported catalysts, the BET surface area and the copper surface area were also determined. These values can be used to explain the different experimental dehydrogenation results obtained. The following definitions were used:

$$Product\ yield = \frac{moles\ isopropanol\ converted\ to\ product}{total\ moles\ isopropanol\ \ fed} \tag{6.1}$$

$$Total\ isopropanol\ conversion = \frac{total\ moles\ isopropanol\ reacted}{total\ moles\ isopropanol\ \ fed} \tag{6.2}$$

$$Product\ selectivity = \frac{moles\ isopropanol\ converted\ to\ product}{total\ moles\ isopropanol\ reacted} \tag{6.3}$$

6.4.1 Al_2O_3 supports

This was the first type of support used for testing. Three different catalysts were prepared for the reaction in the fixed-bed reactor. Three copper percentages (ranging from 13-24 wt % Cu) were chosen. The total surface areas (determined using BET) are presented in **Tables 6.3** to **6.5** for each catalyst. The different catalysts that were used are listed in **Table 6.2**.

When 2-propanol reacted over Cu/Al_2O_3 catalysts, mainly propene formed. The by-products were acetone and diisopropyl ether. Graphs of the propene yield were constructed to illustrate the effect temperature had on this reaction. The following equation describes the reaction:

$$CH_3CHOHCH_3 \prod CH_3\text{-}CH{=}CH_2 + H_2O \qquad (6.4)$$

Table 6.2 Cu/Al_2O_3 catalysts used for the dehydrogenation of 2-propanol

wt % Cu impregnated	Catalyst name
13.2	Catalyst G
18.5	Catalyst A
24	Catalyst B

Catalyst G:

There was a decrease in propene yield above 215 °C for the flow of 1.6 ml/h (liquid hourly space velocity (LHSV) of 0.64 h^{-1}) (**Figure 6.1**). The reason for that behaviour is not clear at this stage. This might be an analytical error. As indicated in **Figures 6.3** the total conversion of isopropanol also decreased sharply at this point. Thus the lower total isopropanol conversion caused a lower propene yield. The propene yield for a flow rate of 3.2 ml/h (LHSV of 1.27 h^{-1}) increased sharply from 180-220 °C and increased gradually from 220-300 °C. The flow rate of 3.2 ml/h achieved the best yields to propene.

It can be seen in **Figure 6.1** that both flow rates of 6.4 (LHSV of 2.55 h^{-1}) and 1.6 ml/h could not achieve higher yields than the flow rate of 3.2 ml/h in the low temperature range. At higher flow rates the total propene conversion decreased due to a shorter catalyst contact time. At a lower flow rate the propene yield also did not reach higher values due to the long residence time which increased the formation of by-products. This can be seen in **Figure 6.2** where the selectivity for the flow rate of 1.6 ml/h is low.

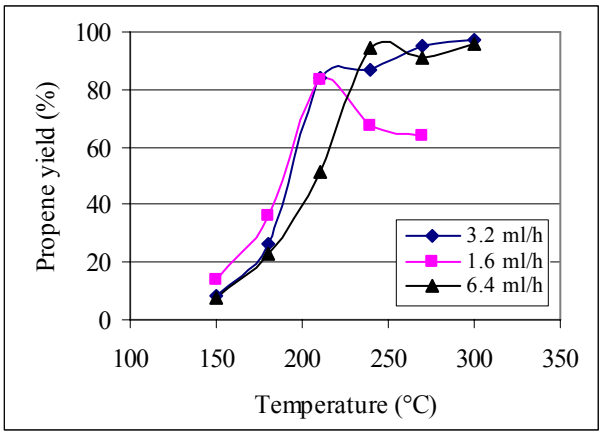

Figure 6.1 Propene yield (Catalyst G)

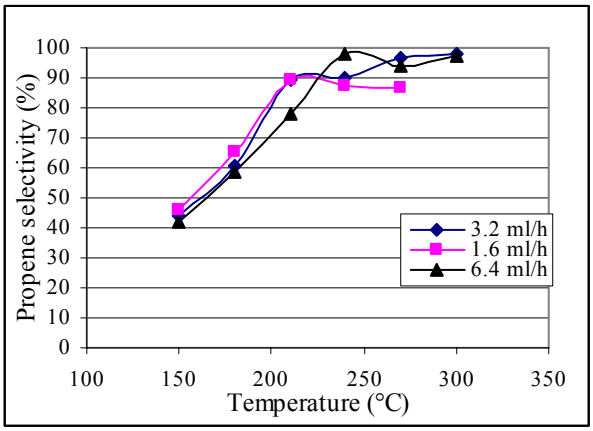

Figure 6.2 Propene selectivity (Catalyst G)

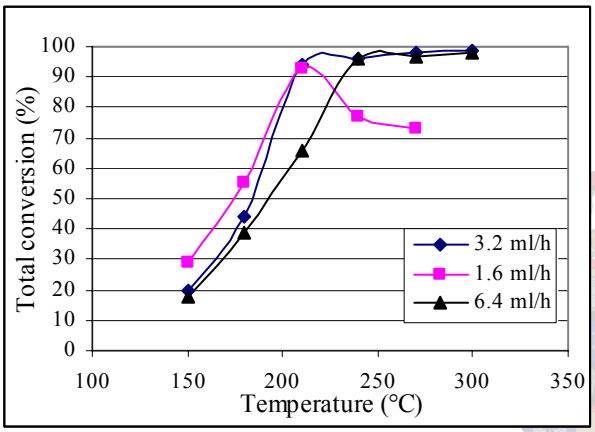

Figure 6.3 Total conversion of isopropanol (Catalyst G)

Table 6.3 Surface area for catalyst G (Al_2O_3)

Cu %	BET area (m^2/g)
13.2	170.8

Catalyst A:

This catalyst showed very good yields to propene. In **Figure 6.4** it can be seen that at 220 °C yields exceeded 95% for flows of 3.2 and 1.6 ml/h. An increase in temperature, increased the propene yield. From 220 to 300 °C, the yields decreased marginally. Between 220 and 300 °C a flow rate of 6.4 ml/h did not result in high yields to propene. This is because of the short contact time at the higher feed rate.

From all the catalysts tested, this catalyst showed the best results for the dehydration of isopropanol. A reaction of this type could be performed at 220 °C to achieve high yields. The lower flow rates resulted in much better yields than the higher flow rates, because of the higher catalyst contact time and lower LHSV's at lower flow rates.

Table 6.4 Surface area for catalyst A (Al_2O_3)

Cu %	BET area (m^2/g)
18.5	139.1

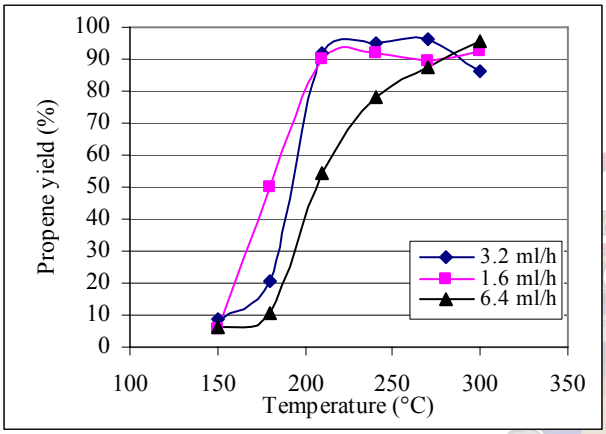

Figure 6.4 Propene yield (Catalyst A)

Catalyst B:

The flow rate of 3.2 ml/h resulted in almost the exact yields as for catalyst A. At temperatures exceeding 220 °C, the yield stayed constant above 98% (**Figure 6.5**). For a flow rate of 1.6 ml/h, the propene yield gradually increased from about 20% to 80% over the entire temperature range. The flow rate of 1.6 ml/h resulted in poorer propene yields. The selectivity towards propene was the highest for the flow rate of 3.2 ml/h where the selectivity was 97.1% at 240 °C (**Figure 6.6**). The selectivity at high temperatures for the flow rate of 1.6 ml/h declined slightly, which indicates that by-products started forming at that flow rate. The selectivity towards propene was also high for the flow rate of 6.4 ml/h.

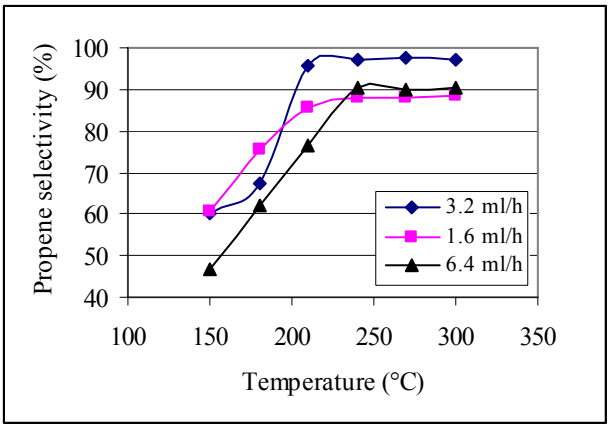

Figure 6.5 Propene yield (Catalyst B)

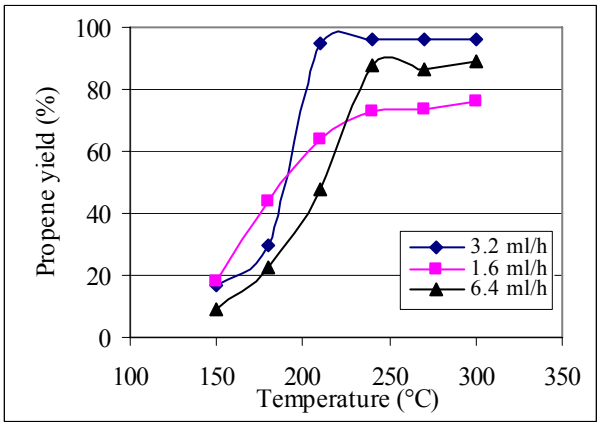

Figure 6.6 Propene selectivity (Catalyst B)

Table 6.5 Surface area for catalyst B (Al_2O_3)

Cu %	BET area (m^2/g)
24	120.0

6.4.1.1 The effect of copper and catalyst surface area

It should be noted that the determination of the Cu surface areas using chemisorption was difficult and gave several problems. The results were not reliable and also were not reproducible. During the reduction of the catalyst in H_2 before analysis several problems were encountered. Some of the problems were bonding between the Cu species and the support sites, the formation of amorphous phases and interactions between different Cu species. Poor reduction thus occurred. For the purpose of this study no other methods were used to determine the Cu surface areas.

Another method for determining Cu surface areas that can be used is N_2O titration. Sivaraj and Kantarao (1988a) explained the N_2O titration method. The nitrous oxide decomposes according to the following equation:

$$N_2O\ (gas) + 2Cu_s \rightarrow (Cu_s)_2O + N_2\ (gas) \qquad (6.5)$$

The metallic surface area (S_H) is determined from

$$S_H = n_m X_m / n_s \quad (6.6)$$

where n_m is the total amount of nitrous oxide molecules that decompose, X_m is the chemisorption stoichiometry and n_s is the amount of copper metal atoms per unit surface area ($1.47*10^{19}$ m^{-2}). The catalyst is first reduced in hydrogen for 5 hours at 250 °C, evacuated (to 10^{-6} Torr) for 2 hours and then reacted with N_2O at 200 Torr and 90 °C. The reaction does not cause a pressure change. After 5 hours of reaction, the remaining N_2O is frozen out in a nitrogen trap and the pressure difference between the initial pressure and final pressure is used to calculate the amount of N_2O that reacted.

Figure 6.7 illustrates the effect that the total catalyst area had on propene yield. These values are yields at a temperature of 210 °C and a flow rate of 3.2 ml/h. Alumina is an acidic support and the deposited copper sites reduced the number of available acidic sites on the catalyst. The result is a decline in the yield of the dehydration product (propene). According to **Figure 6.7** the yield decreased with increasing total surface area. This indicates that the propene yield increased with an increase in Cu concentration. The results from **Figure 6.7** and the fact that the Cu reduces the number of available acidic sites are thus contradicting. Reddy et al. (1999) illustrated that the interaction between copper and alumina has a significant effect on dehydration reactions. This study showed that by supressing the interaction between copper and alumina decreases the conversion to the dehydration product. This indicates that the higher copper concentration led to more interaction between the copper and alumina. This higher interaction between the copper and alumina is favourable conditions for the formation of propene. The conclusion that can be reached is that the combination of Al_2O_3 and Cu is what influences the propene formation. In **Figure 6.10** it also shows low total isopropanol conversion at high Cu concentrations which indicates this situation.

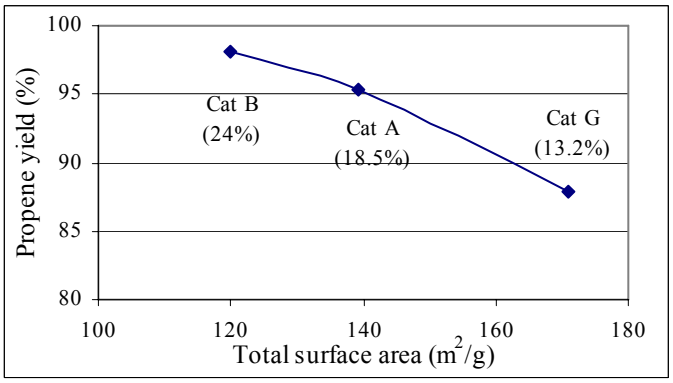

Figure 6.7 Propene yield as a function of total catalyst surface area

In **Figure 6.8** it can be seen that the copper surface area decreases with an increase in copper concentration. According to **Figure 6.9** the total surface area decreased from 175 m^2/g at 8.8 wt Cu % to 120 m^2/g at 24 wt Cu %. This can be explained by the fact that the copper atoms filled the pores of the support as it gets more concentrated with copper.

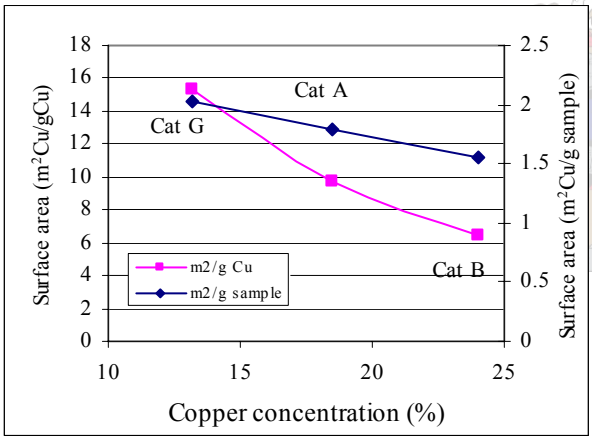

Figure 6.8 Copper surface area as a function of copper concentration

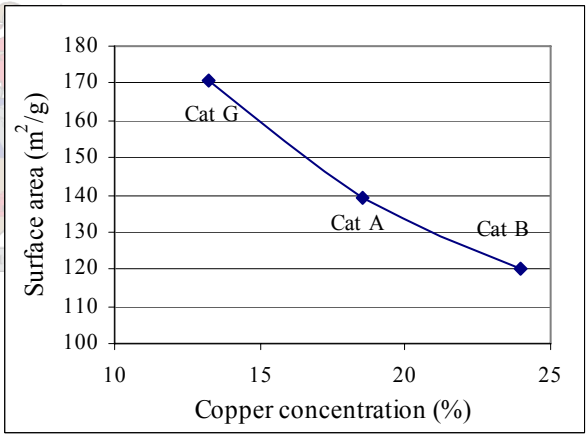

Figure 6.9 Al_2O_3 surface area as a function of copper concentration

6.4.1.2 Total conversion of isopropanol and the conversion to the main by-product

Figures 6.10 and **6.11** summarise the results achieved for the reaction of isopropanol over alumina catalysts. **Figure 6.10** shows the total conversion of isopropanol as a function of copper concentration and reaction temperature. High yields were achieved between 6 and 14 wt % copper and at temperatures between 250 and 290 °C. Very low

conversion of isopropanol were achieved below 135 °C. **Figure 6.11** shows the main by-product (acetone) yield as a function of both copper concentration and reaction temperature. The highest acetone yield was achieved at the lowest temperature (120 °C) and the lowest copper concentration (6%).

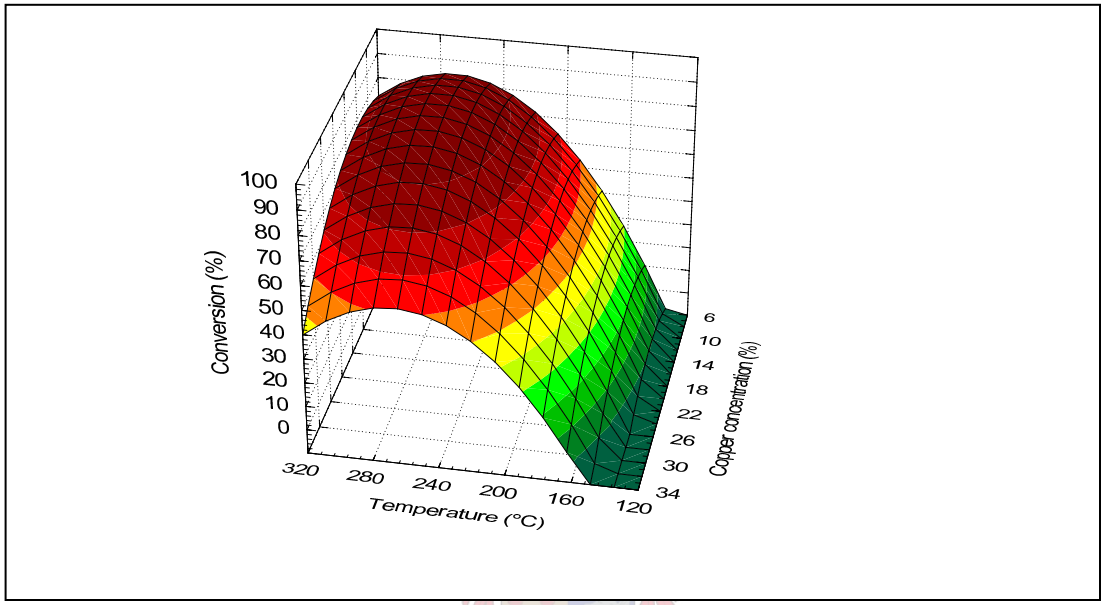

Figure 6.10 Total conversion of isopropanol over Al_2O_3 catalyst as a function of temperature at a flow rate of 3.2 ml/h

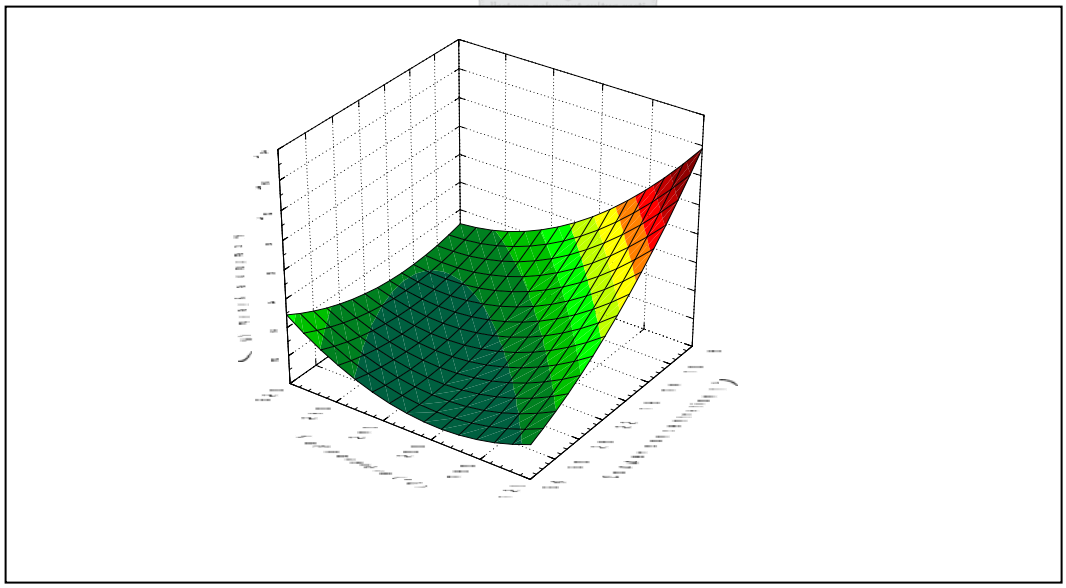

Figure 6.11 Acetone yield over Al_2O_3 catalyst as a function of temperature at a flow rate of 3.2 ml/h

6.4.2 Magnesium oxide supports

Four different catalysts were prepared for the reaction in the fixed-bed reactor. The BET surface areas were determined for these catalysts, but not the Cu surface areas. The different catalysts that were used are named as in **Table 6.6**. **Figures 6.12** to **6.20** show the acetone yield and acetone selectivity as a function of reaction temperature for the four different MgO catalysts. The main product formed over this catalyst was acetone. The by-products that formed were propene and a small amount of 4-methyl pentanone. The following equation demonstrates the main reaction:

$$CH_3CHOHCH_3 \prod C_3H_6O + H_2 \qquad (6.5)$$

Table 6.6 MgO catalysts used

wt % Cu impregnated	Catalyst name	BET (m^2/g)
0	Catalyst A	27.4
10.3	Catalyst C	15.0
16.9	Catalyst D	9.3
24.9	Catalyst E	3.6

Catalyst A:

None of the flow rates indicated in **Figure 6.12** resulted in yields higher than 30%. Acetone yields were low below 300 °C. Very little reaction took place at these temperatures for all flow rates. The selectivity towards acetone varied between 80% and 47% in the temperature range 320-390 °C as presented in **Figure 6.13**. This low selectivities indicates that a high concentration of propene was formed at high temperatures. The reason for this behaviour is because the support was not impregnated with copper, which catalyses the dehydrogenation of isopropanol to acetone. A flow rate of 3.2 ml/h (LHSV of 1.27 h^{-1}) resulted in the highest acetone yields.

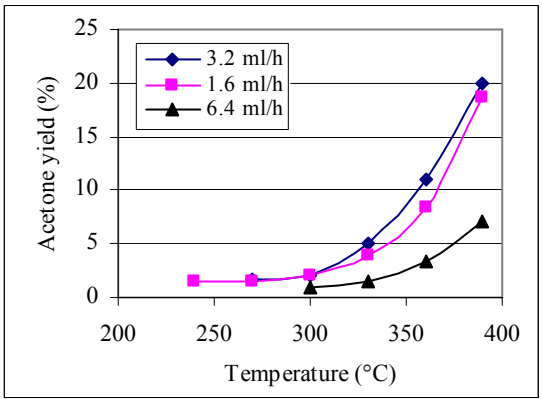

Figure 6.12 Acetone yield (Catalyst A)

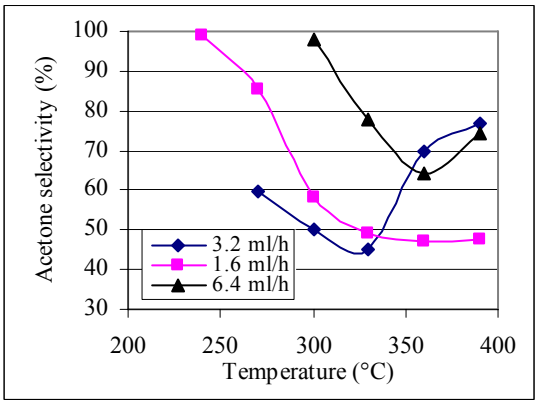

Figure 6.13 Acetone selectivity (Catalyst A)

Catalyst C:

From **Figure 6.14** it can be seen that the flow rate of 1.6 ml/h (LHSV of 0.64 h^{-1}) gave the highest acetone yield for this catalyst. Yields of up to 90% were obtained. The other two flow rates could not achieve these results. The acetone yield dropped due to a shorter catalyst contact time for the higher flow rates of 3.2 and 6.4 ml/h (LHSV of 2.55 h^{-1}). The reaction could not go to completion for the shorter contact time. There was a large difference in the results of catalyst C and catalyst A. When copper is deposited on the support, the propene formation decreased and the acetone formation improved. This indicates that the copper catalyses the reaction and is more active than pure MgO. As indicated in **Table 6.6** the copper content also has an effect on the BET surface area of the catalyst. From **Figure 6.15** it can be seen that the selectivity towards acetone was much better than for catalyst A. The selectivity gradually decreased with an increase of temperature.

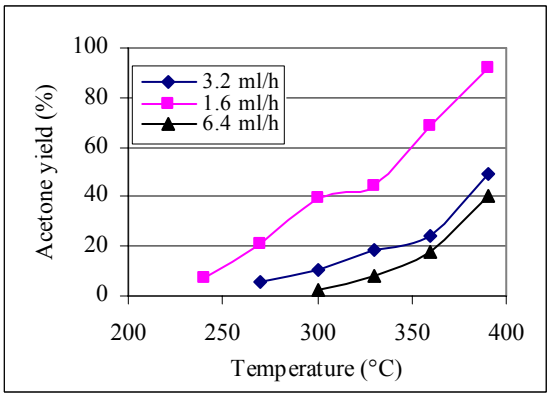

Figure 6.14 Acetone yield (Catalyst C)

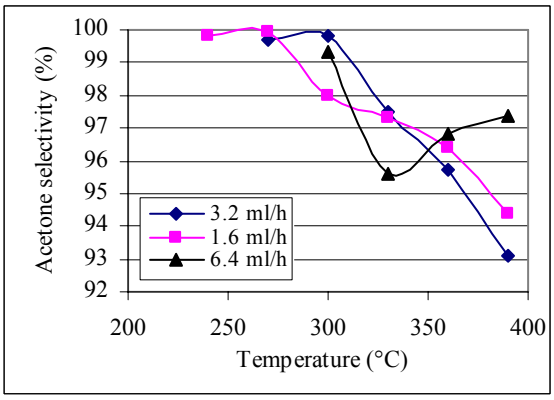

Figure 6.15 Acetone selectivity (Catalyst C)

Catalyst D:

Of the MgO catalysts, this catalyst gave the best results. According to **Figure 6.16**, a flow rate of 1.6 ml/h resulted in the highest yields. The reasons for this are the same as discussed previously at catalyst C. Yields of up to 95% were obtained. A flow rate of 3.2 ml/h resulted in almost the same yields, but at much higher temperatures. Acetone yield and total conversion data **(Figures 6.16** and **6.18)** suggest that an optimum copper surface area was obtained for catalyst D (i.e. for 16.9 wt % Cu). Due to the low surface area of the catalyst (**Table 6.6**), chemisorption analysis was not performed to confirm this. In **Figure 6.17** it can be seen that the selectivity towards acetone above 300 °C was between 94.5% and 99.5%, which is very good.

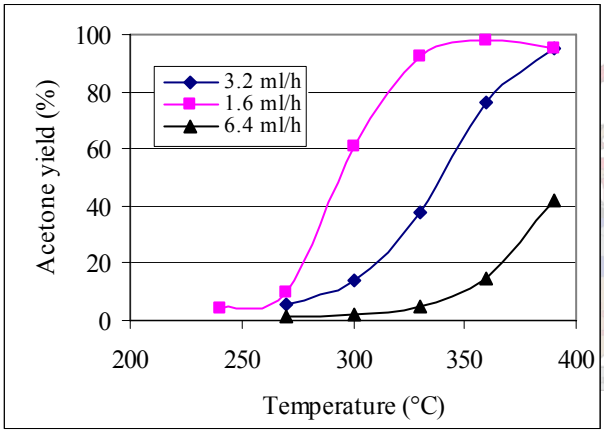

Figure 6.16 Acetone yield (Catalyst D)

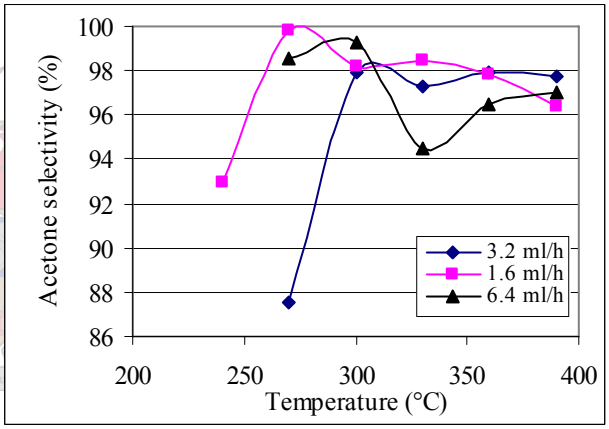

Figure 6.17 Acetone selectivity (Catalyst D)

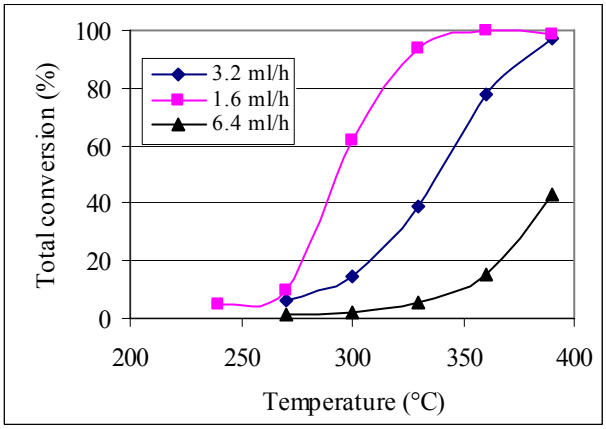

Figure 6.18 Total conversion to acetone (Catalyst D)

Catalyst E:

As in the case of the previous catalysts, the flow rate of 1.6 ml/h resulted in the best results. Yields of 90% could be obtained with this catalyst (**Figure 6.19**). The reaction rate for this catalyst was however slower than that of catalyst D, due to the higher copper content and lower BET surface area. The selectivity also decreased with an increase in temperature as shown in **Figure 6.20**.

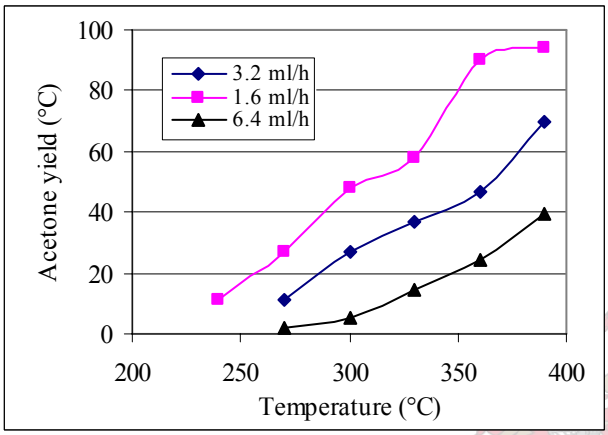

Figure 6.19 Acetone yield (Catalyst E)

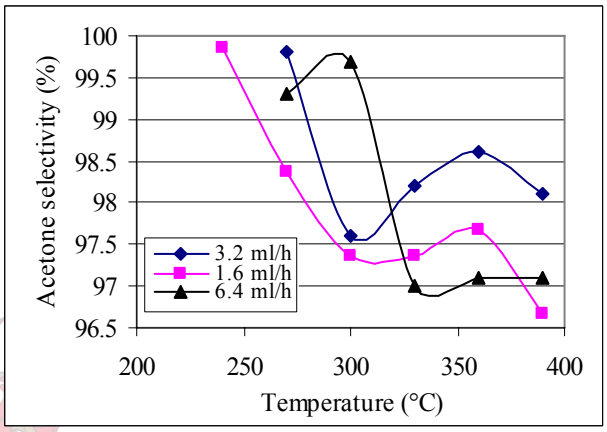

Figure 6.20 Acetone selectivity (Catalyst E)

6.4.2.1 The effect of catalyst surface area

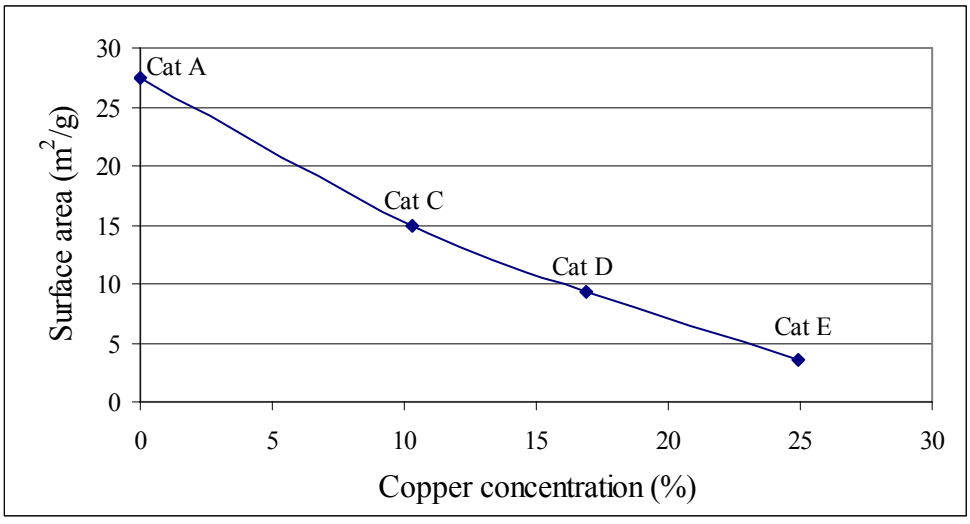

Figure 6.21 MgO surface area as a function of copper concentration

From **Figure 6.21** it can be seen how the total surface area declines with an increase in copper concentration. Compared to the surface area of the alumina catalysts (**Figure 6.9**), these surface areas are much lower. This explains the poor results achieved by the MgO catalysts when comparing the product yield of the two catalysts with each other.

6.4.2.2 Total conversion of isopropanol and the conversion to the main by-product

Figures 6.22 and **6.23** show total isopropanol conversion and propene yield over the entire range of copper concentrations. According to **Figure 6.22**, very high conversions were reached in the temperature range 380-420 °C for catalysts which had copper loadings of between 18 and 25%. It can be seen in **Figure 6.23** that 18% propene yield was obtained at the highest temperature of 420 °C. The maximum by-product formation was observed with a pure MgO catalyst. The copper atoms on the MgO thus suppress propene formation at high temperatures.

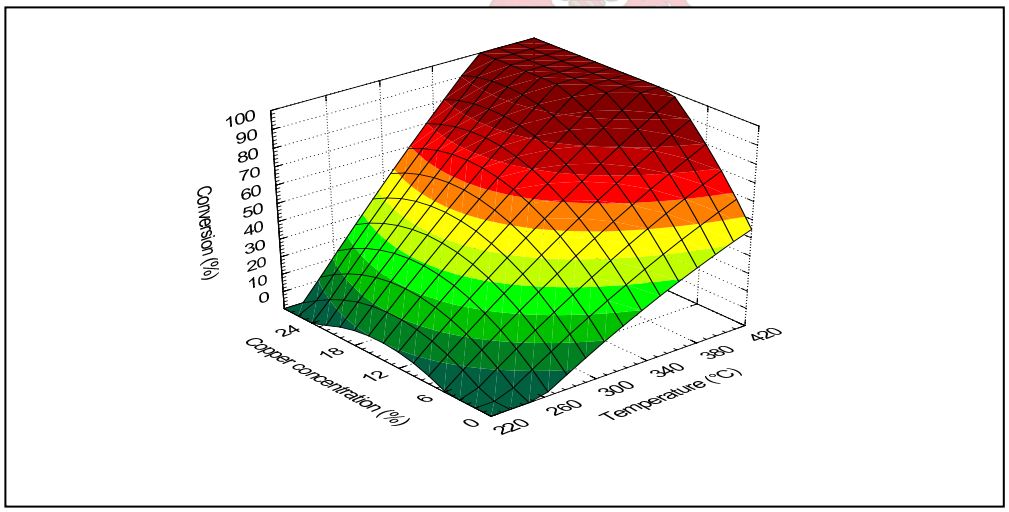

Figure 6.22 Total conversion of isopropanol over MgO catalyst as a function of temperature at a flow rate of 3.2 ml/h

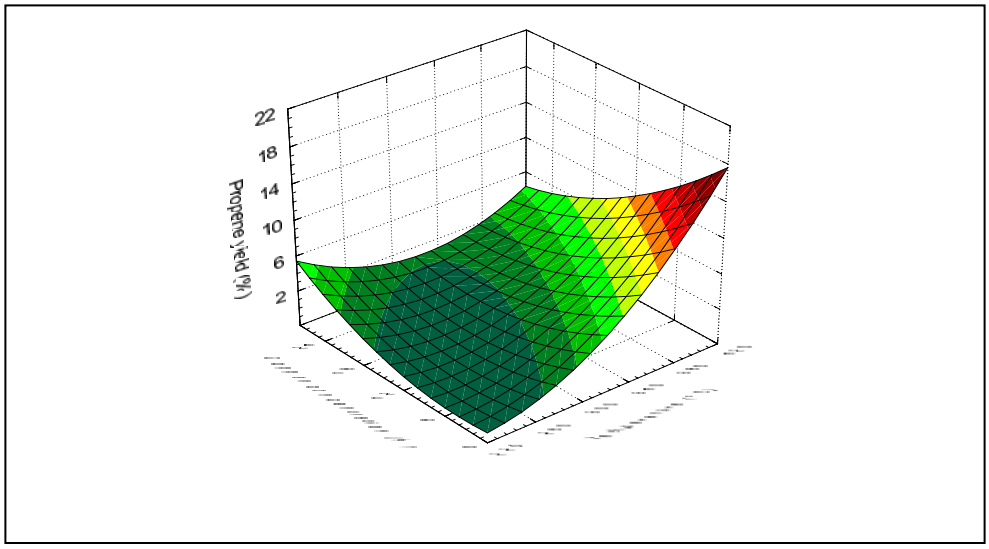

Figure 6.23 Propene yield over MgO catalyst as a function of temperature at a flow rate of 3.2 ml/h

6.4.3 SiO_2 supports

Ten different catalysts were made as listed in **Table 6.7**.

Table 6.7 SiO_2 catalysts used for reactions

wt % Copper impregnated on SiO_2	Name
0	Catalyst A
4.2	Catalyst F
9.2	Catalyst B
11.7	Catalyst G
15	Catalyst H
18.6	Catalyst C
27.7	Catalyst D
9.2 (150-300 microns)	Catalyst Ba
9.1 (850-1180 microns)	Catalyst Bb
9.1 (3 mm)	Catalyst Bc

Figures 6.24 to **6.42** show the acetone yield and selectivities as a function of reaction temperature for the ten different silica catalysts used. To determine what the influence of particle size is on acetone production, three different particle size fractions were made. The surface areas of these different fractions were not determined.

Catalyst A:

No acetone was formed for the pure silica catalyst. The main product was propene. According to **Figure 6.24** very low yields were obtained for a feed flow rate of 6.4 ml/h LHSV of 2.55 h^{-1}). The flow rate of 1.6 ml/h resulted in the highest yields, due to the longer catalyst contact time. For both the flow rates 1.6 and 3.2 ml/h (LHSV's of 0.64 and 1.27 h^{-1}), high yields were obtained at temperatures above 360 °C. The surface area for this catalyst was not determined because the catalyst did not give good results.

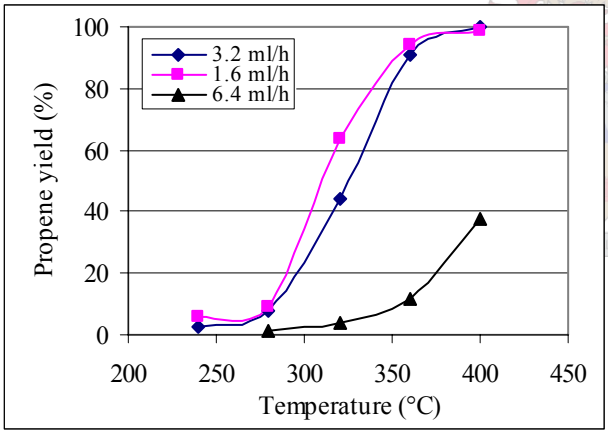

Figure 6.24 Propene yield (Catalyst A)

Catalyst F:

From **Figure 6.25** it can be seen that this catalyst did not result in very high yields to acetone, due to the low copper content (4.7%). At 350 °C, the average yield was 33% which was poor compared to the other catalysts. As indicated in **Figure 6.26** the selectivity to acetone increases with an increase in temperature. From a temperature of 300-440 °C the selectivity increases from between 70-75% to 80-90%. Of all the

catalysts tested this one showed the poorest acetone selectivities. Although the BET surface area of this catalyst was the highest, it performed the worst. Although this catalyst delivered the worst results, it produced more acetone than catalyst A, due to the fact that it was impregnated with copper. This indicates that the copper catalyses the dehydrogenation to acetone. **Tables 6.8** to **6.13** show the total catalyst surface areas for the different silica catalysts.

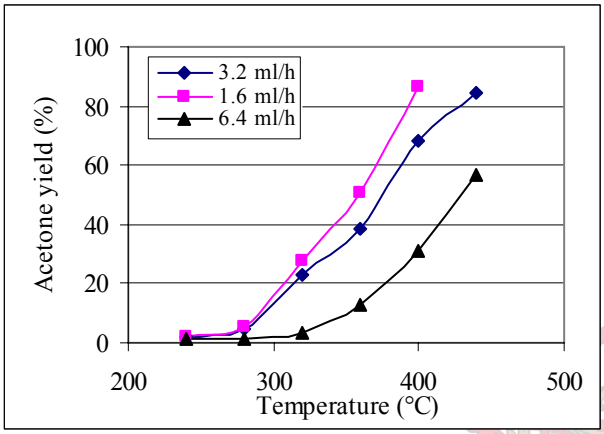

Figure 6.25 Acetone yield (Catalyst F)

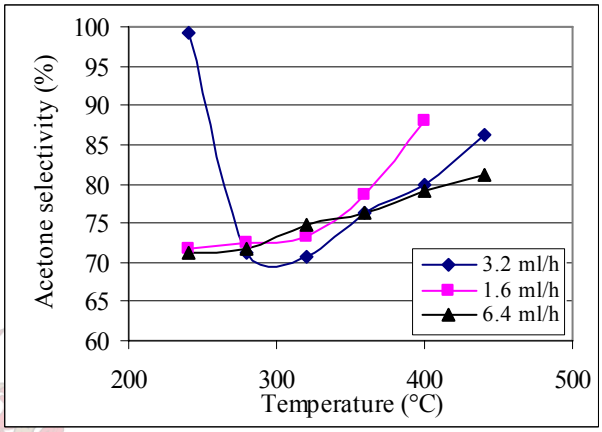

Figure 6.26 Acetone selectivity (Catalyst F)

Table 6.8 Surface area for catalyst F (SiO_2)

Cu %	BET area (m^2/g)
4.2	378

Catalyst B:

Figure 6.27 indicates that above a temperature of 350 °C, acetone yields of 98% were obtained for a feed flow rate of 3.2 and 1.6 ml/h. At 325 °C, a flow rate of 1.6 ml/h resulted in a conversion of 90%. Of the catalysts investigated, this catalyst was found to work the best for the dehydrogenation of 2-propanol. The smaller flow rate resulted in higher yields, due to the longer catalyst contact time. As shown in **Figure 6.29** and discussed in sections 6.4.1 and 6.4.2, the total conversion and acetone yield decreased with an increase in LHSV's and flow rate. The total conversion of isopropanol showed

very high values (99.9% at 390 °C). As shown in **Figures 6.27** and **6.28,** the selectivity towards acetone increased and the acetone yield increased as the temperature increased. For all the silica catalysts, this one showed the best selectivity towards acetone. Catalyst B was used for reactions in the membrane reactor.

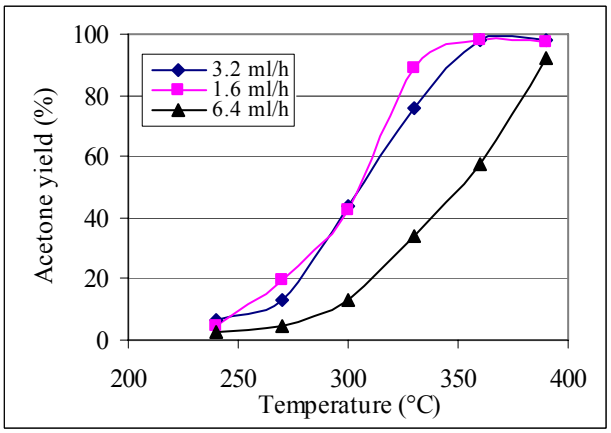

Figure 6.27 Acetone yield (Catalyst B)

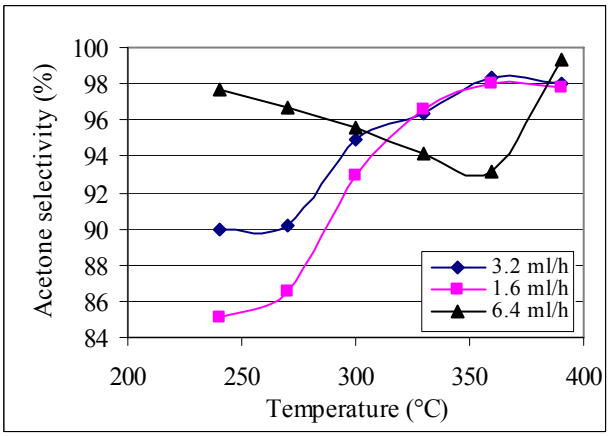

Figure 6.28 Acetone selectivity (Catalyst B)

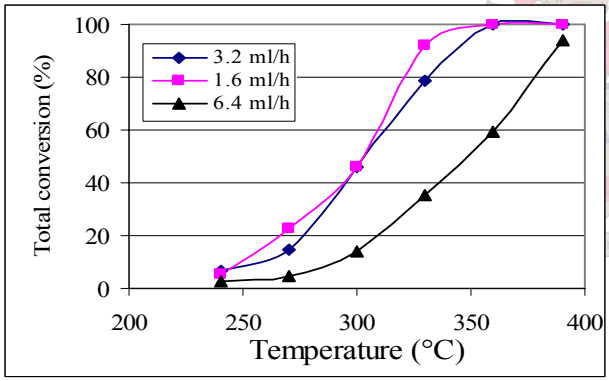

Figure 6.29 Total isopropanol conversion (Catalyst B)

Table 6.9 Surface area for catalyst B (SiO_2)

Cu %	BET area (m^2/g)
9.2	352.7

Catalyst G:

The flow rate of 3.2 and 1.6 ml/h resulted in high yields for this catalyst. The other flow rate resulted in low yields at temperatures below 350 °C, due to shorter catalyst contact

time. The selectivity values above 300 °C varied between 80% and 90%. This is lower than that of Catalyst B. This means more by-products formed with this catalyst with the higher copper concentration. With the previous catalyst it was shown that the copper catalyses the conversion of isopropanol to acetone, but as shown with this catalyst too much, will again decrease the acetone selectivity.

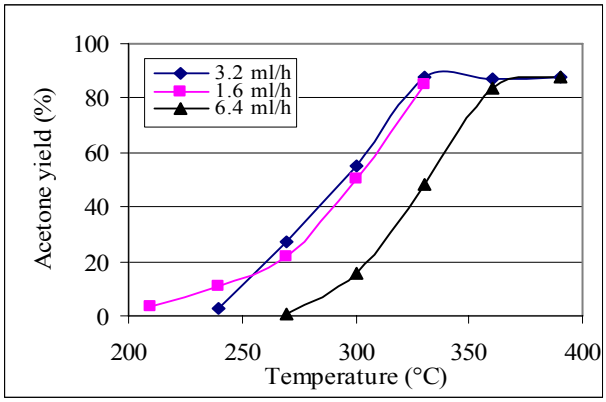

Figure 6.30 Acetone yield (Catalyst G)

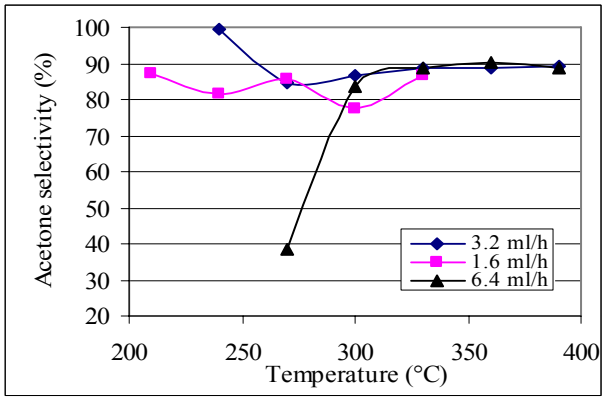

Figure 6.31 Acetone selectivity (Catalyst G)

Table 6.10 Surface area for catalyst G (SiO_2)

Cu %	BET area (m^2/g)
11.7	316

Catalyst H:

For this catalyst the reaction rate was very fast even at low temperatures. For the lower LHSV's and flow rates, due to the longer catalyst contact time, the acetone yield increased rapidly from 10% to 80% in the temperatures range 250 °C to 300 °C (**Figure 6.32**). This occurrence can be attributed to the catalytic properties of copper which content is slightly higher on this catalyst (15%) than that of catalyst B (9.2%). Above 300 °C, the conversion slowly increased to 90%. The selectivity values (**Figure 6.33**) were however lower than those of catalyst B, which explains why catalyst H could not obtain higher yields than catalyst B.

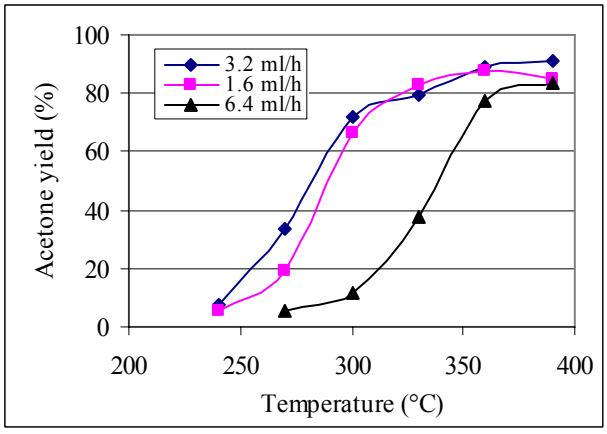

Figure 6.32 Acetone yield (Catalyst H)

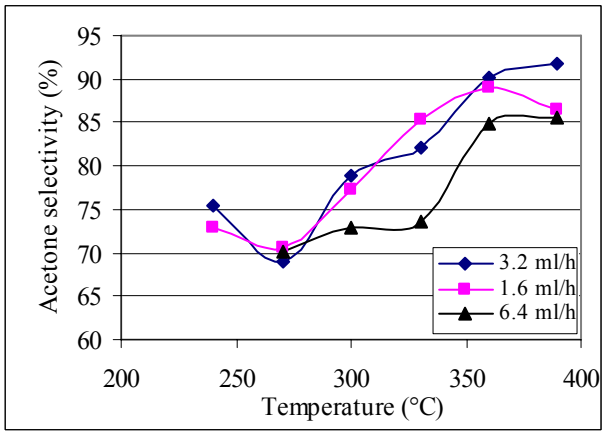

Figure 6.33 Acetone selectivity (Catalyst H)

Table 6.11 Surface area for catalyst H (SiO_2)

Cu %	BET area (m^2/g)
15	307

Catalyst C:

Figure 6.35 shows that the selectivity of this catalyst is quite good. It is better than that of both Catalyst G and H. This is again in contradiction to what was discussed earlier with Catalyst G. Catalyst C however has a much lower total catalyst surface area which should decrease the amount of propene formed. From this it can be said that the combination of the amount of copper impregnated and the BET surface area is what effects the conversion of isopropanol to acetone the most.

Table 6.12 Surface area for catalyst C (SiO_2)

Cu %	BET area (m^2/g)
18.6	275

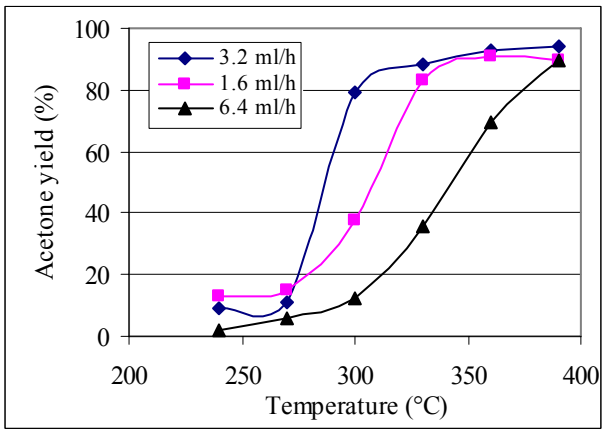

Figure 6.34 Acetone yield (Catalyst C)

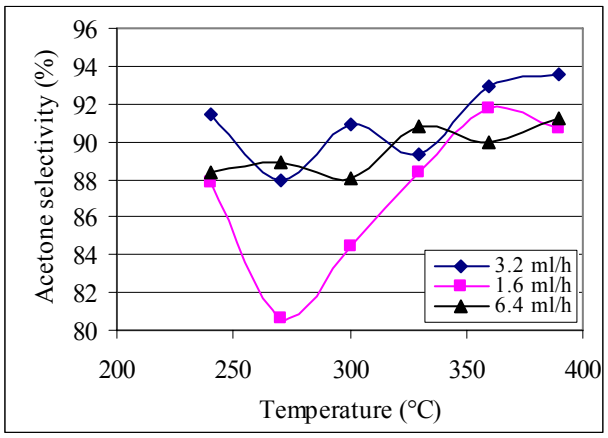

Figure 6.35 Acetone selectivity (Catalyst C)

Catalyst D:

With this catalyst high yields were obtained at 330 °C as shown in **Figure 6.36**. When the temperature increased above 330 °C at flow rates of 1.6 and 3.2 ml/h, the acetone yield decreased slightly. This suggests that there was higher propene formation at the higher temperatures for this catalyst. This is confirmed in **Figure 6.37** where a slight decrease in acetone selectivity is visible in that temperature range. At the higher copper concentration (27.7%), the catalyst surface area decreases. This should lead to a decrease in propene formation (the thermal decomposition product). In this case however the propene formation slightly increased due to the high concentration of copper. The 2-propanol flow rate of 3.2 ml/h gave the highest yields. Below 280 °C, however, a flow rate of 1.6 ml/h resulted in higher yields.

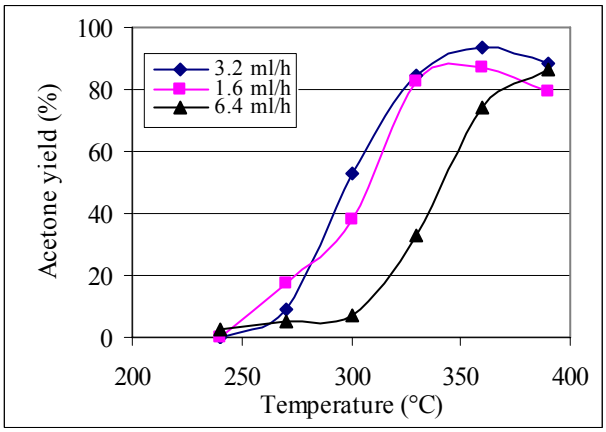

Figure 6.36 Acetone yield (Catalyst D)

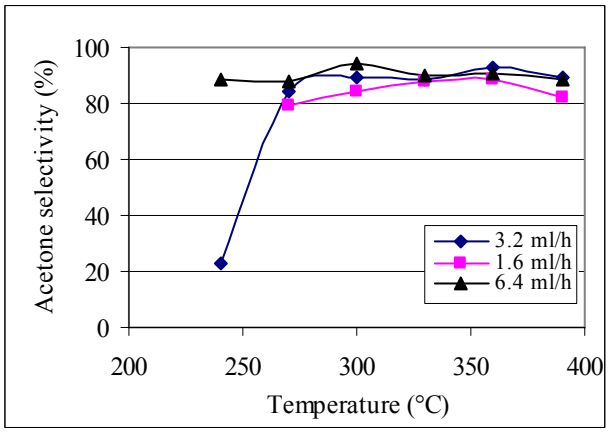

Figure 6.37 Acetone selectivity (Catalyst D)

Table 6.13 Surface area for catalyst D (SiO_2)

Cu %	BET area (m^2/g)
27.7	241

6.4.3.1 Effect of particle size on acetone yield

Cat Ba:

Figure 6.38 shows that the smaller particle size, resulted in very good yields at lower temperatures (240 °C). At 300 °C, the average yield for flow rates 3.2 and 1.6 ml/h was ±80%. This was better than for the bigger particle sizes. However, at temperatures above 300 °C the yield stayed constant.

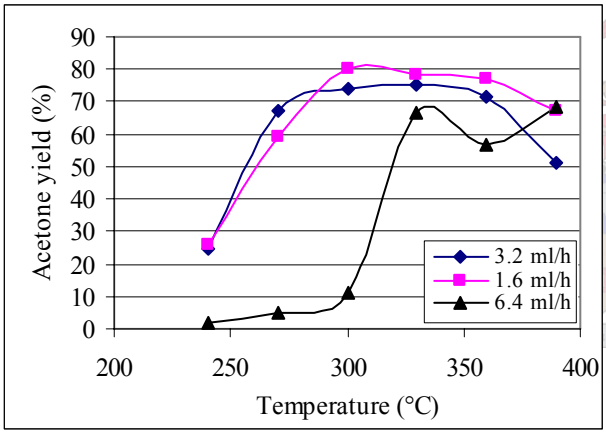

Figure 6.38 Acetone yield (Catalyst Ba)

Cat Bb:

The flow rate 3.2 and 1.6 ml/h showed almost the same characteristics. Yields above 90% could be obtained with a flow of 1.6 ml/h as seen in **Figure 6.39**. This was higher than the acetone yield obtained by catalyst Ba, but at a temperature of about 50 °C higher than the temperature where the optimum yield resulted for catalyst Ba.

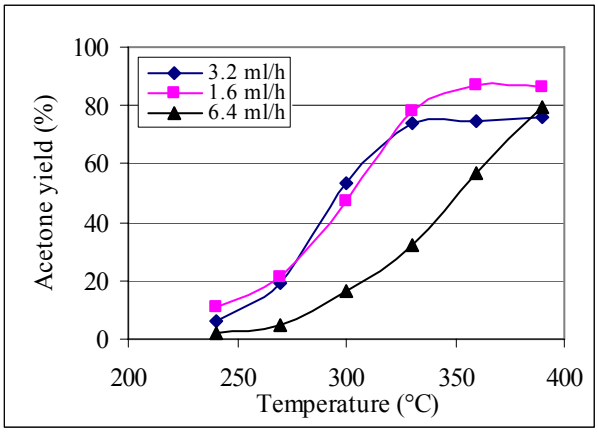

Figure 6.39 Acetone yield (Catalyst Bb)

Cat Bc:

This catalyst was of spherical shape with average diameter 3 mm. This catalyst achieved its highest yields (90%) at 390 °C (**Figure 6.40**).

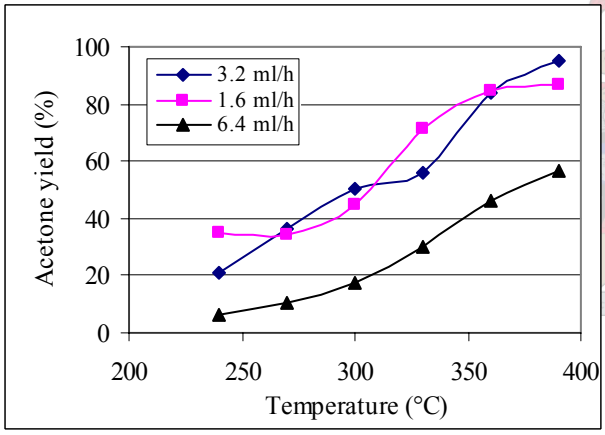

Figure 6.40 Acetone yield (Catalyst Bc)

The effect of particle size can be seen from these three figures (**Figures 6.38** to **6.40**). All three catalysts achieved almost the same maximum acetone yield. The smaller particle size achieved its highest yield at a temperature of 300 °C, the medium size particles at 350 °C and the large particle size at 390 °C.

Figures 6.41 and **6.42** show the effect of catalyst particle size on total isopropanol conversion and propene yield. From **Figure 6.41** it can be seen that the smallest particle size resulted in high total conversions at low temperatures. According to **Figure 6.42** the

smaller particle size produced the most propene. At 390 °C the propene yield is 20%. The slightly bigger particle size (850-1180 microns) achieved a maximum of 12% propene yield. Greater mass transfer resistance can be expected from larger particles. This might slow down the reaction rate. The mass transfer rate should decrease with a decrease in particle size. This is confirmed by **Figures 6.41** and **6.42**.

The decrease of total isopropanol conversion with the use of larger particles can be explained by the fact that channelling of the feed gas occur. When the particle diameter is more than one tenth of the reactor diameter, channelling usually starts occurring. For the circumstance where the 3 mm particle diameter catalyst was used, channelling occurred.

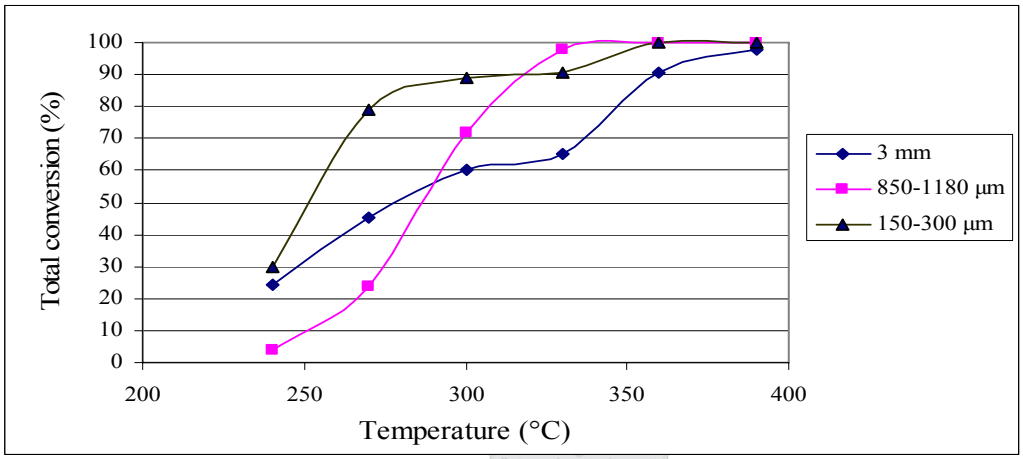

Figure 6.41 Total 2-propanol conversion at a flow rate of 3.2 ml/h for different particle sizes

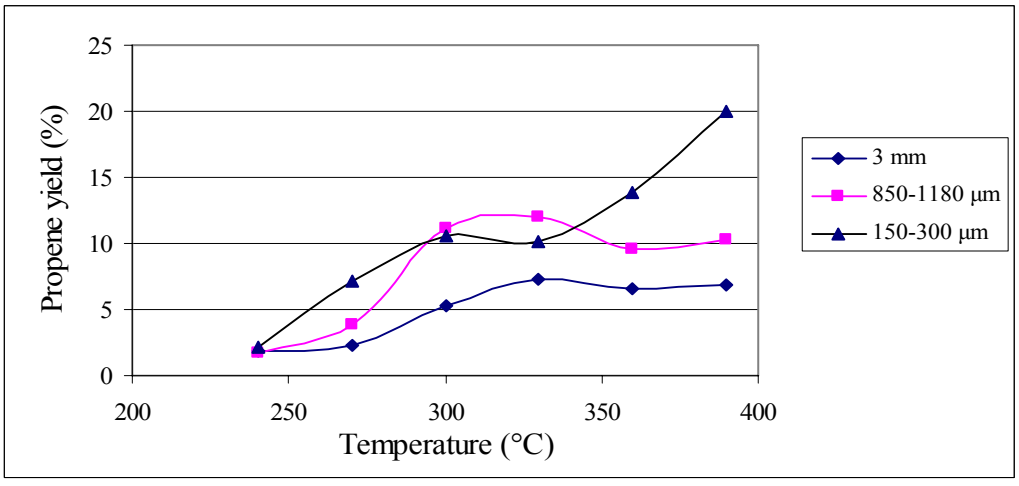

Figure 6.42 Propene yield at a flow rate of 3.2 ml/h for different particle sizes

6.4.3.2 Effect of catalyst surface area

Figure 6.43 illustrates the effect the SiO_2-catalyst surface area had on the acetone yield. These yields were calculated at a temperature of 330 °C for the flow rate of 3.2 ml/h. This means that the SiO_2 surface area plays a large role in obtaining good yields to acetone as indicated by **Figure 6.43**. According to **Figure 6.43** a decrease in acetone yield occurred with an increase in total catalyst surface area. The surface area of the catalyst should decrease with an increase in copper concentration, because this copper fills the pores of the catalyst. This is confirmed in **Figure 6.43**, which also shows the surface area of the catalyst as a function of copper concentration. The total surface area decreased from 380 m^2/g at 4.4% Cu to 240 m^2/g at a copper concentration of 27.7%. From **Figure 6.43** it can be seen that the acetone yield is a function of the catalyst surface area and the copper concentration. There is an optimum level between these two factors. For the purpose of this study it was not required to investigate this characteristic.

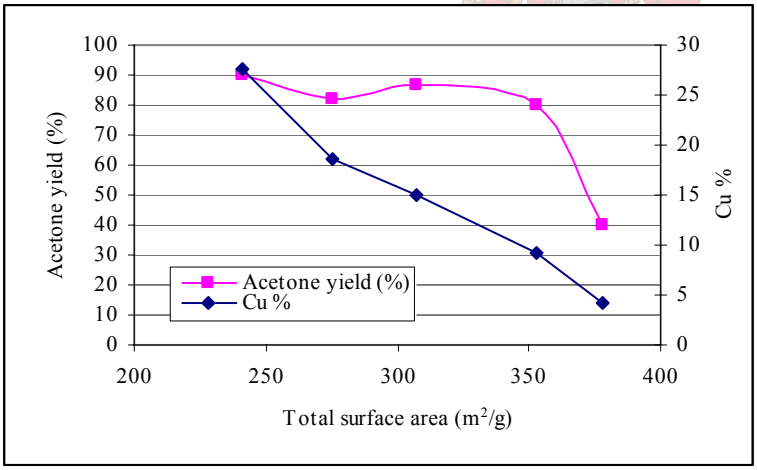

Figure.6.43 Acetone yield and copper concentration as a function of total catalyst surface area

6.4.3.3 Total conversion of isopropanol and the conversion to the main by-product

From **Figure 6.44** it can be seen that at 420 °C all the different catalysts obtained 100% of total conversion of isopropanol. It can also be seen that the temperature to reach 100%

total conversion decreases with an increase in copper concentration. As indicated in **Figure 6.45** the highest by-product formation is obtained with the pure silica catalyst. This was also for the case of the MgO catalysts. The pure silica catalysts however resulted in much higher propene formation (98%).

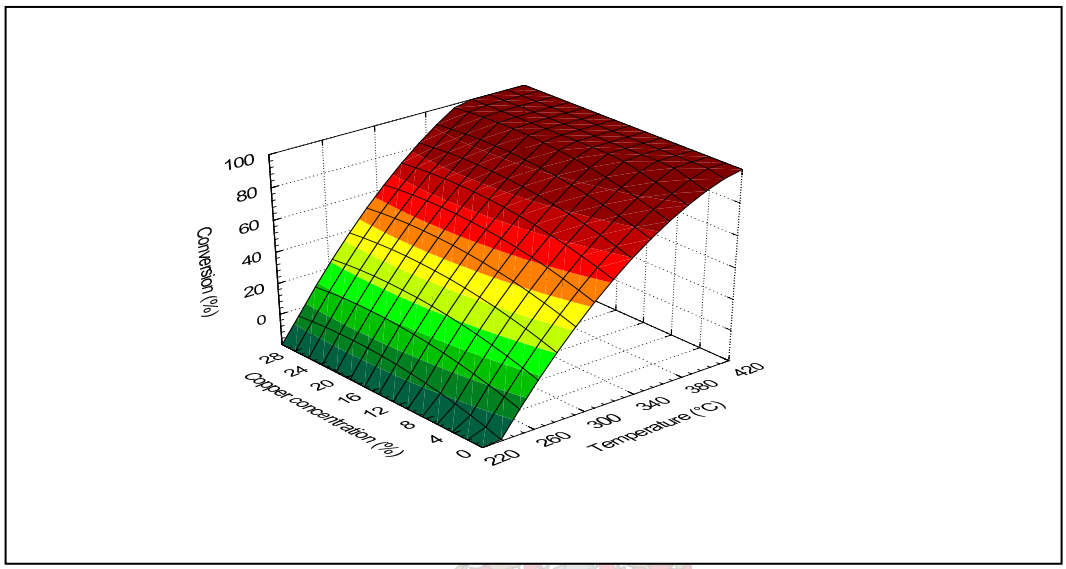

Figure 6.44 Total conversion of isopropanol over silica catalyst as a function of temperature at a flow rate of 3.2 ml/h

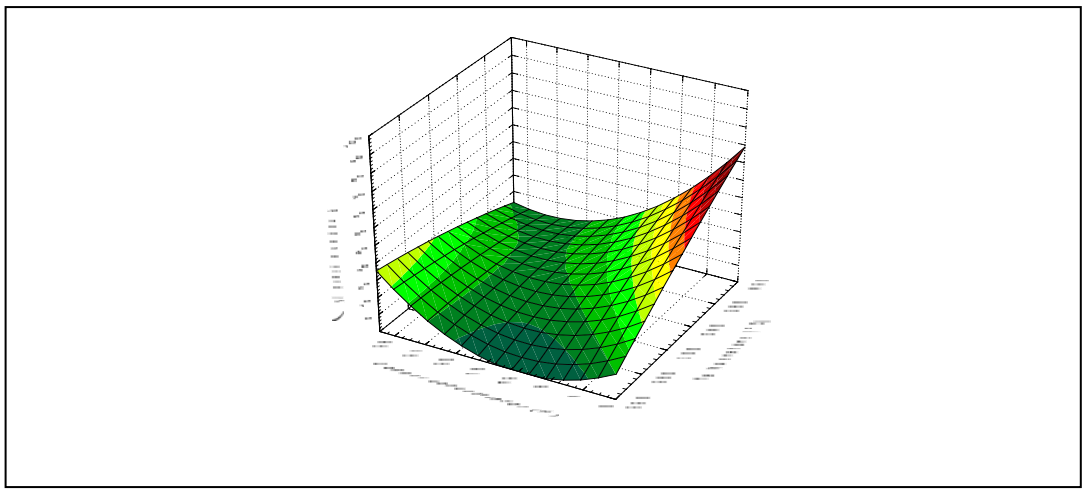

Figure 6.45 Propene yield over silica catalyst as a function of temperature at a flow rate of 3.2 ml/h

6.5 Summary

© Results showed that the alumina support had almost no dehydrogenation activity. Some acetone was formed but most of the isopropanol was converted to propene. This means that the alumina catalyst can be used for dehydration reactions, but they are unsuitable for dehydrogenation reactions in a membrane reactor. The total isopropanol conversion and the propene yield increased with an increase in temperature. An 18.5 wt % Cu on Al_2O_3 gave the highest propene yields. It was shown that the interaction between Cu and alumina is an important factor in dehydration reactions.

© From the MgO-support experiments it could be seen that the conversion depended a lot on the amount of copper impregnated on the catalyst. There was an optimum percentage of copper. The use of Catalyst D (16.9 wt % Cu) resulted in the highest acetone yields. The MgO catalysts showed the lowest total conversion of isopropanol. Due to the low surface area of the support it was unsuitable for further testing in the membrane reactor.

© The surface area of the silica catalyst was about double that of the alumina catalysts and about 10-100 times as much as the surface area of the MgO catalysts. For silica catalysts there were an optimum copper concentration on the support (9.2 wt % Cu) which gave the highest acetone yield. This catalyst achieved the best results and will be used as catalyst for the dehydrogenation of isopropanol reaction in the membrane reactor. It could be seen from all the results of the SiO_2-catalyst that the optimum temperature for this reaction is 330 °C. The two lower flow rates (1.6 and 3.2 ml/h) achieved the highest yields and will be used as flow rates in the membrane reactor. This is because of the increase in the catalyst contact time at the lower LHSV's and flow rates. The selectivities towards acetone decreased with an increase in temperature. The total isopropanol conversion also decreased with an increase in catalyst particle size. It was noticed that the performance of the catalyst was also dependant on the combination of the amount of copper impregnated and the total catalyst surface area.

The performance of the catalysts was as expected and other practical applications for these catalysts include the dehydrogenation of propane to ethylene. This reaction is of industrial importance in many chemical industries.

7. Performance of the membrane reactor

7.1 Introduction

This chapter focuses on all aspects regarding membrane reactors. Hydrogen permeances and hydrogen to nitrogen selectivities were determined experimentally. Furthermore, the conversion of isopropanol to acetone in the membrane reactor was investigated. The dehydrogenation of 2-propanol (with a 9.2 wt % Cu on SiO_2 catalyst) was performed at the same conditions in both a fixed-bed reactor and a membrane reactor. A series of runs were conducted varying the reaction temperature, reaction pressure and feed flow rates. The purpose of the runs was to compare the performance of the membrane reactor with that of a conventional reactor. Two different types of membrane reactors will be evaluated. A brief discussion of the usage of membrane reactors will be given before the results are presented. The same experimental set-up was used as described in sections 3.3 and 3.6.

7.2 Overview of membrane reactors

The combination of membrane separation with catalytic reaction in order to improve yield, selectively or some other performance characteristic, is an active area of research. Applications which have used selective membranes include hydrogen separation and purification, hydrogen recovery from process streams and the use of membrane reactors for H_2-related reactions (e.g., hydrogenation, dehydrogenation, methane reforming, ammonia decomposition, etc.) (Farris, 1993; Saracco, 1994; Collins, 1994; Ionaddis, 1996). An overall conversion can be attained which is much greater than that realised in the conventional reactor, by conducting these reactions in a catalytic membrane reactor. This is due to one product that is selectively permeated through the membrane and out of the reaction environment. These reactions are all equilibrium limited. The removal of the product hydrogen by a permselective membrane deployed along the reaction path can increase the conversion and thus improve process efficiency.

Normally high temperatures are required for endothermic reactions. This is why ceramic membranes or thin palladium films are used instead of polymer-based membranes for high temperature reactions. The interest in research of dehydrogenation reactions increased due to the availability of high hydrogen permselective membranes which can be used at elevated temperatures. Pure palladium membranes for hydrogen separation are, however, limited as hydrogen embrittlement occurs below 300 °C. Recently, palladium composite membranes have sparked much interest. Composite membranes offer the opportunity of making thinner films, which will reduce costs and increase hydrogen permeance. In addition, hydrogen embrittlement is suppressed by alloying the thin palladium film with silver or copper. The process of dehydrogenation when using a catalytic membrane can highly utilise the hydrogen species produced by the reaction. Catalytic membranes plated with palladium are best suited for dehydrogenation reactions as they separate the produced hydrogen from the products. The permeated hydrogen can be used in another reaction if the process requires this.

The improvement of the preparation techniques for producing membranes with very thin palladium or palladium alloy films, should make palladium membrane applications more economically viable.

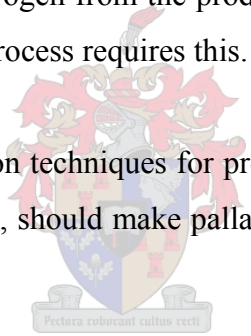

7.3 Permeance and selectivity tests

In this section the hydrogen permeance and H_2 to N_2 selectivity of a composite membrane consisting of palladium-copper alloy and a pure palladium film supported on the inner surface of a porous alumina cylindrical membrane were investigated. The experimental data are presented in appendix F. The H_2 to N_2 selectivity was determined using the following formula:

$$H_2 \text{ to } N_2 \text{ selectivity} = \frac{H_2 \text{ permeance}}{N_2 \text{ permeance}} \qquad (7.1)$$

7.3.1 Palladium plated membrane

This alumina membrane was coated with a palladium film of thickness 5 microns. The selectivity tests were done as described in section 3.6. It has long been known that atomically clean metals dissociate hydrogen molecules and adsorb the resulting atoms very fast (Steward, 1983). **Figure 7.1** shows the effect temperature had on the hydrogen to nitrogen selectivity. Results showed that the membrane selectivity increased with increasing temperature. It is known that transformation of palladium hydride from the α to the β phase is accelerated by increasing hydrogen concentration in palladium at temperatures below 300 °C (Uemiya, 1990). The decreasing H_2 selectivity at the lower temperatures can be attributed to the fact that the H_2 permeance decrease with decreasing temperature from the Arrhenius equation (**equation 2.14**) together with the increase in N_2 permeance with decreasing temperature from the Knudsen diffusion theory (**equations 2.7** and **2.8**). Selectivities of up to 90.6 could be obtained from this membrane. This was achieved at the higher temperatures. At 330 °C the selectivity was 63.

Figure 7.1 Membrane selectivity as a function of temperature (Pd on Al_2O_3)

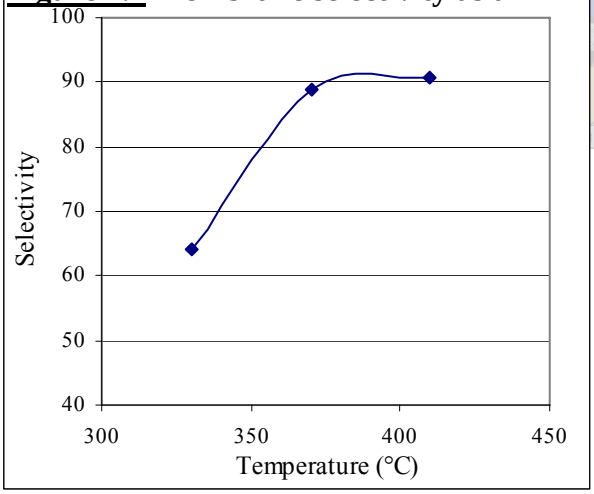

Figure 7.2 Hydrogen permeance as a function of temperature (Pd on Al_2O_3)

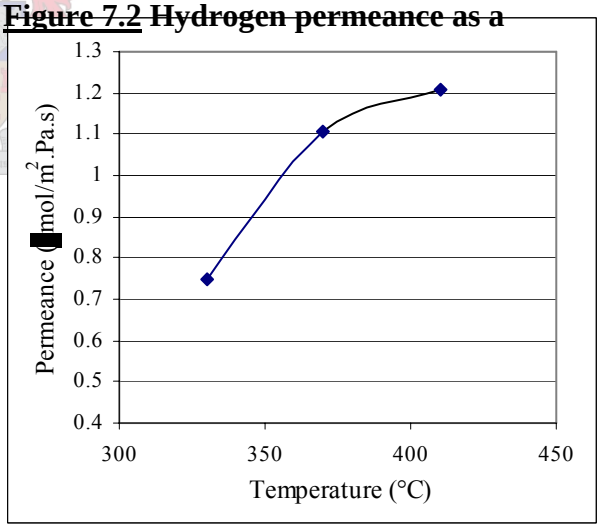

The hydrogen permeance through the membrane can be observed from **Figure 7.2**. The permeance increased with increasing temperature. This is the same as for the selectivity of the membrane. It is known that hydrogen permeates through palladium via a solution-diffusion transport mechanism (Lewis, 1967). Uemiya (1991) reported that the diffusion

of hydrogen through palladium is the rate-determining step for the permeation of hydrogen through palladium membranes. It was also proved that the diffusion of hydrogen through palladium increased with an increase in temperature (Holleck, 1970). This indicates that hydrogen permeance should increase with temperature as in **Figure 7.2**. Furthermore, the hydrogen permeance should increase with temperature as predicted by the Arrhenius equation (**equation 2.14**).

7.3.2 Palladium-copper plated membrane

A 4 micron palladium film was plated on the inside of the membrane with 40% copper thereafter. Hydrogen embrittlement was suppressed by alloying the thin palladium film with copper. **Figure 7.3** shows the effect temperature has on the selectivity of this membrane. This membrane was also heat treated for different time periods to form the Pd-Cu alloy. **Figure 7.3** illustrates the effect the length of time of heat treatment had on the hydrogen selectivity of the supported palladium-copper membranes. The heat treatment was done at 600 °C. After each session of heat treatment (thus after 24, 48, 80 and 110 hours) the selectivity tests were done at the different selected temperatures. Results showed that alloying dramatically decreased the membrane selectivity. Alloying the membrane for 24 hours decreased the selectivity from a maximum of 13.5 to 4. After 24 hours of heat treatment, the selectivity decreased very little.

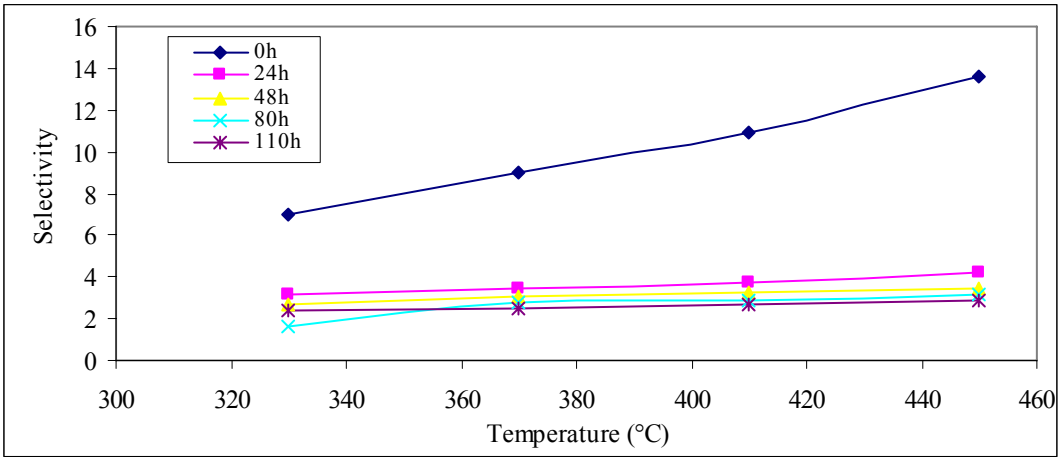

Figure 7.3 Membrane selectivity as a function of temperature (Pd-Cu on Al_2O_3)

The membrane selectivity also increased with increasing temperatures. Before heat treatment of this membrane the selectivity increased from 7 to 13.5 from a temperature 350-450 °C. This effect was explained in section 7.3.1. This membrane's selectivity was much lower than that of the pure palladium coated membrane. From the values it can be seen that the copper suppresses the selectivity of the membrane. The alloy film is not as selective as the pure palladium film.

After both 24 and 110 hours of heat treatment the hydrogen permeance decreased with increasing temperature. This effect can be noticed in **Figure 7.4**. According to the Arrhenius equation (**equation 2.14**) the hydrogen permeance through thick solid films should increase with increasing temperature. This occurred before the membrane was heat treated. According to Knudsen diffusion theory (**equation 2.7** and **2.8**) the hydrogen permeance should decrease with increasing temperature (this happened after heat treatment). The membrane thickness being constant, the differences in the permeation rate and selectivities are caused mainly by changes in the film structure (i.e., microstructure and/or phase structure) during annealing.

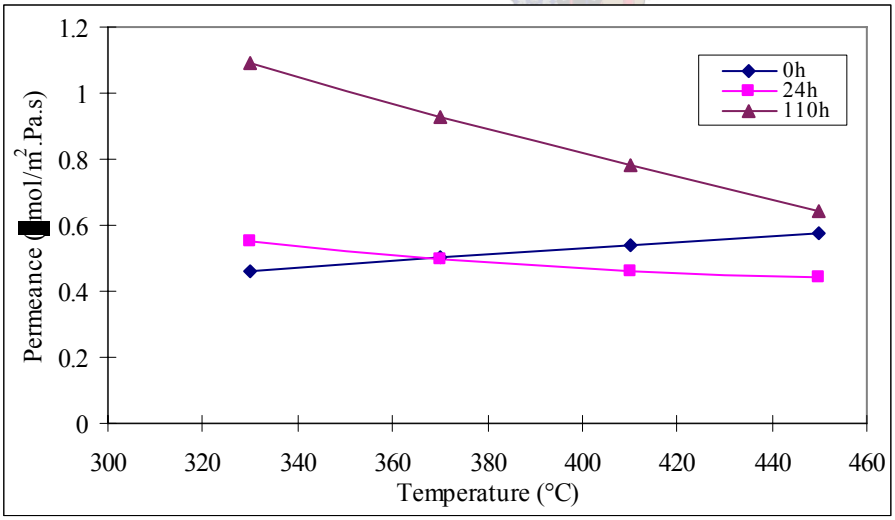

Figure 7.4 Hydrogen permeance as a function of temperature (Pd-Cu on Al_2O_3)

Figures 7.3 and **7.4** demonstrate that during the annealing process definite change of the film structure had occurred, which is responsible for the decrease in permeance rates of the Pd-Cu membrane. This suggests that after heat treatment of the membrane, Knudsen

diffusion occurred and that the hydrogen mainly permeated through defects in the film and not through the film. The Knudsen defects thus correspond to the H_2 selectivities. A possible explanation of this might be that the method for the Cu plating was not good enough. Hence, there is potential for improving the Cu plating method.

7.4 Reactions in the membrane- and fixed-bed reactor

The dehydrogenation of 2-propanol over 9.2 wt % Cu impregnated on SiO_2 was done in two different types of membranes and in a fixed bed reactor. As explained in **Chapter 3** (section 3.9), nitrogen with isopropanol was fed inside the membrane tube and simultaneously argon as a sweep gas was introduced into the outer annular space co-currently. On the one type of membrane only 5 microns of palladium was coated and the other membrane an alloy of palladium and copper was plated. In this section the results of those experiments will be discussed and the performance of the best membrane reactor will be compared to those of the fixed-bed reactor. Two different flow rates of sweep gas were used. Two different flow rates of 2-propanol were also used.

7.4.1 The dehydrogenation of 2-propanol in a palladium coated membrane

Figure 7.5 shows the acetone yields vs. temperature for a 2-propanol flow rate of 3.2 ml/h (LHSV = 0.33 h^{-1}). The higher sweep gas flow rate showed better yields than that of the lower one. The acetone yield should increase by increasing the flow rate of the sweep gas, due to the fact that the removal of hydrogen (one of the products) is increased. The hydrogen permeance through the membrane is increased by increasing the sweep gas flow and thus increasing the difference in the pressures between the inner and outside membrane to provide the driving force for permeance. **Figure 7.6** indicates that the slower feed rate of 1.6 ml/h (LHSV = 0.17 h^{-1}) of 2-propanol achieved slightly higher yields than the faster feed rate. This is due to the longer catalyst contact time. For this flow rate the highest acetone yield achieved is 45%. Also for the flow rate of 1.6 ml/h the higher sweep gas flow rate to some extent achieved higher acetone yields. This is in

agreement with theory as previously discussed for the 3.2 ml/h flow rate. For the Argon:Nitrogen of 2:1 the acetone yield increased from 13-47% over the temperature range 240-320 °C. For the Argon:Nitrogen of 1:1 the yield increased from 10-46% over the same temperature range.

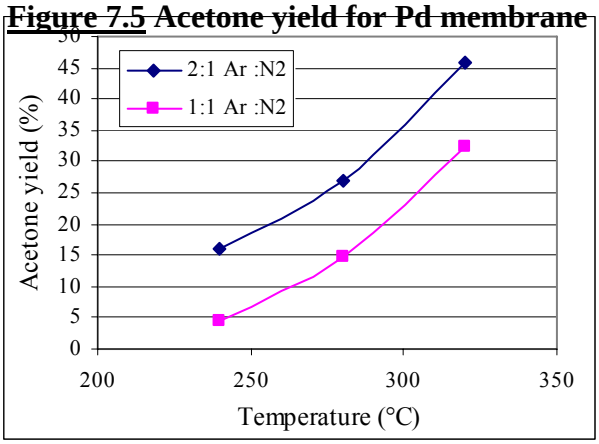

Figure 7.5 Acetone yield for Pd membrane (3.2 ml/h)

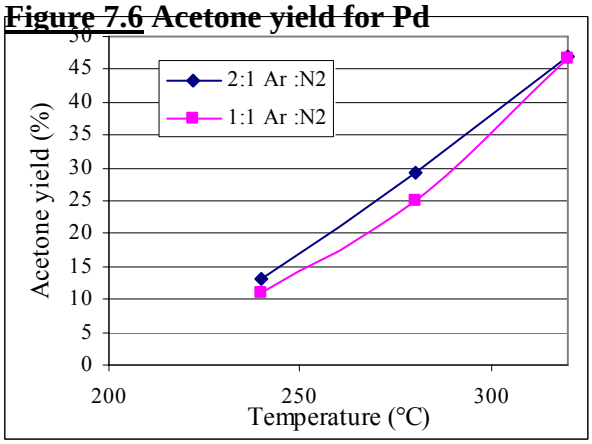

Figure 7.6 Acetone yield for Pd membrane (1.6 ml/h)

7.4.2 The dehydrogenation of 2-propanol in a palladium-copper coated membrane

From **Figures 7.7** and **7.8** it can be seen that the acetone yields are lower than that of pure palladium coated membrane. As discussed in sections 7.3.1 and 7.3.2, the H_2 to N_2 selectivity of this membrane was much lower. Hydrogen is not removed selectively and this will lead to a decrease in acetone yield. From this it follows that when a membrane with a higher selectivity for products is used, the membrane reactor performance will be improved. This copper plated membrane is thus not suitable for reactions in a catalytic membrane.

It is shown in **Figures 7.7** and **7.8** that the 2:1 sweep gas to feed gas ratio performed better than the lower sweep gas to feed gas ratio. This is true for both the flow rates of 2-propanol. This can again be explained by the fact that the H_2 permeance is increased with an increase in sweep gas flow. This leads to a shifting of reaction equilibrium towards the product side. The flow rate of 1.6 ml/h however achieved higher acetone yields than the flow rate of 3.2 ml/h, due to its longer catalyst contact time.

Figure 7.7 Acetone yield for Pd-Cu membrane (3.2 ml/h)

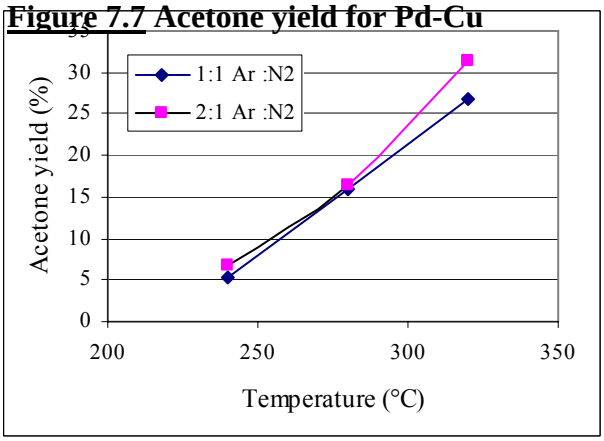

Figure 7.8 Acetone yield for Pd-Cu membrane (1.6 ml/h)

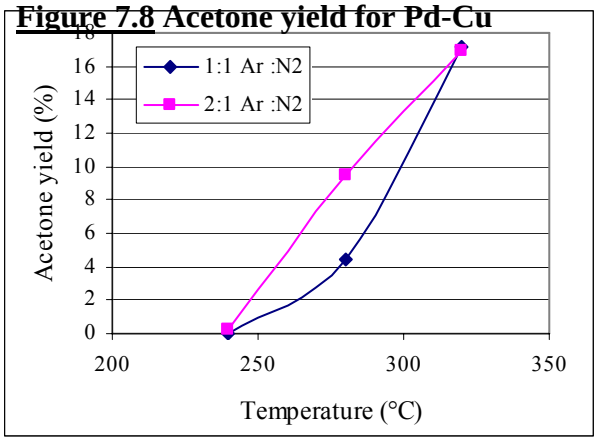

7.4.3 The dehydrogenation of 2-propanol in a fixed-bed reactor

For this reaction the sweep gas was not used. **Figure 7.9** summarises the results obtained from this experiment. The flow rate of 1.6 ml/h of 2-propanol achieved the better results. This flow rate resulted in better results because the reaction time is longer and the reaction thus could reach more completion due to the longer catalyst contact time. The increase in conversion over the temperature range for that flow rate was also faster. The highest acetone yield achieved was 31%.

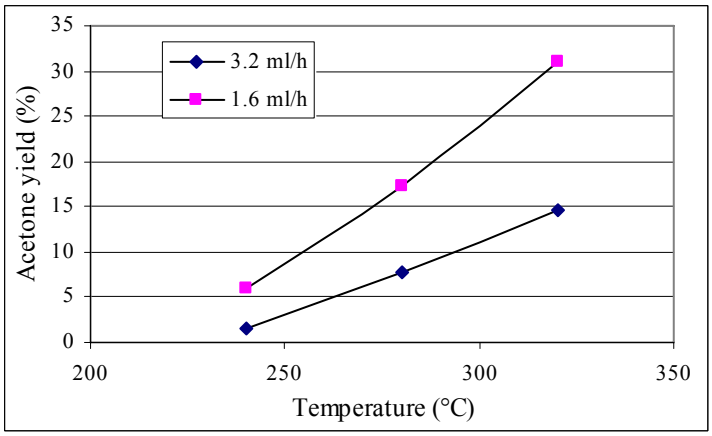

Figure 7.9 Acetone yield for the fixed-bed reactor

7.4.4 Comparison of the membrane reactor against the fixed-bed reactor

The acetone yield will be used to compare these reactor types. The palladium membrane reactor will be used for discussion as it shown the best results. In **Figure 7.10** it can be seen that the palladium membrane reactor achieved better results than the fixed-bed reactor. The acetone yield in the membrane reactor was about 1.5-2.6 times higher than the yields in the fixed-bed reactor. This can be attributed to the fact that the product (hydrogen) is removed by a selective membrane from the reaction zone, which will increase the yield. At 240 °C the acetone yield obtained with the membrane reactor with an Argon:Nitrogen ratio of 2:1 is 16% whereas the yield of the fixed-bed reactor at the same temperature was merely 6%. These results are all for a 2-propanol flow rate of 3.2 ml/h.

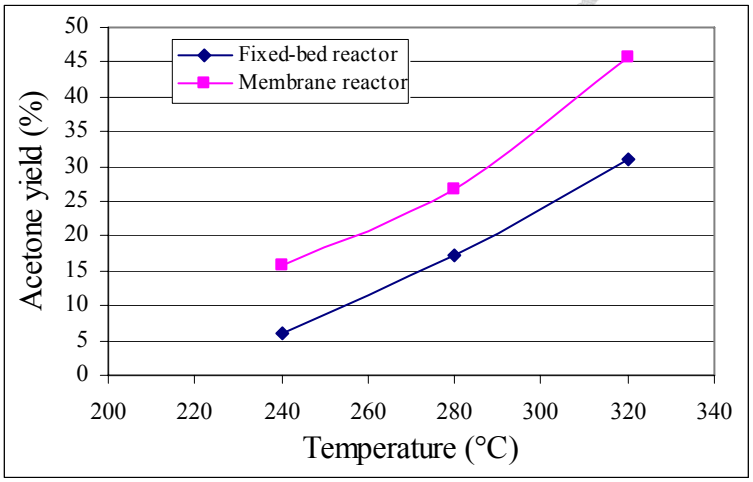

Figure 7.10 Comparison between the Pd membrane reactor and fixed-bed reactor

Keuler (2000) investigated the dehydrogenation of ethanol in a Pd-Ag membrane. **Figure 7.11** compares the performance of the catalytic membrane reactor against the plug-flow reactor. This study also showed that by using the membrane reactor improvements in acetaldehyde yield was obtained.

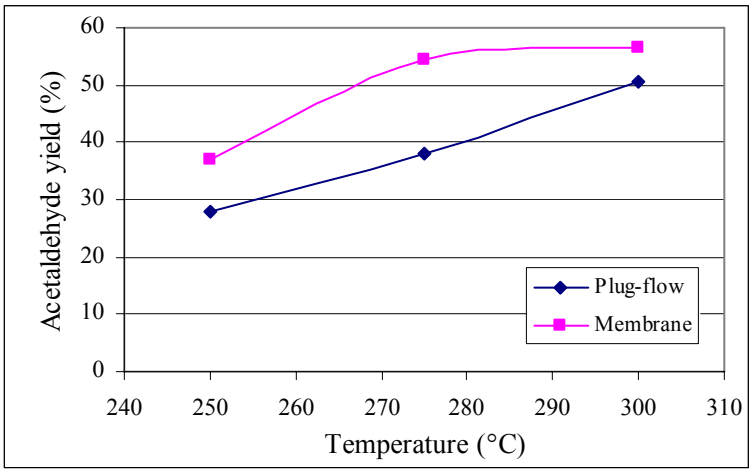

Figure 7.11 Comparison between the Pd-Ag membrane reactor and plug-flow reactor (Keuler, 2000)

7.5 Summary

The dehydrogenation of isopropanol over a 9.2 wt % Cu impregnated silica catalyst was used to study the performance of two kinds of membrane reactors, palladium coated and palladium-copper coated alumina reactors, and a fixed-bed reactor. The palladium-coated membrane achieved the best results. The reason for that is its better H_2 to N_2 selectivity. In the temperature range of 330-410 °C the palladium membrane's H_2 permeance varied from 0.7-1.2 μmol/m^2.Pa.s and the H_2 to N_2 selectivity varied between 63.1 and 90.6. Results also showed that with an increase in sweep gas flow rate, the acetone yield increased, due to more hydrogen that is removed from the product side.

The palladium-copper membrane reactor did not show much better results than the fixed-bed reactor. To form the palladium-copper alloy at high temperature damages the membrane. Hence the selectivity decreases. Results showed that better acetone yield could be achieved by doing dehydrogenation reactions in the membrane reactor. The acetone yields obtained were increased beyond those achievable by the fixed-bed reactor with an increase in flow rate of the sweep gas, that is, in the separation tempo of the

products, especially hydrogen. This kind of reactor however is more expensive than the fixed-bed reactor.

8. Conclusions

This study investigated the performance of alumina membrane reactors for dehydrogenation reactions. The alumina membranes were coated with palladium and copper by an electroless plating method. This method was investigated in detail and the best plating conditions were found.

These membranes were first characterised by using XRD, SEM and PIXE and then used for reactions. XRD experiments confirmed that the copper diffused into the palladium, with broader peaks showing after heat treatment. These results indicated that smaller palladium and copper crystallites formed during the heat treating process. SEM results revealed that films plated on the Atech alumina membranes were not of a dense nature. The results were compared to the SCT membrane, which verified better film structure. PIXE experiments showed the concentration profiles of both copper and palladium across the depth of the membrane. It indicated that the copper and palladium atoms penetrated deep into the pores of the membrane during the preparation method. These characterisation methods confirmed that electroless plating process is one of the best ways to coat alumina membranes.

For the catalytic investigation, the dehydrogenation of 2-propanol was used as model reaction. Different catalysts (Al_2O_3, MgO and SiO_2 impregnated with Cu) were tested and the best one (9.2 wt % Cu on SiO_2) was chosen as catalyst in the membrane reactor. Alumina showed no dehydrogenation activity and the main product that formed was propene. Although MgO resulted in the dehydrogenation of isopropanol, the acetone yields it delivered were very low, due to its low surface area. The silica catalyst exhibited the best results. The total conversion of isopropanol, the acetone selectivity and the acetone yield displayed very good values.

Two different types of membrane reactors were used. One, only coated with palladium and the other coated with palladium and copper. Hydrogen to nitrogen selectivity tests were also carried out on these membranes. Selectivities of up to 90.6 could be reached with the palladium-coated membrane. The palladium-copper plated membrane only achieved selectivities of up to 13. With heat treatment this value decreased even more. The palladium membrane also achieved much better acetone yields for the dehydrogenation of 2-propanol than the palladium-copper membrane and the fixed-bed reactor. The reason for that is its better selectivity. The greater selectivity indicates that more hydrogen would be removed from the product and thus shifting the equilibrium towards the product side of the reaction. The palladium-copper membrane reactor did not reveal much better results than the fixed-bed reactor, due to its poorer selectivity and hydrogen permeance after heat treatment. The film got damaged while heat treating the membrane to form an alloy between copper and palladium. This caused the poorer results. It was demonstrated that better yields could be obtained by using a membrane reactor for dehydrogenation reactions.

9. Future recommendations

In this study it was proved that performing dehydrogenation reactions in membrane reactors can enhance the conversion to the products of these reactions.

Different thicknesses of Pd-Cu alloys in an alumina membrane could be investigated to see if there is any improvement of H_2 permeances and H_2 to N_2 selectivities. Other future work might include the dehydrogenation of propane to ethylene, which is of industrial importance to many chemical industries. Ethylene is used for the production of valuable chemicals such as poly vinyl chloride (PVC) and different grades of polyethylene (LLPDE, HDPE, LPDE, etc.). A hydrogenation reaction that is of industrial importance is the hydrogenation of acetylene. This reaction is used to prevent the build up of coke promoters in the process of producing vinyl chloride.

After this, scale-up investigations could be conducted to see how viable full-scale dehydrogenation/hydrogenation reactions would be in the catalytic membrane reactor.

10. References

Abys JA, 1998, Palladium plating, *Plating and surface finishing*, Vol. 85.

Agarwalla S and Lund CRF, 1992, Use of a membrane reactor to improve selectivity to intermediate products in consecutive catalytic reactions, *Journal of Membrane Science*, Vol. 70.

Al-Shammary AFY and Caga IT, 1991, Palladium-based diffusion membranes as catalysts in ethylene hydrogenation, *Journal of chemical technology and biotechnology*, Vol. 52.

Aramendia MA, et al., 1994, Determination of acid sites in solid catalysts by mass spectrometry, *Rapid Communications in Mass Spectrometry*, Vol. 8.

Aramendia MA, et al., 1995, Contribution of mass spectrometry to the determination of basic sites in solid catalysts, *Rapid Communications in Mass Spectrometry*, Vol. 9.

Aramendia MA, et al., 1996, Magnesium oxides as basic catalysts for organic processes, *Journal of Catalysis*, Vol. 161.

Assubumrungrat S and White DA, 1996, Permeation of ethanol and methanol vapours through a porous alumina membrane, *Chemical Engineering Science*, Vol. 51.

Assabumrungrat S and White DA, 1998, Permeation of acetone and isopropanol vapours through a porous alumina membrane, *Chemical Engineering Science*, Vol. 53, No.7.

Athavale SN and Totlani MK, 1989, Electroless plating of palladium, *Metal Finishing*, Vol. 87.

Atkinson RB, 1964, *U.S. Patent 3,119,709.*

Axelrod SD and Makrides AC, 1964, X-Ray studies of hydrogen-silver-palladium electrodes, *The Journal of Physical Chemistry*, Vol. 68.

Baker RW, et al., 1991, Membrane separation systems - Recent developments and future directions, *Noyes Data Corp*., New Jersey, USA.

Boudart M, 1966, The dehydrogenation of isopropanol on catalysts prepared by sodium borohydride reduction, *AIChE Journal*, Vol. 12.

Buxbaum RE and Marker TL, 1993, Hydrogen transport through non-porous membranes of palladium-coated niobium, tantalum and vanadium, *Journal of Membrane Science*, Vol. 85.

Cahill AE, 1957, *American Ethnological Society Proceedings*, Vol. 44.

Chang H and Saleque MA, 1993, Dependence of selectivity on the preparation method of copper/α-alumina catalysts in the dehydrogenation of cyclohexanol, *Applied Catalysis A: General*, Vol. 103.

Collins JP, 1993, Catalytic decomposition of ammonia in a membrane reactor, *PhD thesis*, Oregan State University, USA.

Collins JP, 1994, Catalytic decomposition of ammonia in a membrane reactor, *Journal of Membrane Science*, Vol. 96.

Cunningham J, et al., 1986, Surface synergisms between copper and its oxides, *Journal of Catalysis*, Vol. 102.

Directory of Chemical Producers-United States, 1981, SRI International, Menlo Park, California.

Dressick WJ, et al., 1994, Covalent binding of Pd catalysts to ligating self-assembled monolayer films for selective electroless metal deposition, *Journal of Electrochemical Society*, Vol. 141, No. 1.

Farris TS and Armor JN, 1993, Liquid phase-hydrogenation using palladium membranes, *Applied Catalysis A*, Vol. 96.

Gaspillo PD, et al., 1998, Dehydrogenation of 2-propanol in reactive distillation column for chemical heat pump, *Journal of Chemical Engineering of Japan*, Vol. 31, No. 3.

Gil A, et al., 1996, Effect of the support and added oxides on the bistability observed in the oxidative dehydrogenation of 2-propanol over copper-supported catalysts, *Catalysis Today*, Vol. 32.

Gil A, et al., 1996, Influence of various metal oxides in the bistability observed in the oxidative dehydrogenation of 2-propanol over copper catalysts, *The Canadian Journal of Chemical Engineering*, Vol. 74.

Goto R, 1970, Purification of hydrogen by selective osmosis with palladium alloy membranes, *Kagaku Kogaku*, Vol. 34.

Gryaznov VM and Smirnov VS, 1974, The reactions of hydrogenations on membrane catalysts, *Russian Chemical Reviev*, Vol. 43.

Gryaznov VM and Smirnov VS, 1977, Selective hydrogenation on membrane catalysts, *Kinetics and Catalysis*, Vol. 18.

Gryaznov VM, 1986, Hydrogen permeable palladium membrane catalysts. An aid to the efficient production of ultra pure chemical and pharmaceuticals, *Fresh Patent 2.595.093.*

Holleck GL, 1970, Diffusion and solubility of hydrogen in palladium and palladium-silver alloys, *The Journal of Physical Chemistry*, Vol. 74, No. 3.

Holt A, et al., 1913, *The Journal of Physical Chemistry*, Vol. 82.

Hongbin Z, et al., 1995, Preparation and characterization of novel porous metal/ceramic catalytic membrane materials, *Catalysis Today*, Vol. 25.

Hsieh HP, 1996, Inorganic membranes for separations and reaction, *Elsevier Science Pub. Co.*, New York.

Hurlbert RC and Konecny JO, 1960, Diffusion of hydrogen through palladium, *The Journal of Chemical Physics*, Vol. 34, No.2.

Ioannides J and Verykios XE, 1996, Application of a dense silica membrane reactor in the reactions of dry reforming and partial oxidation of methane, *Catalysis Letters*, Vol. 36.

Itoh N and Sathe AM, 1997, Hydrogen transport from gas to liquid phase through a palladium membrane, *Journal of Membrane Science*, Vol. 137.

Jayaraman V and Lin YS, 1995, Synthesis and hydrogen permeation properties of ultrathin palladium-silver alloy membranes, *Journal of Membrane Science*, Vol. 104.

Jeyalakshmi R and Jagannadhaswamy B, 1990, Kinetics of dehydrogenation of 2-propanol on $La_{2-x}Sr_xCuO_{4-y}$, *Bulletin of the Chemical Society of Japan*, Vol. 63.

Jia MD, et al., 1994, Ceramic-zeolite composite membranes and their application for separation of vapour/gas mixtures, *Journal of Membrane Science*, Vol. 90.

Karanov AN, et al., 1995, Porous membrane catalysts with Pd-M-clusters for liquid phase hydrogenation of dehydrolinalool, *Catalysis Today*, Vol. 25.

Katona T and Arpad A, 1995, Amorphous catalysts, *Journal of Catalysis*, Vol. 153.

Katona T, et al., 1990, Effects of dehydrogenation of 2-propanol on the structure and catalytic activity of an amorphous copper-zirconium alloy sample, *Catalysis Letters*, Vol. 5.

Katona T, et al., 1994, Dehydration of 2-propanol over Cu-Ti metallic glasses: effect of pretreatments and reaction on the structure and surface properties, *Materials Science and Engineering*, Vol. A181/A182.

Keizer K, et al., 1988, Gas separation mechanisms in microporous modified γ-Al_2O_3 membranes, *Journal of Membrane Science*, Vol. 39.

Kemball C, et al., 1960, *Journal of the American Chemical Society*.

Keuler JN, 1997, Preparation and characterisation of palladium composite membranes, *Thesis towards Masters in Chemical Engineering*, University of Stellenbosch, South Africa.

Keuler JN, 2000, Optimising catalyst and membrane performance and performing a fundamental analysis on the dehydrogenation of ethanol and 2-butanol in a catalytic membrane reactor, *PhD-thesis*, University of Stellenbosch, South Africa.

Kirk RE and Othmer DF, 1978, *Encyclopedia of chemical technology*, Vol. 1, Third Edition.

Koga O, et al., 1980, Adsorption and decomposition of isopropyl alcohol over zinc oxide, *J.C.S. Faraday I*, Vol. 76.

Kokugan T, et al., 1998, Dehydrogenation of pure cyclohexane in the membrane reactor and prediction of conversion by pseudo equilibrium model, *Journal of Chemical Engineering of Japan*, Vol. 31, No. 4.

Krylov OV, 1970, Catalysis by Nonmetals, *Academic Press*, London.

Lewis FA, 1967, The Palladium Hydrogen System, *Academic Press*, London.

Li A and Xiong G, 1996, Preparation of Pd/ceramic composite membrane: 1. Improvement of the conventional preparation technique, *Journal of Membrane Science*, Vol. 110.

Lombard V and Eichner C, 1933, *Bulletin Societe Chimique de France*, Vol. 53.

Lonsdale HK, 1982, The growth of membrane technology, *Journal of Membrane Science*, Vol. 10.

Lukes RM, 1964, *Plating*, Vol. 51.

Lyon SB and Fray DJ, 1984, Determination of hydrogen generated in electrochemical processes by use of a solid electrolyte probe, *British Corrosion Journal*, Vol. 19.

Macauley DJ, et al., 1998, Comparison of processes for selective electroless copper plating on 96% alumina photo-selective activated using chlorinated and non-chlorinated photochemical coatings: photoactivity and reliability studies, *Surface and coatings Technology*, Vol. 101.

Makrides AC, 1964, Absorption of hydrogen by silver-palladium alloys, *The Journal of Physical Chemistry*, Vol. 68.

Mallory GO, 1985, Kinetics of electroless nickel deposition with dimethylamine borane: an empirical rate law, *Plating and Surface Finishing*, Vol. 72.

Mardilovich PP and She Y, 1998, Defect-free palladium membranes on porous stainless-steel support, *AIChE Journal*, Vol. 44, No.2.

Matsubara T and Saito Y, 1991, Mechanism of 2-propanol dehydrogenation catalysed by tin(II)-coordinated iridium(III) complexes, *Journal of Molecular Catalysis*, Vol. 66.

Meng N, et al., 1997, Improvements on the thermal efficiency of chemical heat pump involving the reaction couple of 2-propanol dehydrogenation and acetone hydrogenation, *International journal of hydrogen energy*, Vol. 22, No. 4.

Mishra KG and Paramguru RK, 1999, Kinetics and mechanism of electroless copper deposition at moderate-to-high copper ion and low-to-moderate formaldehyde concentrations, *Metallurgical and Materials Transactions B*, Vol. 30B.

Pepe F, et al., 1985, Catalytic behaviour and surface chemistry of copper/alumina catalysts for isopropanol decomposition, *Journal of catalysis*, Vol. 91.

Perry RH and Green D, 1984, *Perry's Chemical Engineers' Handbook*, McGraw-Hill International Editions.

Reddy GK, et al., 1999, Effect of support modification by carbon coverage in the dehydrogenation activity of Cu/Al_2O_3 catalyst, *Catalysis Letters*, Vol. 59.

Rhoda RN, 1959, Electroless palladium plating, *Transaction Institution of Metal Finishing*, Vol. 36.

Riedel W, 1980, The ductility of electroplated and chemically deposited coatings, *Galvanotechnik*, Vol. 71.

Saracco G and Specchia V, 1994, Catalytic inorganic membrane reactors: present experience and future opportunities, *Catalysis Reviews Science*, Vol. 36.

Saubestre EB, 1959, *American Ethnological Society Proceedings*, Vol. 46.

Saubestre EB, 1965, *Plating*, Vol. 52.

Schneble FW, et al., 1967, *U.S. Patent 3,310,430.*

Shindo Y, et al., 1989, High performance reactor using a membrane, *AIChE Symposium Series 272*, Vol. 85.

Shipley CR, 1984, Historical highlights of electroless plating, *Plating and Surface Finishing*, Vol. 71.

Shu J, et al., 1991, Catalytic palladium-based membrane reactors: A review, *The Canadian Journal of Chemical Engineering*, Vol. 69.

Shu J and Grandjean BPA, 1993, Simultaneous deposition of Pd an Ag on porous stainless steel by electroless plating, *Journal of Membrane Science*, Vol. 77.

Silberg PA and Bachman CH, 1958, *The Journal of Physical Chemistry*, Vol. 29.

Sivaraj C, et al., 1988, Characterization of copper/alumina catalysts prepared by deposition-precipitation using urea hydrolysis, *Applied Catalysis*, Vol. 45.

Stern M and Geary AL, 1957, *Journal of Electrochemical Society*, Vol. 104.

Steward SA, 1983, Review of hydrogen isotope permeability through metals, *Lawrence Livermore National Laboratory*, UCRL-53441.

Stoltz B, et al., 1998, Electroless Cu plating of alumina treated with cw CO_2 laser radiation, *Part of the SPIE Conference on smart electronics and MEMS*, San Diego, California.

Szabo Z, et al., 1975, The joint application of flow-system and the micropulse techniques for a comparative study of 2-propanol decomposition over MgO, CaO and SrO, *Journal of Catalysis*, Vol. 39.

Takata K and Suziki T, 1993, Permeation of hydrogen in vanadium I. Experimental details, *Materials Science and Engineering A*, Vol. 163.

Takata K and Suziki T, 1993, Permeation of hydrogen in vanadium I. Theoretical details, *Material Science and Engineering A*, Vol. 163.

Tamaru K, et al., 1980, The mechanisms of the decomposition reaction of 2-propanol on zinc oxide, *Zeitschrift fuer Physikalische Chemie (Wiesbaden)*, Vol. 110.

Teichner SJ, 1967, *Bulletin Societe Chimique de France*, Vol. 8.

Uemiya S, et al., 1991a, Hydrogen permeable palladium-silver alloy membrane supported on porous ceramics, *Journal of Membrane Science*, Vol. 56.

Uemiya S, et al., 1991b, Separation of hydrogen through palladium thin film supported on a porous glass tube, *Journal of Membrane Science*, Vol. 56.

Ullmann F, 1993, *Ullmann's encyclopedia of industrial chemistry*, Vol. A22.

Wood BJ, 1968, Dehydrogenation of cyclohexane on a hydrogen-porous membrane, *Journal of Catalysis*, Vol. 11.

Yamshita M, et al., 1991, Mechanism of 2-propanol dehydrogenation with suspended nickel fine-particle catalyst, *The Chemical Society of Japan*, Vol. 64, No. 2.

Yashima T, et al., 1974, Decomposition of 2-propanol over alkali cation exchanged zeolites, *Journal of Catalysis*, Vol. 33.

Yeung KL and Sebastian JM, 1995, Novel preparation of Pd/Vycor composite membranes, *Catalysis Today*, Vol. 25.

Yeung KL, et al., 1999, Palladium composite membranes by electroless plating technique: Relationships between plating kinetics, film microstructure and membrane performance, *Journal of Membrane Science*, Vol. 159.

Appendix A

(List of chemicals)

Name	**Purity**	**Supplier**
Ammonia solution	25 wt %	Saarchem
$AgNO_3$	99.9999%	Aldrich
$Cu(NO_3)_2 \cdot 3H_2O$	>99%	ACE
Isopropanol	99.8% (0.02% H2O)	Merck
Hydrazine	35 wt % solution	Aldrich
MgO	>97%	Merck
$Na_2EDTA \cdot 2H_2O$	>99%	Saarchem
$(NH_3)_4PdCl_2 \cdot H_2O$	99.99%	Aldrich
$PdCl_2$	59%	Merck
$SnCl_2 \cdot 2H_2O$	>98%	Fluka

Appendix B

(Electroless plating data)

Electroless palladium plating

Time (h)	Mass of container (g)	Mass of container (+Water)(g)	Mass of container (+Water) (+Pd solution)(g)	Atomic Adsorption Value(ppm)	Real concentration (ppm)
	Membrane 1				
0	14.2013	29.3131	29.9298	39.78	1014.560937
1	14.0657	29.1259	29.7603	1.73	42.79895649
2	14.1313	29.2027	29.8252	0.39	9.832322892
	Membrane 2				
0					2045
1.5	14.4146	29.6543	30.2624	40.5	1055.477553
2	14.2151	29.4333	30.0457	2.43	62.81573808
	Membrane 3				
0					2181
0.5	14.3253	29.4428	30.069	63	1583.923826
1	14.431	30.7847	31.6295	38	773.6067708
1.5	14.2279	30.0306	30.632	1.05	28.64034752
	Membrane 4				
0.5	14.4278	24.5534	25.1205	68.07	1283.463391
1	14.3472	24.5418	25.1969	56.69	938.8940513
1.5	14.416	24.423	25.0673	55.75	921.6358451
2	14.6247	24.7887	25.321	38.25	768.6144561
3	14.3971	24.4922	25.1148	9.93	170.9392242
	Membrane 5				
0.5	14.2009	24.2723	24.7709	68.3	1447.916165
1	14.2279	23.9734	24.6134	51.93	842.6859609
1.5	14.4067	24.6392	25.2719	53.33	915.8228481
2	14.3215	24.3496	24.9139	43.32	813.1539394

3	14.2615	23.852	24.4739	12.86	211.1777842

Appendix C

(PIXE data)

Membrane 1h

Datafile(*.gup)	Sample	Ni(ppm)	Cu(ppm)	Pd(ppm)	Au(ppm)	Chi^2
nr120141	1h	0.0	20049.8	306150.7	3567.9	0.853
nr120142	1h	0.0	27186.3	333545.3	1730.2	0.940
nr120143	1h	3.4	17382.7	151114.1	986.9	0.629
nr120144	1h	2.3	9496.9	69151.7	1133.6	0.752
nr120145	1h	0.0	8736.6	70582.3	930.8	0.750
nr120146	1h	8.1	8798.6	63303.1	903.2	0.740
nr120147	1h	0.0	9160.3	54326.5	911.4	0.764
nr120148	1h	0.0	10027.6	52580.4	885.9	0.636
nr120149	1h	0.0	11355.7	54377.1	942.2	0.616
nr120150	1h	11.4	11151.5	45320.2	907.0	0.650

	Statistical error				Fitting error			
	Ni	Cu	Pd	Au	Ni	Cu	Pd	Au
nr120141	0.0	0.8	0.8	3.2	0.00	3.55	3.23	4.40
nr120142	0.0	0.6	0.7	4.9	0.00	3.28	3.08	5.27
nr120143	482.3	0.8	1.1	6.5	225.77	0.99	1.37	5.73
nr120144	464.1	1.1	1.7	6.2	288.35	6.76	6.22	8.18
nr120145	0.0	1.2	1.6	7.0	0.00	6.49	5.98	8.36
nr120146	135.2	1.2	1.8	7.2	100.21	6.71	6.55	8.65
nr120147	0.0	1.1	1.9	6.8	0.00	6.99	6.82	8.95
nr120148	0.0	1.1	2.0	6.7	0.00	7.30	6.91	9.08
nr120149	0.0	1.0	2.0	6.9	0.00	7.30	6.96	9.08
nr120150	110.9	1.0	2.1	6.8	67.54	7.84	7.58	9.59

Membrane 2

Datafile(*.gup)	Sample	Ni(ppm)	Cu(ppm)	Pd(ppm)	Au(ppm)	Chi^2
nr180254	2	0.0	44798.9	310915.2	1711.1	1.029
nr180255	2	0.0	43469.2	345782.5	1482.7	0.892
nr180256	2	3.9	30407.7	242250.0	1433.2	0.984
nr180257	2	0.0	20218.0	127235.4	1040.5	0.602
nr180258	2	0.0	16018.0	84127.5	1029.2	0.707
nr180259	2	4.6	14236.0	68865.8	983.7	0.598
nr180260	2	0.0	13391.1	58316.7	986.1	0.620
nr180261	2	0.0	13762.2	55481.4	1105.3	0.603
nr180262	2	2.3	12806.4	51483.7	1300.3	0.762
nr180263	2	2.4	8580.0	29364.7	1247.5	0.710
nr180264	2	7.8	6219.1	21031.7	1424.7	0.650
nr180265	2	7.7	5975.0	15770.0	1266.4	0.513

	Statistical error				Fitting error			
	Ni	Cu	Pd	Au	Ni	Cu	Pd	Au
nr180254	0.0	0.5	0.8	5.1	0.00	3.19	3.11	5.39
nr180255	0.0	0.5	0.7	5.5	0.00	3.16	2.90	5.74
nr180256	545.4	0.6	0.9	5.4	308.92	3.57	3.45	5.83
nr180257	0.0	0.8	1.2	6.3	0.00	4.96	4.52	7.34
nr180258	0.0	0.8	1.5	6.5	0.00	5.73	5.50	7.75
nr180259	280.5	0.9	1.7	6.0	200.54	6.39	6.10	8.28
nr180260	0.0	0.9	1.9	6.2	0.00	6.69	6.56	8.54
nr180261	0.0	0.9	2.0	6.1	0.00	6.69	6.70	8.28
nr180262	532.9	0.9	1.9	5.5	360.90	7.17	7.00	8.39
nr180263	398.9	1.2	2.7	5.7	300.74	2.24	3.45	5.23
nr180264	117.0	1.4	3.2	5.3	92.56	11.02	11.23	11.61
nr180265	121.0	1.4	3.8	5.7	91.74	1.55	4.32	4.93

Membrane 2h

Datafile(*.gup)	Sample	Ni(ppm)	Cu(ppm)	Pd(ppm)	Au(ppm)	Chi^2
nr160210	2h	0.0	66675.1	334511.1	1267.0	1.088
nr160211	2h	6.4	57843.5	322860.7	1177.7	0.946
nr160212	2h	0.0	39598.8	250624.8	1176.3	0.976
nr160213	2h	0.0	18006.4	121689.8	1133.9	0.670
nr160214	2h	0.0	11254.0	57267.3	1090.6	0.707
nr160215	2h	0.0	11494.4	35124.5	1238.8	0.636
nr160216	2h	0.0	18181.7	48383.5	1122.0	0.803
nr160217	2h	11.5	20151.6	55431.8	1125.2	0.696
nr160218	2h	9.2	23408.0	61986.8	1138.8	0.630
nr160219	2h	17.4	22036.8	58669.8	1067.3	0.726
nr160220	2h	13.0	14881.8	38228.3	769.5	0.577
nr160221	2h	15.8	13592.8	32395.8	957.5	0.516
nr160222	2h	34.6	15539.0	38015.8	1136.6	0.573
nr160223	2h	5.0	16602.8	40197.7	1442.1	0.546
nr160224	2h	7.5	14022.0	35951.1	1376.9	0.559

	Statistical error				Fitting error			
	Ni	Cu	Pd	Au	Ni	Cu	Pd	Au
nr160210	0.0	0.4	0.8	6.2	0.00	2.97	2.96	6.20
nr160211	475.1	0.4	0.8	6.2	243.11	3.04	2.96	6.37
nr160212	0.0	0.5	0.9	6.0	0.00	3.48	3.45	6.41
nr160213	0.0	0.8	1.3	6.0	0.00	5.14	4.69	7.29
nr160214	0.0	1.0	1.8	5.8	0.00	6.86	6.63	8.45
nr160215	0.0	1.0	2.5	5.7	0.00	8.51	8.64	9.60
nr160216	0.0	0.8	2.1	6.2	0.00	1.66	2.63	5.53
nr160217	146.3	0.8	1.9	6.1	103.42	6.92	6.84	8.49
nr160218	197.2	0.7	1.8	6.0	129.69	6.68	6.38	8.34
nr160219	107.3	0.7	1.9	6.4	57.83	6.73	6.36	8.44
nr160220	107.6	0.9	2.3	7.9	85.21	1.20	2.72	6.71
nr160221	87.3	0.9	2.5	6.7	59.74	8.62	8.95	10.21
nr160222	46.9	0.9	2.3	6.1	34.23	8.41	8.03	9.57

nr160223	307.8	0.8	2.3	5.3	171.35	7.73	7.97	8.81
nr160224	190.0	0.9	2.4	5.7	112.93	8.02	8.09	9.06

Membrane 3h

Datafile(*.gup)	Sample	Ni(ppm)	Cu(ppm)	Pd(ppm)	Au(ppm)	Chi^2
nr160175	3h	4.5	96840.0	254662.6	1222.0	0.998
nr160176	3h	0.0	50153.3	239763.0	1067.8	0.815
nr160177	3h	0.0	14853.5	132246.5	865.8	0.777
nr160178	3h	0.0	6366.3	65386.0	551.5	0.645
nr160179	3h	3.7	1235.0	11209.1	721.2	0.536
nr160180	3h	2.4	1206.8	3768.0	782.3	0.608
nr160181	3h	0.0	2832.9	9164.9	1075.8	0.472
nr160182	3h	0.0	5384.6	21094.8	1003.1	0.443
nr160183	3h	0.0	6476.9	29543.2	717.8	0.544
nr160184	3h	0.0	3816.7	16278.7	959.0	0.430

	Statistical error				Fitting error			
	Ni	Cu	Pd	Au	Ni	Cu	Pd	Au
nr160175	932.9	0.3	0.9	6.3	434.92	3.27	3.29	6.49
nr160176	0.0	0.5	0.9	6.7	0.00	3.49	3.41	6.92
nr160177	0.0	0.9	1.2	7.0	0.00	4.93	4.50	7.74
nr160178	0.0	1.3	1.7	9.1	0.00	7.13	6.25	10.45
nr160179	135.1	3.2	4.7	7.5	150.11	3.05	5.15	6.58
nr160180	179.9	3.2	7.7	7.1	232.03	3.13	9.32	6.16
nr160181	0.0	2.1	4.8	6.0	0.00	2.11	5.52	5.21
nr160182	0.0	1.5	3.1	6.1	0.00	11.15	11.17	12.12
nr160183	0.0	1.4	2.7	7.6	0.00	9.44	9.25	11.28
nr160184	0.0	1.8	3.7	7	0.00	1.89	4.04	5.68

Appendix D

(Response factors)

Response factors

2-Propanol :Acetone					
Mass(g) Pr2	Mass(g) Acetone	GC % Pr2	GC % Acetone	True mass % Pr2	Acetone
1.804	0.2101	90.39	9.61	89.57	10.43
1.607	0.4009	81.88	18.12	80.03	19.97
1.198	0.8243	61.38	38.62	59.24	40.76
1.0247	1.4608	53.99	45.76	41.23	58.77

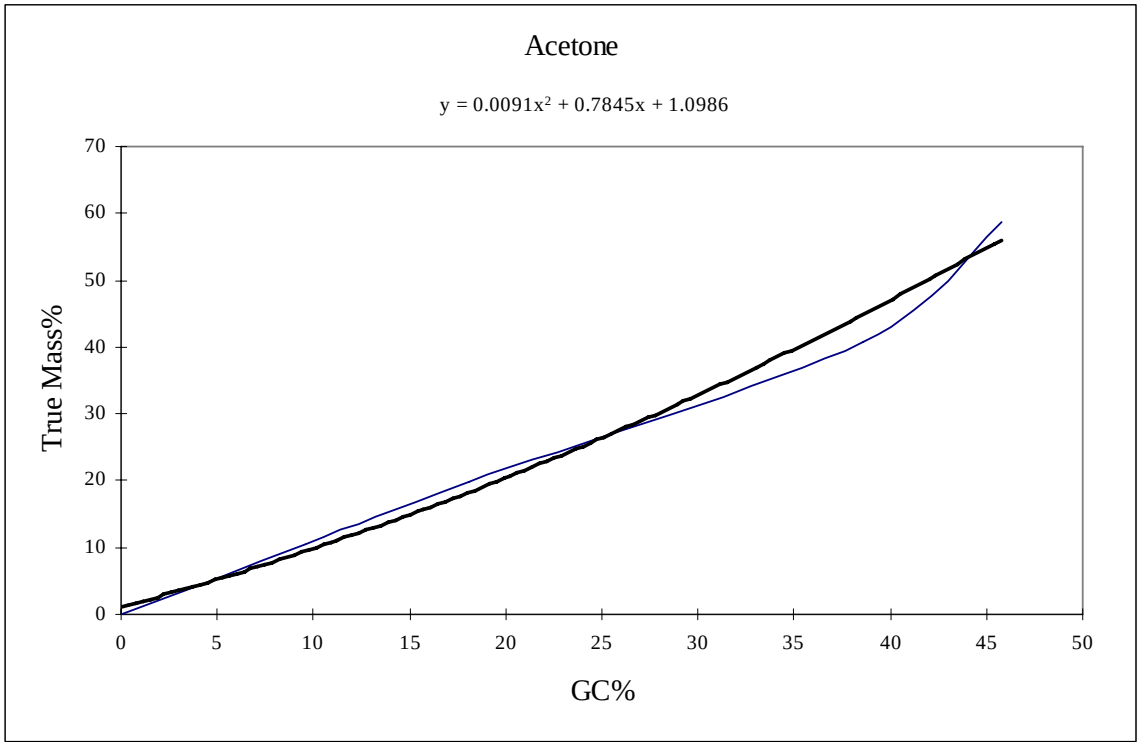

2-propanol:Di-isopropylether					
Mass(g) Pr2	Mass(g) Di-iso	GC % Pr2	GC % Di-iso	True mass % Pr2	Di-iso
1.8022	0.2014	84.7	15.3	89.948	10.052
1.6023	0.3995	71.8	28.2	80.043	19.957
1.2013	0.7987	51.32	48.68	60.065	39.935
0.8117	1.2391	29.99	69.59	39.580	60.420

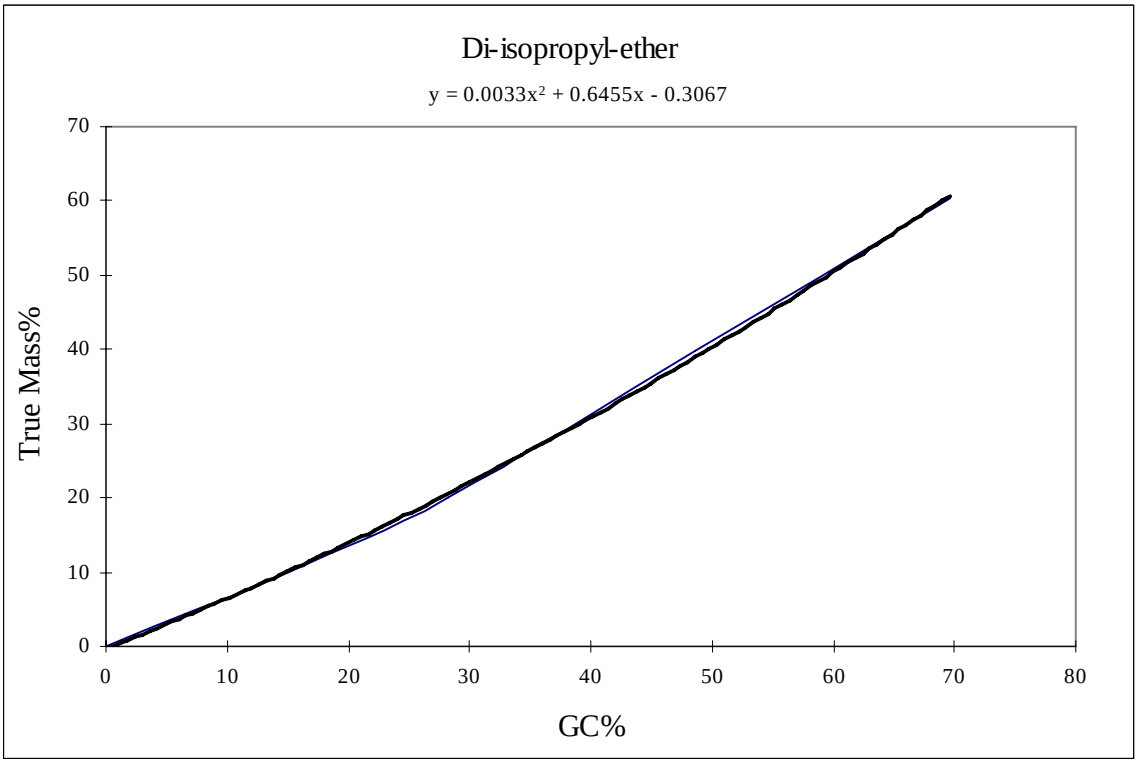

2-Propanol: N2								
Mol Ratio	cm3/min	ml/h	GC Ave %		True mass flowrate(g/min)		True mass%	
(Pr2:N2)	N2	Pr2	N2	Pr2	Pr2	N2	Pr2	N2
01:02	69	6.4	51.73	48.27	0.08	0.09	49.42	50.58
01:04	137	6.4	66.01	33.99	0.08	0.17	32.98	67.02
01:08	137	3.2	75.81	24.19	0.04	0.17	19.75	80.25

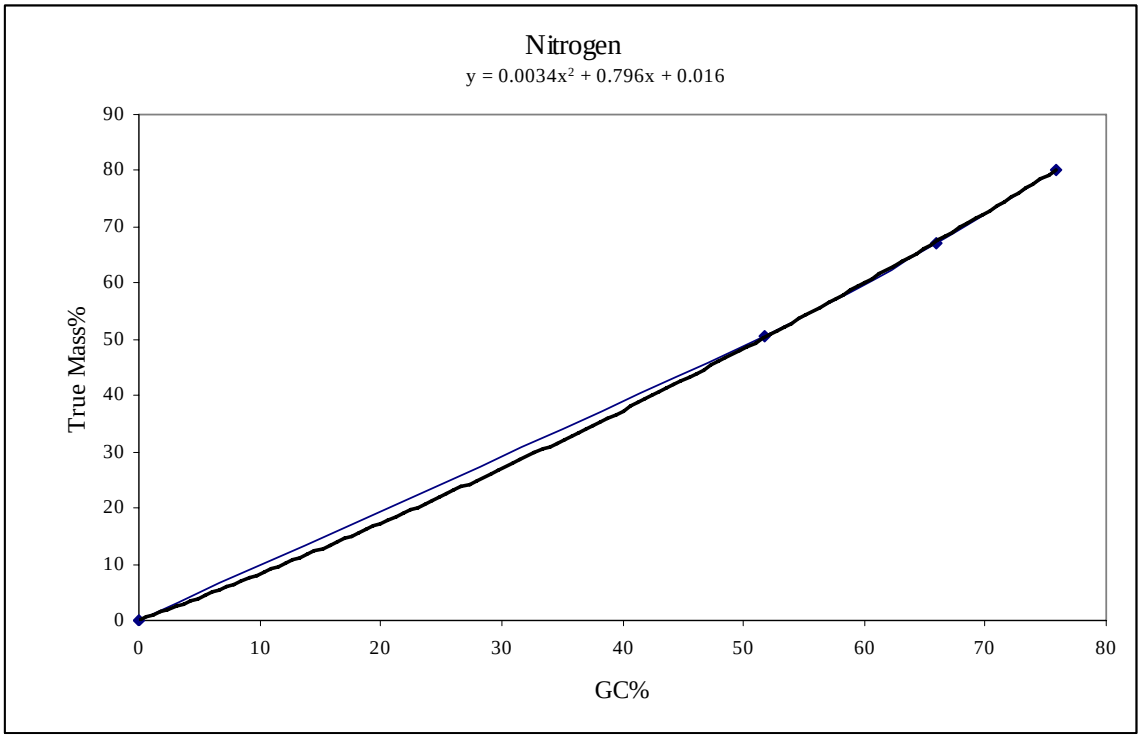

Appendix E

(Catalytic investigation)

Al_2O_3 catalysts

Cat A: 850-1180 micron Alumina

18.5% Cu on alumina
2-Propanol:Nitrogen =1:4

Run	Pr2 (ml\h)	T (°C)	%propene	% 2-propanone	% propan-2-ol	di-isopropyl ether	% phenol	total
Pr2kta1	3.2	150	5.9	0.00	90.89	3.20	0.00	100
Pr2kta2	3.2	180	21.0	0.00	64.60	14.44	0.00	100
Pr2kta3	3.2	210	94.5	5.53	0.00	0.00	0.00	100
Pr2kta4	3.2	240	96.2	3.09	0.00	0.00	0.67	100
Pr2kta5	3.2	270	97.8	2.20	0.00	0.00	0.00	100
Pr2kta6	3.2	300	89.4	0.00	9.34	0.00	1.25	100
Pr2kta7	1.6	150	0.0	0.00	96.73	3.25	0.00	100
Pr2kta8	1.6	180	56.3	3.00	25.65	14.17	0.89	100
Pr2kta9	1.6	210	92.3	2.73	3.74	0.00	1.22	100
Pr2kta10	1.6	240	94.7	1.70	3.56	0.00	0.00	100
Pr2kta11	1.6	270	92.9	0.00	7.05	0.00	0.00	100
Pr2kta12	1.6	300	94.8	0.00	5.17	0.00	0.00	100
Pr2kta13	6.4	150	2.2	0.00	96.57	1.27	0.00	100
Pr2kta14	6.4	180	7.7	0.00	85.81	6.44	0.00	100
Pr2kta15	6.4	210	63.1	0.00	31.20	5.66	0.00	100
Pr2kta16	6.4	240	84.0	0.00	15.07	0.95	0.00	100
Pr2kta17	6.4	270	91.6	2.81	5.55	0.00	0.00	100
Pr2kta18	6.4	300	97.3	2.73	0.00	0.00	0.00	100

Cat B: 850-1180 micron Alumina

24% Cu on alumina
2-Propanol:Nitrogen =1:4

Run	Pr2 (ml\h)	T (°C)	%propene	% 2-propanone	% propan-2-ol	di-isopropyl ether	% phenol	total
Pr2kta1	3.2	150	19.43	1.44	72.41	3.85	1.11	98
Pr2kta2	3.2	180	34.20	0.00	53.28	11.66	0.00	99
Pr2kta3	3.2	210	94.45	1.29	1.77	0.24	1.65	99
Pr2kta4	3.2	240	96.64	0.87	1.54	0.00	0.00	99
Pr2kta5	3.2	270	96.83	0.79	1.42	0.00	0.00	99
Pr2kta6	3.2	300	96.76	0.88	1.50	0.00	0.00	99
Pr2kta7	1.6	150	20.61	1.47	70.99	5.04	0.70	99
Pr2kta8	1.6	180	50.06	2.16	34.58	11.36	0.97	99
Pr2kta9	1.6	210	71.18	1.49	22.93	2.73	0.80	99
Pr2kta10	1.6	240	79.31	1.05	17.18	1.70	0.00	99
Pr2kta11	1.6	270	79.83	0.00	17.63	1.53	0.00	99
Pr2kta12	1.6	300	80.29	0.00	17.17	1.40	0.00	99
Pr2kta13	6.4	150	7.20	0.00	90.42	1.93	0.00	100
Pr2kta14	6.4	180	25.70	0.00	63.56	10.74	0.00	100
Pr2kta15	6.4	210	54.59	0.00	31.93	12.84	0.00	99
Pr2kta16	6.4	240	91.02	0.83	7.18	0.35	0.00	99
Pr2kta17	6.4	270	89.77	0.00	8.83	0.69	0.00	99
Pr2kta18	6.4	300	92.17	0.59	6.41	0.38	0.00	100

Cat G: 850-1180 micron Alumina

13.2% Cu on alumina
2-Propanol:Nitrogen =1:4

Run	Pr2 (ml\h)	T (°C)	%propene	% 2-propanone	% propan-2-ol	di-isopropyl ether	% phenol	total
Pr2ktg1	3.2	150	5.55	1.43	89.36	3.66	0.00	100
Pr2ktg2	3.2	180	28.91	5.46	48.78	16.86	0.00	100
Pr2ktg3	3.2	210	88.80	4.23	6.97	0.00	0.00	100
Pr2ktg4	3.2	240	92.51	2.48	7.01	0.00	0.00	102
Pr2ktg5	3.2	270	96.69	2.27	1.02	0.00	0.00	100
Pr2ktg6	3.2	300	98.20	1.78	0.00	0.00	0.00	100
Pr2ktg7	1.6	150	12.39	10.22	67.70	9.69	0.00	100
Pr2ktg8	1.6	180	41.70	11.24	32.02	15.05	0.00	100
Pr2ktg9	1.6	210	87.52	2.27	9.23	0.00	0.98	100
Pr2ktg10	1.6	240	74.48	1.08	22.01	0.44	1.95	100
Pr2ktg11	1.6	270	72.01	1.26	25.30	0.56	0.84	100
Pr2ktg12	1.6	300	27.09	0.00	71.04	1.42	0.00	100
Pr2ktg13	6.4	150	4.24	0.00	93.72	2.04	0.00	100
Pr2ktg14	6.4	180	24.53	4.03	56.89	14.55	0.00	100
Pr2ktg15	6.4	210	59.09	4.59	25.62	10.71	0.00	100
Pr2ktg16	6.4	240	96.21	2.40	1.40	0.00	0.00	100
Pr2ktg17	6.4	270	93.22	1.61	4.27	0.00	0.88	100
Pr2ktg18	6.4	300	97.15	1.45	1.40	0.00	0.00	100

MgO catalysts

Cat A: 850-1180 microns MgO
0% Cu on MgO
2-Propanol: Nitrogen=1:4

Run	2-Propanol	T(°C)	Propene	Acetone	2-Propanol	4-methyl pentanone	Total
	ml/h						
1	3.2	390	15.29	22.84	61.88	0.00	100
2	3.2	360	12.81	13.62	73.57	0.00	100
3	3.2	330	7.42	6.23	86.35	0.00	100
4	3.2	300	1.04	1.62	97.34	0.00	100
5	3.2	270	0.61	1.21	98.18	0.00	100
6	3.2	240					
7	1.6	240	0.00	0.95	99.05	0.00	100
8	1.6	270	0.33	1.08	98.59	0.00	100
9	1.6	300	1.79	1.85	96.36	0.00	100
10	1.6	330	4.91	4.45	90.64	0.00	100
11	1.6	360	10.93	10.42	78.65	0.00	100
12	1.6	390	22.15	23.67	54.18	0.00	100
13	6.4	390	2.99	7.02	89.99	0.00	100
14	6.4	360	2.35	3.35	94.31	0.00	100
15	6.4	330	0.53	1.09	98.38	0.00	100
16	6.4	300	0.00	0.33	99.67	0.00	100
17	6.4	270					
18	6.4	240					

Cat C: 850-1180 microns MgO
10.3% Cu on MgO
2-Propanol: Nitrogen=1:4

Run	2-Propanol	T(°C)	Propene	Acetone	2-Propanol	4-methyl pentanone	Total
	ml/h						
1	3.2	390	4.40	48.06	47.15	0.39	100.00
2	3.2	360	1.35	23.42	74.69	0.54	100.00
3	3.2	330	0.57	17.76	81.68	0.00	100.00
4	3.2	300	0.00	10.01	89.99	0.00	100.00
5	3.2	270	0.00	4.85	95.15	0.00	100.00
6	3.2	240	0.00	2.81	97.19	0.00	100.00
7	1.6	240	0.00	6.72	93.28	0.00	100.00
8	1.6	270	0.00	20.01	79.99	0.00	100.00
9	1.6	300	0.98	37.84	61.17	0.00	100.00
10	1.6	330	1.51	43.16	55.33	0.00	100.00
11	1.6	360	3.17	66.58	30.24	0.00	100.00
12	1.6	390	6.54	89.42	4.04	0.00	100.00
13	6.4	390	1.28	37.76	60.96	0.00	100.00
14	6.4	360	0.71	16.53	82.76	0.00	100.00
15	6.4	330	0.45	7.32	92.24	0.00	100.00
16	6.4	300	0.00	1.68	98.32	0.00	100.00
17	6.4	270	0.00	1.07	98.93	0.00	100.00
18	6.4	240					

Cat D: 850-1180 microns MgO
16.9% Cu on MgO
2-Propanol: Nitrogen=1:4

Run	2-Propanol	T(°C)	Propene	Acetone	2-Propanol	4-methyl pentanone	Total
	ml/h						
1	3.2	390	2.78	91.39	5.83	0.00	100.00
2	3.2	360	2.01	73.36	24.63	0.00	100.00
3	3.2	330	1.33	36.88	61.79	0.00	100.00
4	3.2	300	0.36	13.30	83.29	3.05	100.00
5	3.2	270	0.95	4.91	94.14	0.00	100.00
6	3.2	240	0.00	1.33	98.67	0.00	100.00
7	1.6	240	0.41	3.87	95.72	0.00	100.00
8	1.6	270	0.00	9.06	90.94	0.00	100.00
9	1.6	300	1.36	58.83	39.82	0.00	100.00
10	1.6	330	1.76	88.57	9.68	0.00	100.00
11	1.6	360	2.65	94.13	1.71	1.51	100.00
12	1.6	390	4.32	91.82	0.93	2.92	100.00
13	6.4	390	1.58	40.30	58.13	0.00	100.00
14	6.4	360	0.65	13.81	85.53	0.00	100.00
15	6.4	330	0.35	4.40	95.25	0.00	100.00
16	6.4	300	0.00	1.67	98.33	0.00	100.00
17	6.4	270	0.00	0.54	99.46	0.00	100.00
18	6.4	240					

Cat E: 850-1180 microns MgO
24.9% Cu on MgO
2-Propanol: Nitrogen=1:4

Run	2-Propanol	T(°C)	Propene	Acetone	2-Propanol	4-methyl pentanone	Total
	ml/h						
1	3.2	390	1.65	67.57	30.42	0.36	100.00
2	3.2	360	0.82	44.91	54.27	0.00	100.00
3	3.2	330	0.82	35.27	63.92	0.00	100.00
4	3.2	300	0.80	25.98	73.22	0.00	100.00
5	3.2	270	0.00	10.31	89.69	0.00	100.00
6	3.2	240	0.00	2.62	97.38	0.00	100.00
7	1.6	240	0.00	10.39	89.61	0.00	100.00
8	1.6	270	0.55	26.01	73.44	0.00	100.00
9	1.6	300	1.61	46.38	52.01	0.00	100.00
10	1.6	330	1.93	55.70	42.37	0.00	100.00
11	1.6	360	2.64	86.74	10.62	0.00	100.00
12	1.6	390	3.97	91.11	4.92	0.00	100.00
13	6.4	390	1.45	38.45	60.10	0.00	100.00
14	6.4	360	0.91	23.67	75.42	0.00	100.00
15	6.4	330	0.53	13.61	85.86	0.00	100.00
16	6.4	300	0.00	4.30	95.70	0.00	100.00
17	6.4	270	0.00	1.68	98.32	0.00	100.00
18	6.4	240					

SiO_2 catalysts

Cat A: 2-Propanol: Nitrogen=1:4
0% Cu on SiO_2
850-1180 microns SiO_2

Run	Propanol-2	T(°C)	Propene	Acetone	Pr2	4-methyl pentanone	Total
	ml/h						
1	3.2	440	100.00	0.00	0.00	0.00	100.00
2	3.2	400	100.00	0.00	0.00	0.00	100.00
3	3.2	360	93.41	0.00	6.59	0.00	100.00
4	3.2	320	55.20	0.00	44.80	0.00	100.00
5	3.2	280	13.01	0.00	86.99	0.00	100.00
6	3.2	240	4.11	0.00	95.89	0.00	100.00
7	1.6	240	9.59	0.00	90.41	0.00	100.00
8	1.6	280	14.58	0.00	85.42	0.00	100.00
9	1.6	320	72.58	0.00	27.42	0.00	100.00
10	1.6	360	96.01	0.00	3.99	0.00	100.00
11	1.6	400	99.13	0.00	0.87	0.00	100.00
12	1.6	440					
13	6.4	440					
14	6.4	400	48.75	0.00	51.25	0.00	100.00
15	6.4	360	18.06	0.00	81.94	0.00	100.00
16	6.4	320	7.14	0.00	92.86	0.00	100.00
17	6.4	280	2.47	0.00	97.53	0.00	100.00
18	6.4	240					

Cat B: 2-Propanol: Nitrogen =1:4
9.2% Cu on SiO_2
850-1180 microns SiO_2

Run	Propanol-2	T(°C)	Propene	Acetone	2-Propanol	4-methyl pentanone	Total
	ml/h						
1	3.2	390	2.48	96.83	0.69	0.00	100.00
2	3.2	360	2.21	97.26	0.53	0.00	100.00
3	3.2	330	3.46	73.62	22.92	0.00	100.00
4	3.2	300	2.87	42.78	54.35	0.00	100.00
5	3.2	270	1.78	12.76	85.46	0.00	100.00
6	3.2	240	0.86	5.83	93.31	0.00	100.00
7	1.6	240	1.03	4.37	94.59	0.00	100.00
8	1.6	270	3.75	19.51	76.75	0.00	100.00
9	1.6	300	3.94	41.76	54.30	0.00	100.00
10	1.6	330	3.81	86.16	10.03	0.00	100.00
11	1.6	360	2.50	96.43	1.07	0.00	100.00
12	1.6	390	2.80	96.49	0.71	0.00	100.00
13	6.4	390	2.68	88.73	8.60	0.00	100.00
14	6.4	360	2.31	55.93	41.75	0.00	100.00
15	6.4	330	1.95	33.06	64.99	0.00	100.00
16	6.4	300	1.01	12.34	86.65	0.00	100.00
17	6.4	270	0.42	4.18	95.41	0.00	100.00
18	6.4	240	0.00	1.79	98.21	0.00	100.00

Cat C: 2-Propanol: Nitrogen =1:4
18.6% Cu on SiO_2
850-1180 microns SiO_2

Run	Propanol-2	T(°C)	Propene	Acetone	2-Propanol	4-methyl pentanone	Total
	ml/h						
1	3.2	390	7.62	91.62	0.00	0.76	100.00
2	3.2	360	8.46	91.54	0.00	0.00	100.00
3	3.2	330	10.68	75.98	13.34	0.00	100.00
4	3.2	300	8.58	71.18	20.25	0.00	100.00
5	3.2	270	1.83	10.41	87.76	0.00	100.00
6	3.2	240	1.09	8.81	90.10	0.00	100.00
7	1.6	240	2.22	12.61	85.17	0.00	100.00
8	1.6	270	4.29	14.80	80.92	0.00	100.00
9	1.6	300	8.22	38.15	53.63	0.00	100.00
10	1.6	330	12.64	83.06	4.31	0.00	100.00
11	1.6	360	9.60	89.15	1.25	0.00	100.00
12	1.6	390	10.72	88.41	0.00	0.86	100.00
13	6.4	390	10.10	88.52	1.37	0.00	100.00
14	6.4	360	9.08	68.68	22.23	0.00	100.00
15	6.4	330	4.42	35.37	60.20	0.00	100.00
16	6.4	300	2.09	12.16	85.75	0.00	100.00
17	6.4	270	0.91	5.42	93.67	0.00	100.00
18	6.4	240	0.31	1.49	98.20	0.00	100.00

Cat D: 2-Propanol: Nitrogen =1:4
27.7% Cu on SiO_2
850-1180 microns SiO_2

Run	Propanol-2	T(°C)	Propene	Acetone	2-Propanol	4-methyl pentanone	Total
	ml/h						
1	3.2	390	11.97	87.44	0.00	0.59	100.00
2	3.2	360	8.24	91.76	0.00	0.00	100.00
3	3.2	330	12.65	83.97	3.38	0.00	100.00
4	3.2	300	7.43	52.79	39.78	0.00	100.00
5	3.2	270	2.16	9.01	88.83	0.00	100.00
6	3.2	240	1.16	0.00	98.84	0.00	100.00
7	1.6	240	2.57	0.00	97.43	0.00	100.00
8	1.6	270	5.57	17.83	76.60	0.00	100.00
9	1.6	300	8.39	38.32	53.29	0.00	100.00
10	1.6	330	13.14	82.32	4.54	0.00	100.00
11	1.6	360	12.49	86.46	1.05	0.00	100.00
12	1.6	390	19.11	80.89	0.00	0.00	100.00
13	6.4	390	12.61	86.04	1.35	0.00	100.00
14	6.4	360	9.16	73.45	17.39	0.00	100.00
15	6.4	330	4.42	32.85	62.73	0.00	100.00
16	6.4	300	0.53	6.50	92.97	0.00	100.00
17	6.4	270	0.86	4.79	94.35	0.00	100.00
18	6.4	240	0.37	1.84	97.78	0.00	100.00

Cat F: 2-Propanol: Nitrogen =1:4
4.2% Cu on SiO_2
850-1180 microns SiO_2

Run	Propanol-2	T(°C)	Propene	Acetone	2-Propanol	Total
	ml/h					
1	3.2	440	15.11	84.89	0.00	100.00
2	3.2	400	18.81	70.58	10.62	100.00
3	3.2	360	13.61	40.32	46.07	100.00
4	3.2	320	11.12	24.67	64.21	100.00
5	3.2	280	2.41	4.71	92.89	100.00
6	3.2	240	0.00	1.38	98.62	100.00
7	1.6	240	0.97	1.64	97.40	100.00
8	1.6	280	2.52	5.32	92.16	100.00
9	1.6	320	11.53	29.03	59.44	100.00
10	1.6	360	15.61	52.64	31.75	100.00
11	1.6	400	13.61	86.39	0.00	100.00
12	1.6	440				
13	6.4	440	14.92	58.48	26.60	100.00
14	6.4	400	9.66	32.27	58.08	100.00
15	6.4	360	4.81	13.04	82.16	100.00
16	6.4	320	1.57	3.49	94.93	100.00
17	6.4	280	0.74	1.13	98.13	100.00
18	6.4	240	0.55	0.68	98.77	100.00

Cat G: 2-Propanol: Nitrogen =1:4
11.7% Cu on SiO_2
850-1180 microns SiO_2

Run	Propanol-2	T(°C)	Propene	Acetone	2-Propanol	4-methyl pentanone	Total
	ml/h						
1	3.2	390	12.08	86.79	0.00	1.13	100.00
2	3.2	360	12.83	86.57	0.00	0.60	100.00
3	3.2	330	12.92	87.08	0.00	0.00	100.00
4	3.2	300	9.88	55.38	34.74	0.00	100.00
5	3.2	270	5.89	27.38	66.73	0.00	100.00
6	3.2	240	0.00	2.23	97.77	0.00	100.00
7	1.6	240	0.61	2.91	96.48	0.00	100.00
8	1.6	270	2.97	10.62	86.41	0.00	100.00
9	1.6	300	4.46	22.03	73.51	0.00	100.00
10	1.6	330	16.40	52.51	31.09	0.00	100.00
11	1.6	360	15.00	85.00	0.00	0.00	100.00
12	1.6	390					
13	6.4	390	12.87	87.13	0.00	0.00	100.00
14	6.4	360	10.48	83.02	6.49	0.00	100.00
15	6.4	330	7.31	48.40	44.29	0.00	100.00
16	6.4	300	3.67	15.36	80.97	0.00	100.00
17	6.4	270	0.74	0.00	99.26	0.00	100.00
18	6.4	240					

Cat H: 2-Propanol: Nitrogen =1:4
15% Cu on SiO_2
850-1180 microns SiO_2

Run	Propanol-2	T(°C)	Propene	Acetone	2-Propanol	4-methyl pentanone	Total
	ml/h						
1	3.2	390	9.51	89.29	0.00	1.19	100.00
2	3.2	360	11.40	88.09	0.00	0.51	100.00
3	3.2	330	19.09	80.91	0.00	0.00	100.00
4	3.2	300	20.95	74.46	4.60	0.00	100.00
5	3.2	270	16.96	36.77	46.27	0.00	100.00
6	3.2	240	3.14	7.87	88.99	0.00	100.00
7	1.6	240	2.64	5.71	91.65	0.00	100.00
8	1.6	270	9.34	20.38	70.28	0.00	100.00
9	1.6	300	21.03	69.24	9.74	0.00	100.00
10	1.6	330	15.95	83.32	0.73	0.00	100.00
11	1.6	360	12.49	86.80	0.71	0.00	100.00
12	1.6	390	14.95	85.05	0.00	0.00	100.00
13	6.4	390	15.97	84.03	0.00	0.00	100.00
14	6.4	360	15.55	78.43	6.02	0.00	100.00
15	6.4	330	15.12	39.80	45.08	0.00	100.00
16	6.4	300	5.34	12.34	82.33	0.00	100.00
17	6.4	270	2.92	5.61	91.47	0.00	100.00
18	6.4	240					

Cat Ba: 2-Propanol: Nitrogen =1:4
9.2% Cu on SiO_2
Fraction = 150-300 microns

Run	Propanol-2	T(°C)	Propene	Acetone	2-Propanol	4-methyl pentanone	Total
	ml/h						
1	3.2	390	39.04	60.96	0.00	0.00	100.00
2	3.2	360	23.21	74.96	0.00	1.83	100.00
3	3.2	330	11.60	75.12	0.00	0.00	86.73
4	3.2	300	11.03	73.70	0.00	0.00	84.73
5	3.2	270	6.77	65.83	21.54	0.00	94.13
6	3.2	240	2.08	23.98	71.58	0.00	97.64
7	1.6	240	2.91	25.16	70.29	0.00	98.36
8	1.6	270	9.83	59.46	26.85	0.00	96.15
9	1.6	300	14.22	80.62	0.00	0.00	94.84
10	1.6	330	13.64	78.37	4.09	0.32	96.41
11	1.6	360	18.27	78.38	0.00	0.63	97.27
12	1.6	390	25.54	71.33	0.00	0.93	97.80
13	6.4	390	26.90	73.10	0.00	0.00	100.00
14	6.4	360	12.71	57.87	27.44	0.00	98.02
15	6.4	330	7.11	65.54	27.35	0.00	100.00
16	6.4	300	3.25	10.98	84.75	0.00	98.97
17	6.4	270	1.19	4.49	94.32	0.00	100.00
18	6.4	240	0.00	1.07	97.83	0.00	98.90

Cat Bb: 2-Propanol: Nitrogen =1:4
9.2% Cu on SiO_2
Fraction = 850-1180 microns

Run	Propanol-2	T(°C)	Propene	Acetone	2-Propanol	Total
	ml/h					
1	3.2	390	21.34	78.66	0.00	100.00
2	3.2	360	22.21	77.79	0.00	100.00
3	3.2	330	22.88	77.12	0.00	100.00
4	3.2	300	12.56	54.11	33.32	100.00
5	3.2	270	3.43	18.74	77.84	100.00
6	3.2	240	0.83	5.47	93.70	100.00
7	1.6	240	2.36	10.50	87.15	100.00
8	1.6	270	5.38	21.58	73.04	100.00
9	1.6	300	14.93	49.43	35.64	100.00
10	1.6	330	16.03	79.00	4.97	100.00
11	1.6	360	12.83	86.63	0.54	100.00
12	1.6	390	13.87	85.85	0.28	100.00
13	6.4	390	13.52	79.54	6.94	100.00
14	6.4	360	11.22	57.22	31.56	100.00
15	6.4	330	7.35	32.83	59.82	100.00
16	6.4	300	4.33	16.78	78.89	100.00
17	6.4	270	1.19	4.76	94.04	100.00
18	6.4	240	0.00	1.53	98.47	100.00

Cat Bc: 2-Propanol: Nitrogen =1:4
9.2% Cu on SiO_2
Fraction = 3mm

Run	Propanol-2	T(°C)	Propene	Acetone	2-Propanol	Total
	ml/h					
1	3.2	390	4.31	91.73	3.96	100.00
2	3.2	360	5.18	81.43	13.38	100.00
3	3.2	330	3.58	54.32	42.10	100.00
4	3.2	300	3.64	49.10	47.26	100.00
5	3.2	270	3.42	35.92	60.65	100.00
6	3.2	240	1.48	20.01	78.52	100.00
7	1.6	240	2.58	33.81	63.61	100.00
8	1.6	270	3.24	33.57	63.18	100.00
9	1.6	300	7.21	44.83	47.96	100.00
10	1.6	330	9.96	71.07	18.98	100.00
11	1.6	360	9.05	83.48	7.47	100.00
12	1.6	390	9.37	85.28	5.34	100.00
13	6.4	390	4.92	55.24	39.85	100.00
14	6.4	360	5.42	45.31	49.27	100.00
15	6.4	330	4.05	29.57	66.38	100.00
16	6.4	300	3.06	17.22	79.72	100.00
17	6.4	270	2.62	10.31	87.08	100.00
18	6.4	240	1.88	5.84	92.29	100.00

Appendix F

(Membrane tests)

Permeance and selectivity tests

Palladium plated membrane

Run	Gas	T(control)	T(reactor)	delta P	Flow meter	Bubble vol	t1(s)	t2(s)	t3(s)
		(°C)	(°C)	(mbar)	(cm^3/min)	(cm^3)			
1	H_2	340	330	340	600	90	7.78	7.79	7.8
2	H_2	340	330	260	450	90	10.34	10.36	10.35
3	H_2	340	330	171	300	90	15.6	15.6	15.62
4	H_2	340	330	86	150	60	20.75	20.8	20.76
5	N_2	339	331	220	14	4	36.32	36.32	36.32
6	N_2	340	332	395	22	4	19.13	19.13	19.15
7	N_2	340	332	589	31	4	12.25	12.25	12.27
8	H_2	378	370	240	600	90	7.78	7.8	7.78
9	H_2	378	371	181	450	90	10.44	10.45	10.46
10	H_2	378	370	123	300	90	15.63	15.64	15.62
11	H_2	378	370	64	150	60	20.81	20.8	20.85
12	N_2	379	371	170	12	4	45.41	45.4	45.42
13	N_2	379	371	390	22	4	19.34	19.34	19.35
14	N_2	379	371	600	32	4	11.94	11.96	11.95
15	H_2	420	409	243	600	90	7.59	7.6	7.57
16	H_2	422	409	181	450	90	10.41	10.41	10.42
17	H_2	422	409	119	300	90	15.56	15.6	15.58
18	H_2	422	409	60	150	60	21	21	21.03
19	N_2	421	409	176	11	4	44.57	44.58	44.6
20	N_2	420	410	395	21	4	18.9	18.91	18.9
21	N_2	420	410	590	32	4	12.16	12.16	12.18

Palladium-copper plated membrane

Tests after 0 hours of heat treatment at 600 °C.

Run	Gas	T(control)	T(reactor)	delta P	Flow meter	Bubble vol	t1(s)	t2(s)	t3(s)
		(°C)	(°C)	(mbar)	(cm^3/min)	(cm^3)			
1	H_2	469	447	428	600	90	7.81	7.88	7.85
2	H_2	470	452	310	450	90	10.50	10.50	10.51
3	H_2	472	452	209	300	90	15.81	15.81	15.80
4	H_2	470	453	100	150	60	20.91	20.94	20.91
5	N_2	470	453	200	33	4	10.41	10.37	10.40
6	N_2	472	453	400	70	4	5.00	4.97	5.01
7	N_2	468	454	600	107	20	15.87	15.88	15.85
8	H_2	430	414	479	600	90	7.66	7.69	7.70
9	H_2	425	414	357	450	90	10.50	10.44	10.47
10	H_2	424	412	235	300	90	15.78	15.75	15.74
11	H_2	424	410	116	150	60	20.91	20.97	20.95
12	N_2	428	410	180	35	4	10.22	10.28	10.25
13	N_2	425	411	400	75	4	4.50	4.56	4.56
14	N_2	425	413	600	113	20	14.57	14.56	14.56
15	H_2	382	368	559	600	90	7.78	7.77	7.74
16	H_2	380	367	412	450	90	10.53	10.47	10.51
17	H_2	379	370	269	300	90	15.70	15.65	15.66
18	H_2	380	369	130	150	60	20.78	20.82	20.79
19	N_2	380	369	170	33	4	11.00	11.03	11.01
20	N_2	380	369	377	77	4	4.36	4.43	4.40
21	N_2	380	369	590	122	20	13.76	13.78	13.80
22	H_2	337	328	632	600	90	7.81	7.87	7.85
23	H_2	339	328	469	450	90	10.47	10.47	10.48
24	H_2	340	328	308	300	90	15.81	15.75	15.78
25	H_2	337	329	155	150	60	20.97	21.03	21.01
26	N_2	339	329	170	39	4	9.38	9.25	9.32
27	N_2	338	331	377	85	4	4.03	4.03	4.03
28	N_2	340	329	588	131	20	12.68	12.69	12.70

Tests after 24 hours of heat treatment at 600 °C.

Run	Gas	T(control)	T(reactor)	delta P	Flow meter	Bubble vol	t1	t2	t3
		(°C)	(°C)	(mbar)	(cm^3/min)	(cm^3)			
1	H_2	470	451	544	600	90	7.88	7.87	7.85
2	H_2	472	453	408	450	90	10.62	10.53	10.56
3	H_2	468	453	273	300	90	15.94	15.91	15.91
4	H_2	468	454	135	150	60	21.13	21.16	21.15
5	N_2	471	454	222	87	4	3.53	3.56	3.59
6	N_2	470	454	390	156	20	10.47	10.47	10.47
7	N_2	471	454	588	244	30	10.13	10.10	10.11
8	H_2	428	412	548	600	90	7.91	7.87	7.90
9	H_2	424	412	414	450	90	10.60	10.53	10.50
10	H_2	425	412	275	300	90	15.75	15.81	15.81
11	H_2	426	411	139	150	60	21.22	21.25	21.22
12	N_2	425	412	203	86	10	9.16	9.13	9.16
13	N_2	426	412	394	176	20	9.28	9.28	9.28
14	N_2	425	412	588	276	30	8.94	8.97	8.95
15	H_2	380	368	535	600	90	7.78	7.75	7.76
16	H_2	380	369	404	450	90	10.54	10.43	10.56
17	H_2	381	369	273	300	90	15.87	15.90	15.88
18	H_2	383	369	136	150	60	21.22	21.09	21.14
19	N_2	381	370	180	88	10	9.37	9.38	9.38
20	N_2	381	370	390	200	20	8.25	8.22	8.23
21	N_2	380	370	590	319	30	7.72	7.78	7.73
22	H_2	338	329	520	600	90	7.66	7.63	7.70
23	H_2	338	329	394	450	90	10.46	10.44	10.42
24	H_2	340	330	265	300	90	15.75	15.72	15.74
25	H_2	342	330	133	150	60	21.18	21.12	21.15
26	N_2	340	330	180	97	10	8.44	8.41	8.42
27	N_2	339	331	383	220	20	7.41	7.47	7.42
28	N_2	339	330	580	349	30	7.16	7.06	7.10

Tests after 48 hours of heat treatment at 600 °C.

Run	Gas	T(control)	T(reactor)	delta P	Flow meter	Bubble vol	t1	t2	t3
		(°C)	(°C)	(mbar)	(cm^3/min)	(cm^3)			
1	H_2	470	453	480	600	90	7.91	7.90	7.90
2	H_2	472	453	360	450	90	10.53	10.56	10.56
3	H_2	468	453	244	300	90	15.84	15.87	15.85
4	H_2	469	453	123	150	60	21.47	21.41	21.45
5	N_2	470	454	196	102	10	7.68	7.74	7.68
6	N_2	470	454	377	212	20	7.78	7.80	7.81
7	N_2	472	454	600	350	30	7.06	7.05	7.04
8	H_2	425	412	447	600	90	7.60	7.63	7.61
9	H_2	425	411	335	450	90	10.32	10.32	10.31
10	H_2	425	410	232	300	90	15.84	15.80	15.81
11	H_2	425	410	120	150	60	21.25	21.26	21.25
12	N_2	425	412	220	156	10	5.88	5.90	5.95
13	N_2	427	412	389	262	20	6.41	6.40	6.43
14	N_2	425	412	600	426	30	6.03	6.00	6.02
15	H_2	381	369	413	600	90	7.62	7.60	7.58
16	H_2	378	369	314	450	90	10.43	10.40	10.45
17	H_2	381	369	215	300	90	15.59	15.60	15.58
18	H_2	381	369	112	150	60	21.41	21.43	21.45
19	N_2	380	370	210	143	10	5.66	5.70	5.66
20	N_2	382	370	385	303	20	5.50	5.47	5.51
21	N_2	381	370	600	495	30	5.13	5.10	5.15
22	H_2	340	330	391	600	90	8.00	8.03	8.01
23	H_2	340	330	302	450	90	10.62	10.63	10.62
24	H_2	340	330	206	300	90	16.09	16.10	16.09
25	H_2	339	330	110	150	60	21.44	21.44	21.43
26	N_2	339	331	203	172	10	5.15	5.15	5.14
27	N_2	340	331	385	341	20	4.97	5.00	4.98
28	N_2	340	331	600	572	30	4.38	4.40	4.40

Tests after 80 hours of heat treatment at 600 °C.

Run	Gas	T(control)	T(reactor)	delta P	Flow meter	Bubble vol	t1	t2	t3
		(°C)	(°C)	(mbar)	(cm^3/min)	(cm^3)			
1	H_2	470	453	432	600	90	8.03	8.04	8.00
2	H_2	470	452	329	450	90	10.72	10.71	10.72
3	H_2	470	453	223	300	90	16.22	16.20	16.24
4	H_2	470	453	117	150	60	21.37	21.38	21.38
5	N_2	470	454	200	122	10	6.69	6.80	6.80
6	N_2	470	454	390	265	20	6.31	6.32	6.30
7	N_2	470	454	592	431	30	5.90	5.95	5.85
8	H_2	425	412	394	600	90	8.06	8.05	8.08
9	H_2	425	413	299	450	90	10.78	10.80	10.78
10	H_2	425	412	205	300	90	16.05	16.00	16.08
11	H_2	425	413	104	150	60	21.40	21.38	21.40
12	N_2	425	413	203	154	20	11.03	11.00	11.03
13	N_2	425	413	400	327	30	7.66	7.68	7.65
14	N_2	425	413	585	515	40	6.50	6.52	6.54
15	H_2	380	369	358	600	90	7.88	7.88	7.89
16	H_2	380	369	275	450	90	10.63	10.60	10.65
17	H_2	380	369	187	300	90	16.00	15.99	16.03
18	H_2	379	369	97	150	60	21.25	21.28	21.25
19	N_2	381	370	165	141	20	11.47	11.50	11.46
20	N_2	380	370	400	378	30	6.57	6.60	6.61
21	N_2	380	370	600	617	40	5.56	5.60	5.55
22	H_2	340	330	336	600	90	7.97	7.99	8.00
23	H_2	339	329	257	450	90	10.66	10.66	10.69
24	H_2	340	330	178	300	90	15.97	15.96	16.00
25	H_2	340	330	90	150	60	21.28	21.28	21.29
26	N_2	340	331	200	191	20	4.28	4.32	4.30
27	N_2	340	330	400	431	30	3.87	3.89	3.86
28	N_2	340	331	600	707	40	3.69	3.70	3.68

Tests after 110 hours of heat treatment at 600 °C.

Run	Gas	T(control)	T(reactor)	delta P	Flow meter	Bubble vol	t1	t2	t3
		(°C)	(°C)	(mbar)	(cm^3/min)	(cm^3)			
1	H_2	470	452	364	600	90	7.90	7.91	7.92
2	H_2	471	453	275	450	90	10.62	10.60	10.62
3	H_2	470	452	186	300	90	15.97	15.97	15.92
4	H_2	470	452	94	150	60	21.13	21.14	21.10
5	N_2	471	453	207	168	10	4.75	4.76	4.80
6	N_2	471	453	401	351	20	4.75	4.74	4.76
7	N_2	470	453	590	554	30	4.59	4.60	4.58
8	H_2	425	410	324	600	90	7.69	7.70	7.72
9	H_2	425	411	250	450	90	10.06	10.08	10.07
10	H_2	426	411	168	300	90	15.50	15.51	15.52
11	H_2	426	411	85	150	60	20.53	20.53	20.55
12	N_2	425	412	203	214	10	3.81	3.80	3.82
13	N_2	426	412	390	423	20	3.94	3.95	3.97
14	N_2	425	412	592	692	30	3.69	3.70	3.68
15	H_2	380	371	292	600	90	7.46	7.45	7.46
16	H_2	380	371	222	450	90	10.28	10.30	10.28
17	H_2	380	371	150	300	90	15.50	15.50	15.50
18	H_2	380	371	77	150	60	20.60	20.61	20.60
19	N_2	380	370	205	263	10	3.22	3.24	3.25
20	N_2	380	371	382	503	20	3.28	3.29	3.30
21	N_2	380	371	604	838	30	2.90	2.90	2.92
22	H_2	339	330	264	600	90	7.44	7.45	7.46
23	H_2	339	331	199	450	90	10.18	10.20	10.18
24	H_2	340	331	135	300	90	15.56	15.56	15.60
25	H_2	339	331	69	150	60	21.09	21.09	21.10
26	N_2	339	331	210	316	10	2.72	2.70	2.71
27	N_2	339	331	382	581	20	2.94	2.94	2.96
28	N_2	339	331	594	934	30	2.56	2.58	2.53

Appendix G

(List of presentations)

List of presentations

Characterising palladium-copper alloy membranes using SEM, XRD ad PIXE, *Snapshot presentation*, SAIChe (Western Cape branch) Chemical Engineering R&D Conference, University of Stellenbosch, 2 November 1998.

Characterising palladium-copper alloy membranes using SEM, XRD ad PIXE, *Poster presentation*, SAIChe (Western Cape branch) Chemical Engineering R&D Conference, University of Stellenbosch, 2 November 1998.

Development of an alumina membrane reactor using dehydrogenation reactions, Post graduate conference, University of Stellenbosch, July 1999.